LEGIBILITY NOTICE

A major purpose of the Technical Information Center is to provide the broadest dissemination possible of information contained in DOE's Research and Development Reports to business, industry, the academic community, and federal, state and local governments.

Although a small portion of this report is not reproducible, it is being made available to expedite the availability of information on the research discussed herein.

ORNL/TM--11234

DE89 016936

ADVANCED NEUTRON SOURCE FINAL PRECONCEPTUAL REFERENCE CORE DESIGN

G. L. Copeland
W. R. Gambill
R. M. Harrington
J. A. Johnson
F. J. Peretz
H. Reutler
J. M. Ryskamp
D. L. Selby
C. D. West
G. L. Yoder

Date Published - August 1989

Prepared by the
OAK RIDGE NATIONAL LABORATORY
Oak Ridge, Tennessee 37831
operated by
MARTIN MARIETTA ENERGY SYSTEMS, INC.
for the
U.S. DEPARTMENT OF ENERGY
under Contract No. DE-AC05-84OR21400

CONTENTS

LIST OF ACRONYMS

ANS	Advanced Neutron Source
ANSL	Advanced Neutron Source (cross section) Library
ATR	Advanced Test Reactor
BNL	Brookhaven National Laboratory
BOC	Beginning of cycle
CFR	*Code of Federal Regulations*
CPBT	Core pressure boundary tube
DOE	Department of Energy
EOC	End of cycle
GDC	General Design Criteria
HFIR	High Flux Isotope Reactor
IBL	Incipient boiling limit
ID No.	Identity number
ILL	Institut Laue Langevin
INEL	Idaho National Engineering Laboratory
NIST	National Institute for Standards and Technology
NRC	Nuclear Regulatory Commission
ORNL	Oak Ridge National Laboratory

LIST OF FIGURES

LIST OF TABLES

ADVANCED NEUTRON SOURCE FINAL PRECONCEPTUAL REFERENCE CORE DESIGN

G. L. Copeland
W. R. Gambill
R. M. Harrington
J. A. Johnson
F. J. Peretz
H. Reutler
J. M. Ryskamp
D. L. Selby
C. D. West
G. L. Yoder

ABSTRACT

The preconceptual design phase of the Advanced Neutron Source (ANS) Project ended with the selection of a reference reactor core that will be used to begin conceptual design work. The new reference core consists of two involute fuel elements, of different diameters, aligned axially with a small axial gap between them. The use of different element diameters permits a separate flow of coolant to be provided for each one, thus enhancing the heat removal capability and increasing the thermal-hydraulic margins. The improved cooling allows the elements to be relatively long and thin, so self-shielding is reduced and an acceptable core life can be achieved with a relatively small loading of highly enriched uranium silicide fuel clad in aluminum.

The new reference design has a fueled volume of 67.4 L, each element having a heated length of 474 mm and a radial fuel thickness of 66 mm. The end-of-cycle peak thermal flux in the large heavy-water reflector tank around the core is estimated to be in the range of 0.8 to 1.0 × 10^{20} $m^{-2} \cdot s^{-1}$.

---

1. INTRODUCTION

During the preconceptual design phase of the Advanced Neutron Source (ANS) Project, a particular approach to the evolution of a core design was adopted: the ANS Project Office, with guidance from the technical participants in the project, selected a "reference core" (Fig. 1). The reference core was examined in depth for ~1 year, with all members of the project team (core physics, thermal-hydraulics, engineering design, cold source design) basing their work on the same reference core. In this way, a fairly detailed understanding of the merits, performance, and disadvantages of the core was obtained, based on consistent calculations and experiments. After thorough review of

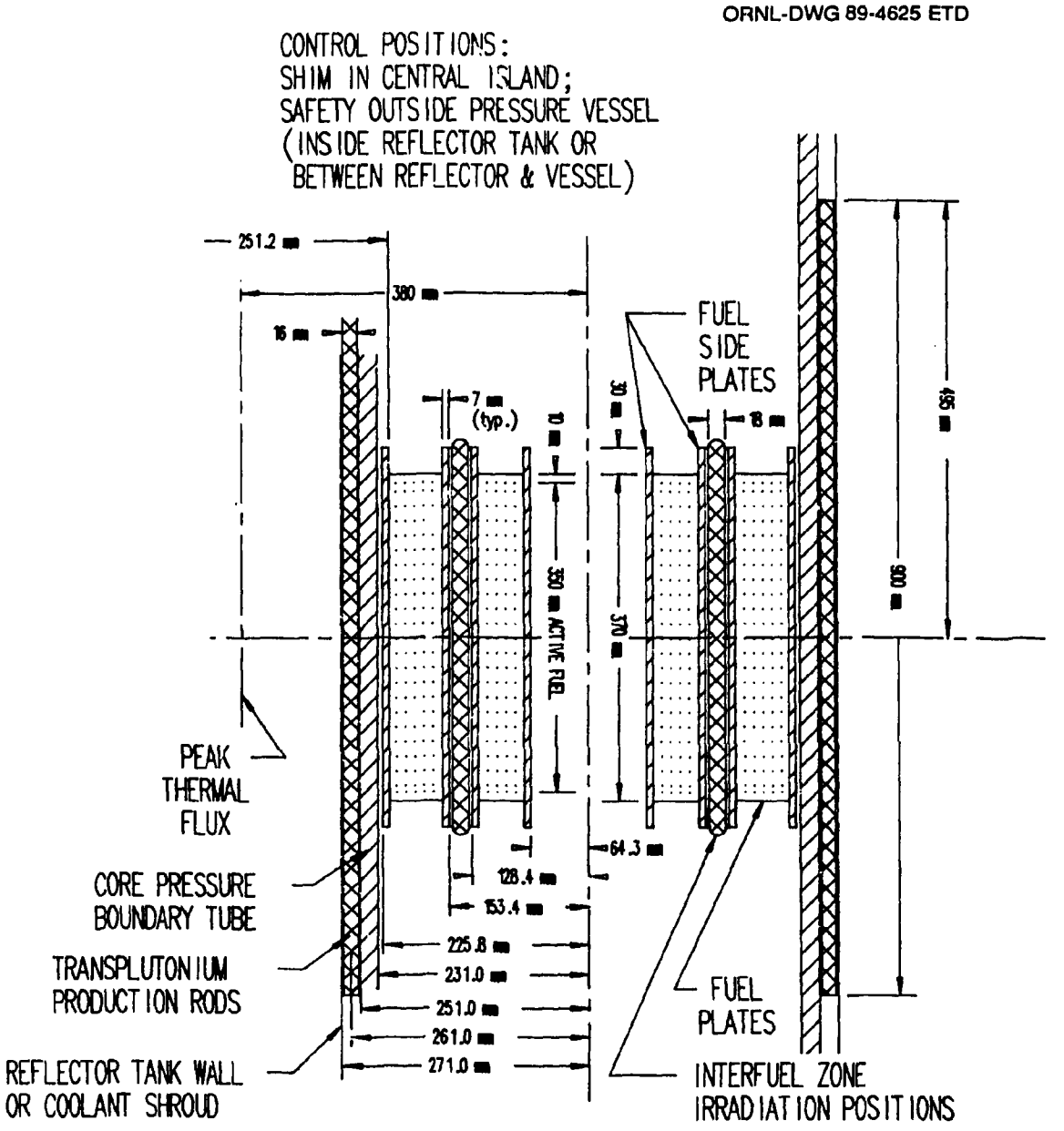

Fig. 1. Reference single core.

the knowledge gained and of proposals for improved designs, a new reference core was adopted that offered better performance and other benefits. The process was repeated, and the new reference core (Fig. 2) was subjected to critical review and extensive analysis. Alternative features, with the potential for enhancement of the core performance or safety margins, were examined and discussed. Finally, at the end of the preconceptual design phase, an intensive period of analysis, review, and

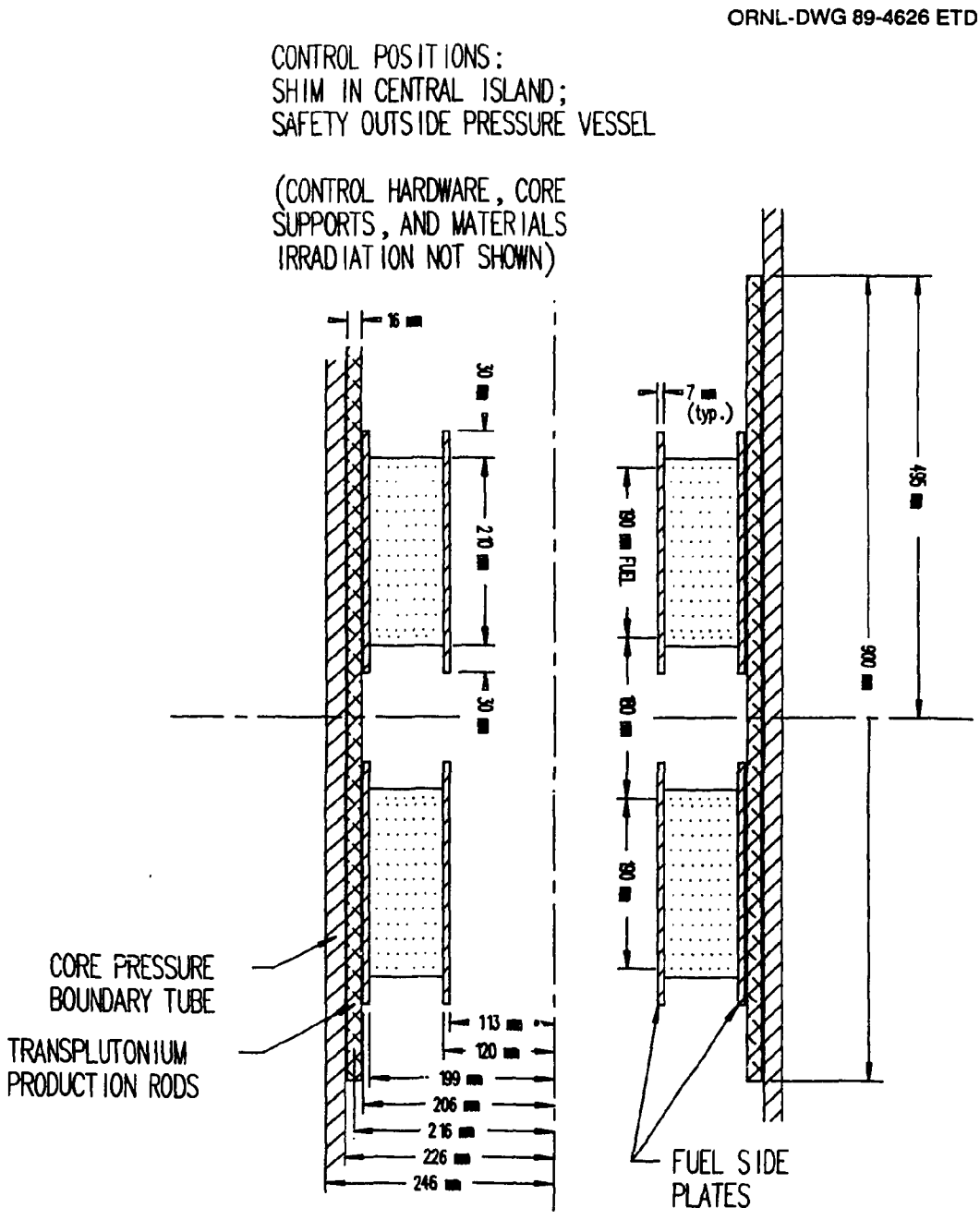

Fig. 2. INT-1 core.

comparison of various core design possibilities resulted in the selection of a final reference core from this phase of the project. This core (Fig. 3) is the one with which the project has begun conceptual design.

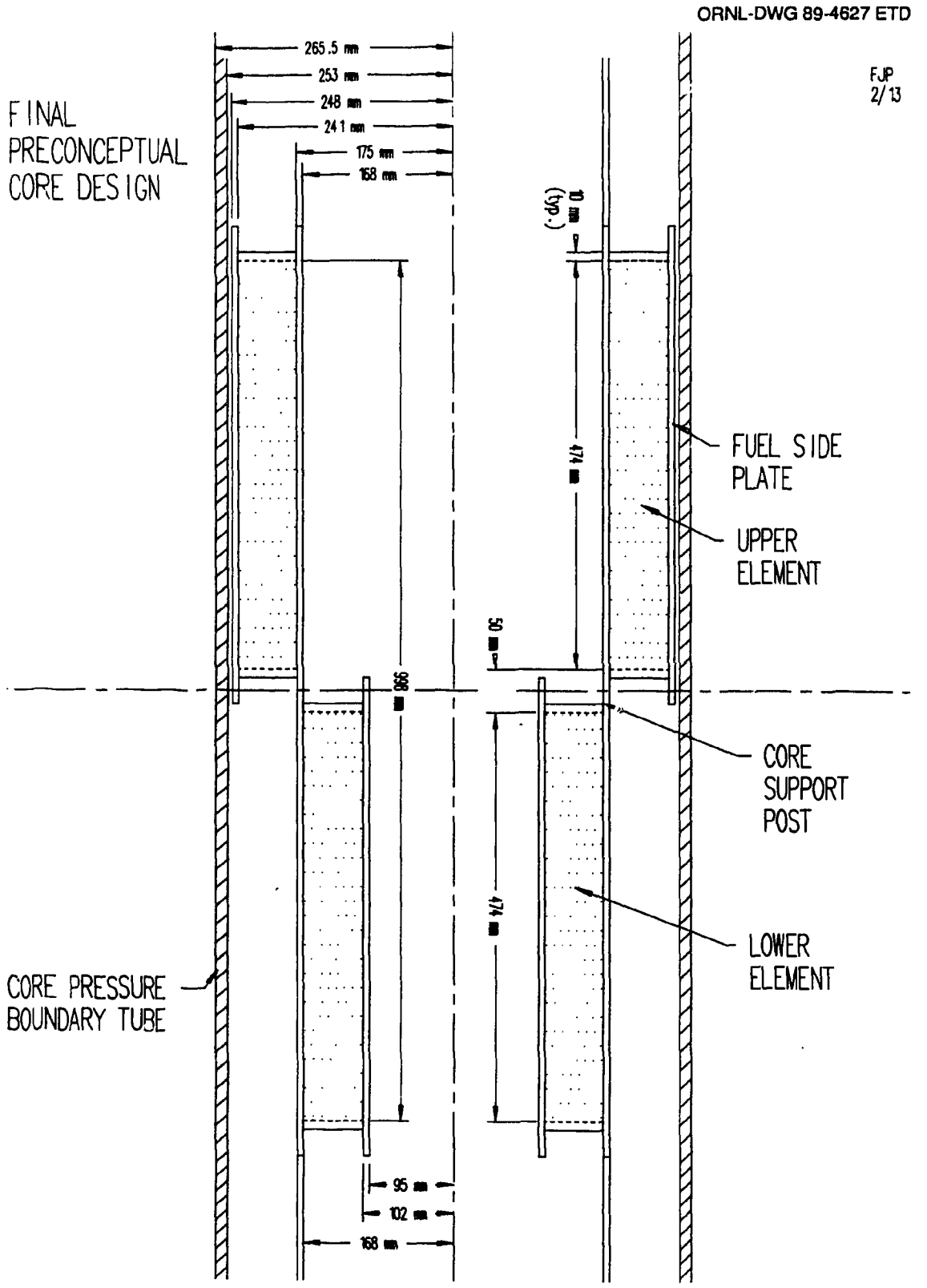

Fig. 3. PS-2 core.

The studies leading to the final preconceptual reference design were guided by a committee, known for historical reasons as the PS-2 Committee, composed of the ANS Project Managers whose resources would be employed in the work. The committee was supported, and most of the calculations were performed, by members of the project technical staff.

PS-2 Committee	ANS staff
R. M. Harrington	R. G. Alsmiller
D. L. Selby	J. A. Johnson (Secretary)
P. B. Thompson	H. Reutler, Interatom
C. D. West (Chairman)	J. M. Ryskamp, Idaho National Engineering Laboratory
	G. L. Copeland
	W. R. Gambill
	L. M. Jordan
	J. March-Leuba
	B. S. Maxon
	B. H. Montgomery
	L. C. Oakes
	F. J. Peretz
	R. T. Primm, III
	P. B. Thompson
	G. L. Yoder

This report describes the basis for the selection of the final preconceptual core design.

2. PREVIOUS REFERENCE CORES

The first reference core (Fig. 1) was based heavily on the highly successful High Flux Isotope Reactor (HFIR). The design comprised two concentric annular elements of involute, aluminum-clad plates of 93% enriched uranium silicide (U_3Si_2) fuel particles dispersed in a powder of aluminum. Developed by Argonne National Laboratory and Babcock and Wilcox, this silicide fuel form offers a higher thermal conductivity at a higher fuel density than the older oxide and aluminide fuels – a major advantage for a high-power, compact core. All the ANS reference cores are considered to be immersed in a large heavy-water reflector tank.

The first reference core had a fueled volume of 35 L and a nominal power level of 270 MW (7.7 MW/L average power density), although it was recognized that the formation of low-conductivity oxide on the heated surface of the aluminum cladding significantly limits the core life at such a higher power density. A research program to study the formation of oxide under ANS-like thermal-hydraulic conditions, but out-of-pile, was initiated. Another program was begun, at Idaho National Engineering Laboratory (INEL), to analyze existing measurements of oxide thickness on the Advanced Test Reactor (ATR) fuel plates.

One of the alternative core designs that was studied called for a 55-L core at 270 MW (4.9 MW/L): it was suggested that such a power density might be accommodated even in the presence of oxide and that the loss of neutron flux compared with the reference core would be only 10 to 20% (see Fig. 4). Another alternative,[1] proposed earlier by INEL, called for two identical elements composed of arcuate fuel plates, as used in the ATR, to be separated axially by a plenum region (Fig. 5). It was argued that in the plenum, warm water exiting from the first element could be mixed with or displaced by unheated water from a bypass flow, thus lowering the inlet temperature to the second element. The improved cooling of the second element would permit a higher power density to be accepted, even in the presence of oxide: indeed, the proposed split core had an even higher power density (355 MW in 40 L or 8.9 MW/L) than the original reference design core. However, later calculations[2] indicated that there would not be significant mixing or flow

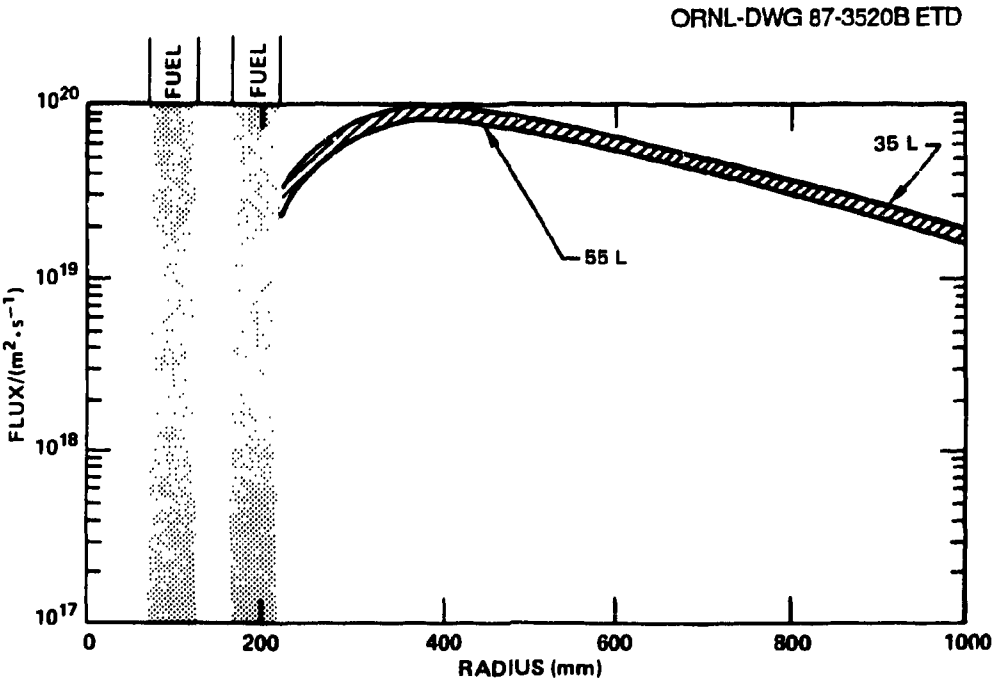

Fig. 4. Unperturbed thermal fluxes for different core volumes.

displacement in the plenum region unless some unspecified devices were introduced to promote such effects.

In February 1988, a workshop was organized to compare proposed designs for a new reference core.[3] The new design selected at the workshop (Fig. 2) adopted the best features from various proposals; it consisted of two axially separated elements of involute fuel plates. It was recognized that separating the elements would not, alone, provide the mixing or displacement of coolant necessary to enhance cooling of the second element; indeed, in that respect the HFIR-like concentric elements have an advantage because each element receives a separate flow of fresh coolant at its inlet. However, this and other disadvantages of the reference split-core design were outweighed by the neutronic benefits of the axial split: a larger volume of high thermal flux in the reflector, a lower gamma and fast neutron contamination of the thermal neutron peak, a higher worth for control elements in the central hole, and a lower reactivity of the individual elements.

The workshop also recognized the potential advantages of a proposal to use flow baffles (Fig. 6) to divert coolant from the first element

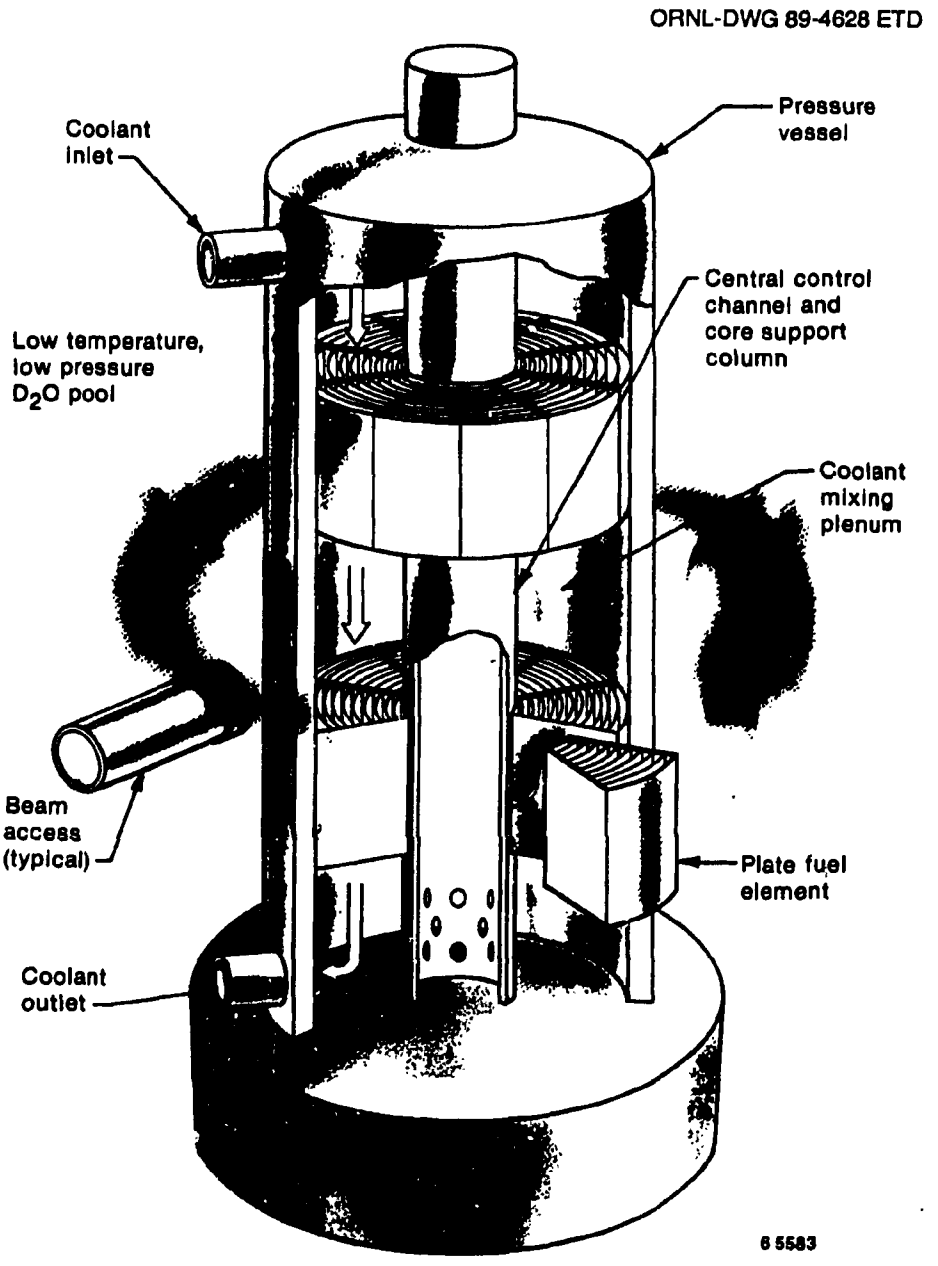

Fig. 5. Original INEL split-core proposal.

away from the second element, thus preserving the advantage of separate coolant streams for the two fuel assemblies. However, such a scheme could not be adopted as a reference core because the ANS Project Office has, as a design constraint, adopted a policy that achievement of the minimum design criteria should not rely on the success of any new or

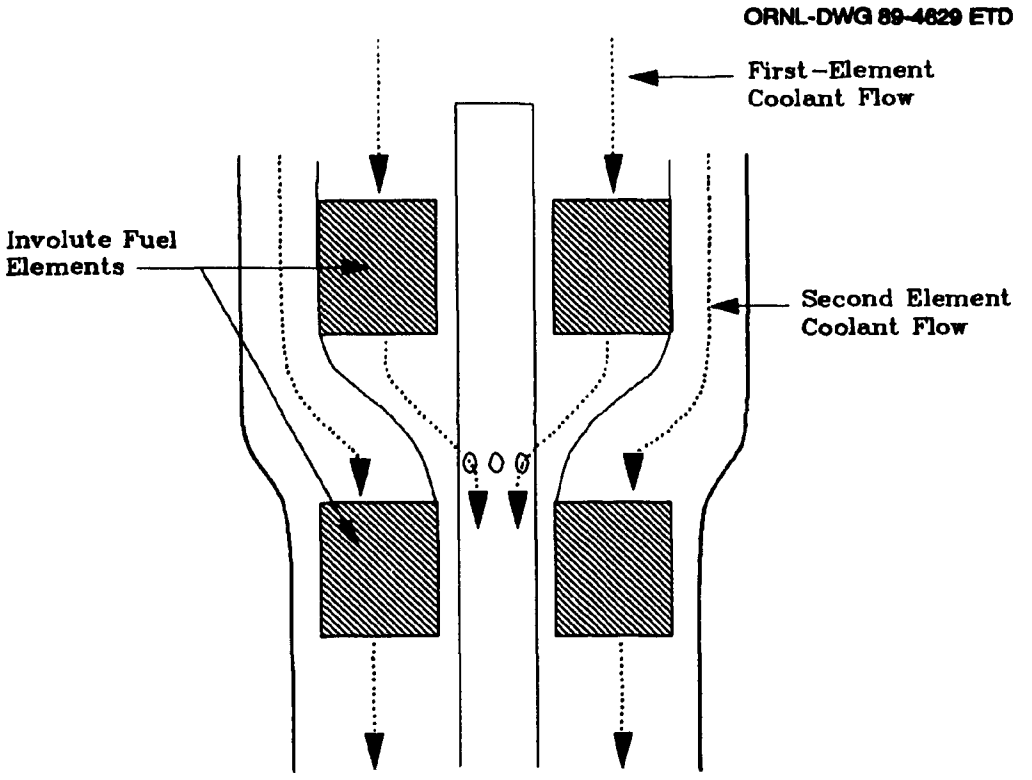

Fig. 6. Original proposal for diverting coolant to provide better cooling to second element.

unproven inventions. The flow divertor proposed at that time, involving substantial radial flow velocities and potential hydraulic problems (e.g., flow separation and flow maldistribution), had to be considered unproven. Similar arguments applied to the idea of mixing devices in the plenum, so no credit was taken for such mixing in calculating the performance of the new reference core.

Since the Core Comparison Workshop, results from the oxide formation research program have indicated that the oxide growth rate in out-of-pile experiments may increase significantly when the heat flux is raised.[4] In addition, the thermal-hydraulic safety margins (e.g., the margins to incipient boiling and critical heat flux) can be greatly increased by accepting the rather small decrease in the reflector peak thermal neutron flux that accompanies an increase in core volume (Fig. 7). Therefore, strong incentives emerged to consider larger cores with lower power density, a conclusion reached independently by one of

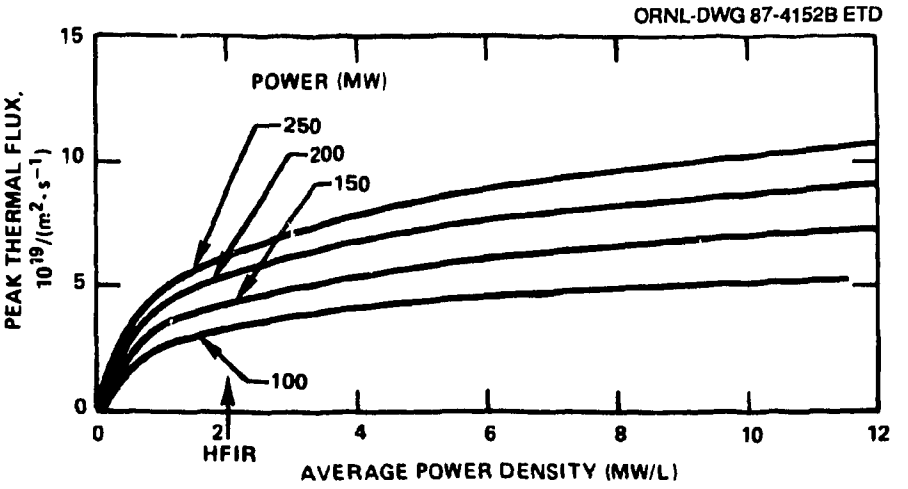

Fig. 7. Neutron flux/core volume or neutron flux/power density sensitivities.

1988's several ANS review committees.[5] To some extent the diminution of neutron flux resulting from a larger core volume can be offset by increasing the power level – if the power increase is proportionately smaller than the volume increase, the average power density is decreased. It also seems likely that with a greater volume available for fuel distribution, an optimally graded large core would yield a lower ratio of peak-to-average power density than a small one, thus reducing the peak heat flux (which largely determines the thermal-hydraulic margins).

In addition, a geometry was identified that provides separate cooling streams to the two elements of an axially split core without requiring radial diversion of the flow (see Fig. 8 and Appendix A), thus avoiding the possible flow separation problems of the original divertor concept.

Accordingly, a good deal of effort was devoted to analyzing larger cores with the new geometry to understand and optimize the core design. A three-element version (Fig. 9) was also extensively analyzed to see if there were performance advantages that might warrant the added cost and complication. The greater length of the flow diversion path in the three-element design reduces the radial acceleration of the coolant, thus avoiding the possibility of flow separation.

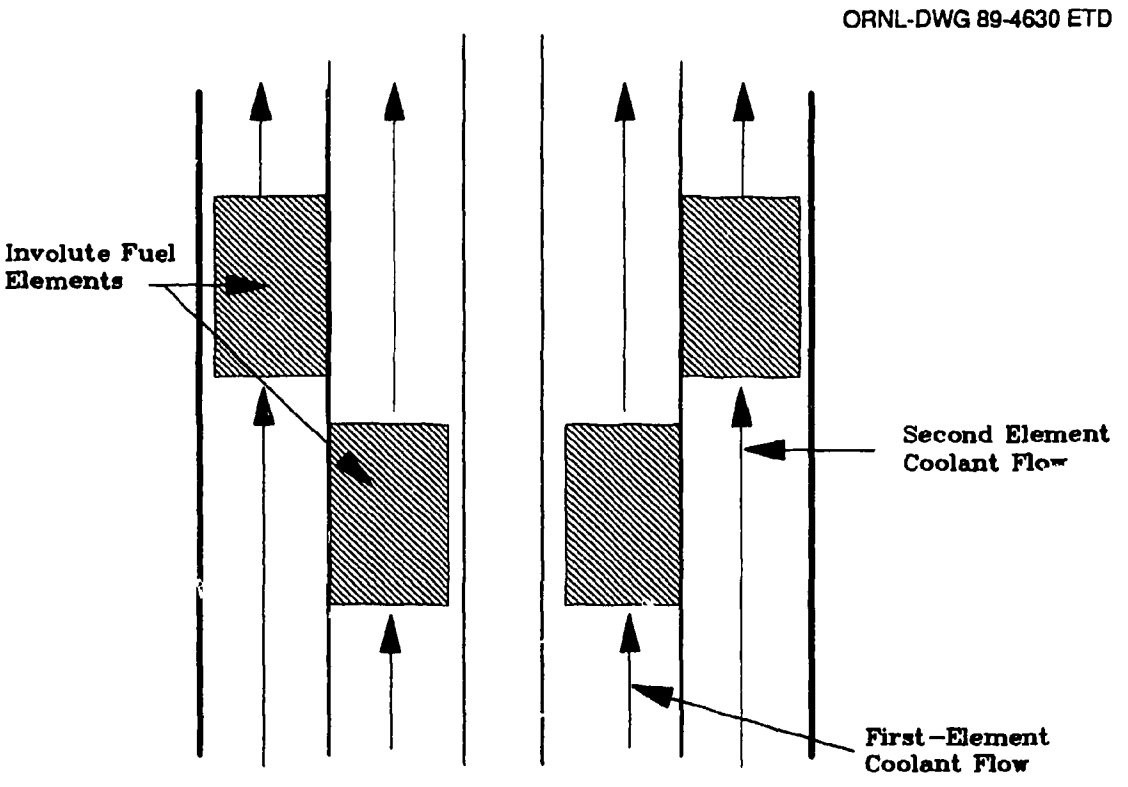

Fig. 8. Modified proposal for providing separate coolant flows to each element.

The results of these analyses, the conclusions drawn from them, and the design eventually chosen as the final preconceptual core design are described in this report.

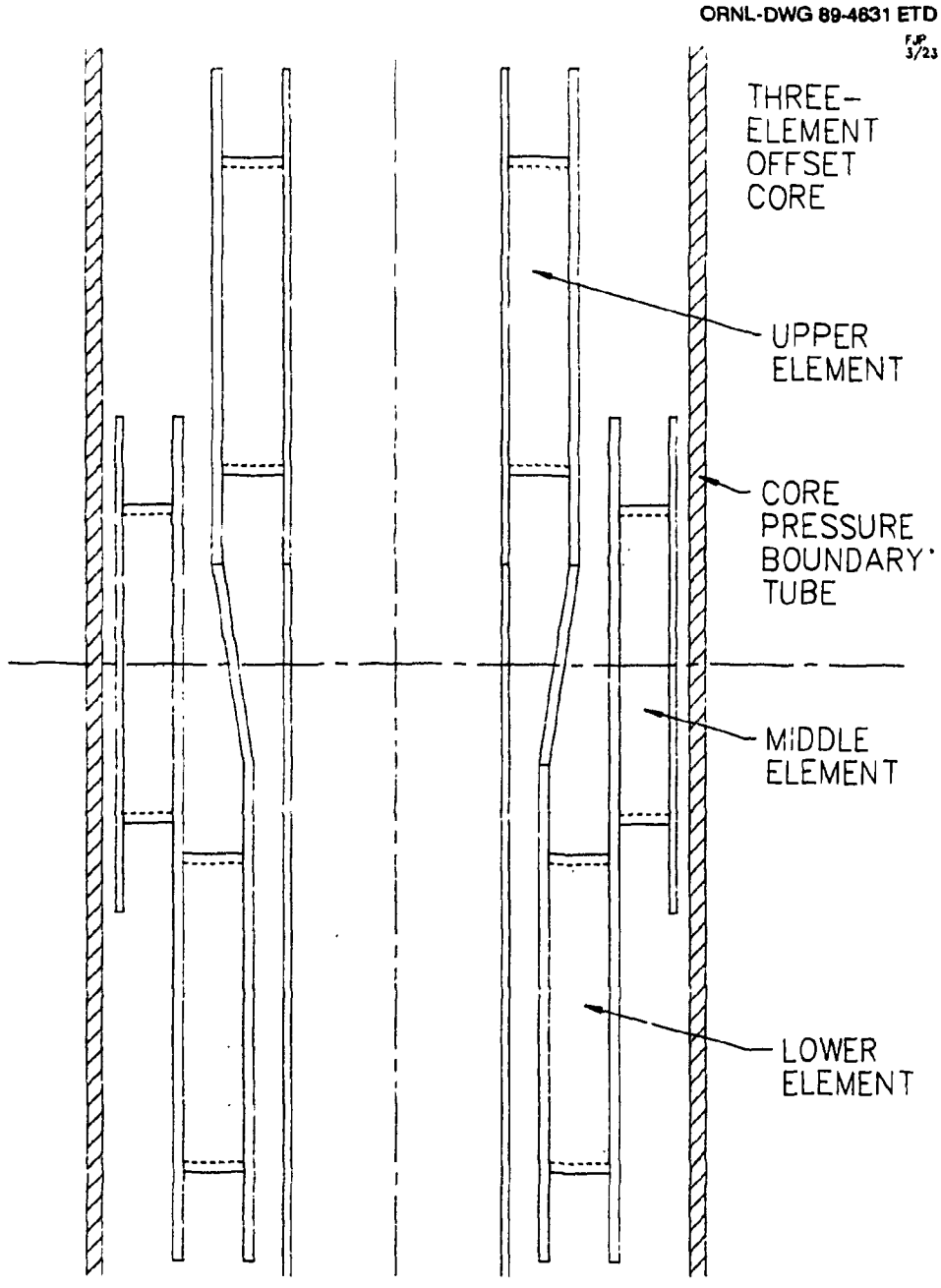

Fig. 9. Three-element offset core.

3. CONSTRAINTS ON CORE PERFORMANCE

3.1 SAFETY LIMITATIONS

The Department of Energy (DOE) regulations and policies provide both deterministic and probabilistic requirements for the design of reactors. DOE Order 5480.6 mandates compliance with the Nuclear Regulatory Commission (NRC) regulation prescribed in 10 *CFR* 50, Appendix A, "General Design Criteria for Nuclear Power Plants." The General Design Criteria (GDC) are a collection of 64 requirements for the design features and capabilities of nuclear plant components and systems. The most germane of these to the present discussion is GDC 10: "Reactor Design. The reactor core and associated coolant, control, and protection systems shall be designed with appropriate margin to assure that specified acceptable fuel design limits are not exceeded during any condition of normal operation, including the effects of anticipated operational occurrences." It was, of course, impossible to perform the full range of analyses implied by GDC 10 for every core design investigated for the PS-2 core design selection task. Instead, the maximum safe operating thermal power for each core was calculated based on the incipient boiling limit (IBL); uncertainties were conservatively multiplied in the calculations. This conservative combination of uncertainties guarantees a margin of 10 to 15% between 100% power and the power level at which boiling might begin at the hot spot.

The acceptable fuel design limit is actually well above the IBL because a significant amount of boiling can occur in a coolant channel before the critical heat flux is exceeded. The reactor protection system can, therefore, easily maintain the fuel within acceptable design limits during anticipated operational occurrences by causing the control rods to be inserted to shut down the reactor before 110 to 115% power is exceeded or before a similar variation of the significant primary coolant system variables: coolant inlet pressure, temperature, and flow. A RELAP5 computer code model of the ANS core and coolant systems is being developed to verify the adequacy of fuel cooling for a full range of anticipated and design basis operational occurrences.

Following NRC and DOE safety objectives, the safety criteria for the ANS reactor are stated in probabilistic terms.[2] The full assessment of the influence of uncertainties in core dimensions and operating conditions therefore requires a proper statistical combination of the various effects. The data required for such an analysis will not be available until conceptual design work is well advanced, and therefore an alternative approach (believed to be conservative) was adopted during preconceptual design. In this approach, the major known uncertainties (in coolant gap, water temperature, inlet pressure, and local fuel loading) are combined in a multiplicative way; that is, all the major uncertainties are assumed to take their worst possible value simultaneously. Simple pencil-and-paper calculations and comparison with results from the Monte Carlo statistical code used by INEL to analyze ATR operating conditions indicate that the multiplicative approach may be conservative by 10 to 15% in setting the IBL for the ANS reactor.

Two other safety limitations were considered in the PS-2 search for a new core design: total core thermal power and core power density. These limitations were regarded in a qualitative sense. The desire to reduce the core power density was one of the motivations for embarking upon the PS-2 process. Lower core power density improves core inherent safety performance in beyond-design-basis events, for example, those involving natural circulation. Total core power level is proportional to the fission product inventory that could become a source term in the event of a severe accident. When other factors were similar, the core design alternative having a lower thermal power was favored in the selection process.

3.2 INCIPIENT BOILING LIMIT

For a given coolant velocity, inlet pressure, inlet temperature, and coolant channel width, the maximum power density that can be accommodated by the fuel element without encountering incipient boiling near the outlet depends upon the heated length. The results of some calculations by W. R. Gambill are given in Table 1; his results are plotted in Fig. 10, along with a least-squares fit, straight-line correlation.

Table 1. IBLs (multiplicative combination of major uncertainties)

Fueled volume (L)	Number of elements	Geometry	Heated length (mm)	Incipient boiling power[a] (MW)	Incipient boiling power density[b] (MW/L)	Figure No.[c]
41	3	Offset	208	316	7.707	B.3
41	2	Offset	310	280	6.829	B.7
41	2	In-line	431	229	5.585	B.1
50	3	Offset	254	365	7.300	B.4
50	2	Offset	379	310	6.200	B.8
50	2	Offset	455	270	5.400	B.15
60	3	Offset	304	413	6.883	B.12
60	2	Offset	455	324	5.400	B.9

[a]Calculations by W. R. Gambill. Inlet pressure = 4.14 MPa, inlet temperature = 49°C, coolant velocity in core = 27.4 m/s, and nominal channel gap = 1.27 mm. Power is defined as the heat convected from the fuel plates into the coolant: fission power would be ~5% higher.

[b]Incipient boiling power divided by fueled volume.

[c]In Appendix B.

Gambill's calculational methods, and the uncertainty factors he used, are described in Appendix C. The correlation was calculated with the linear regression routine of Universal Technical Systems' TK SOLVER program.

Similar calculations by N. C. J. Chen, using a partially modified version of a very early HFIR thermal-hydraulic computer code,[6] gave results that showed the same trends, but generally a 4 to 10% lower IBL. For the purpose of the PS-2 Committee, which was to compare different designs, the figures from the simpler manual calculations were used, while efforts continued to reconcile the two sets of calculations.

The straight-line relationship can be used to define the maximum permissible power density (from an incipient boiling viewpoint) for cores with a heated length, from inlet to outlet, in the range covered

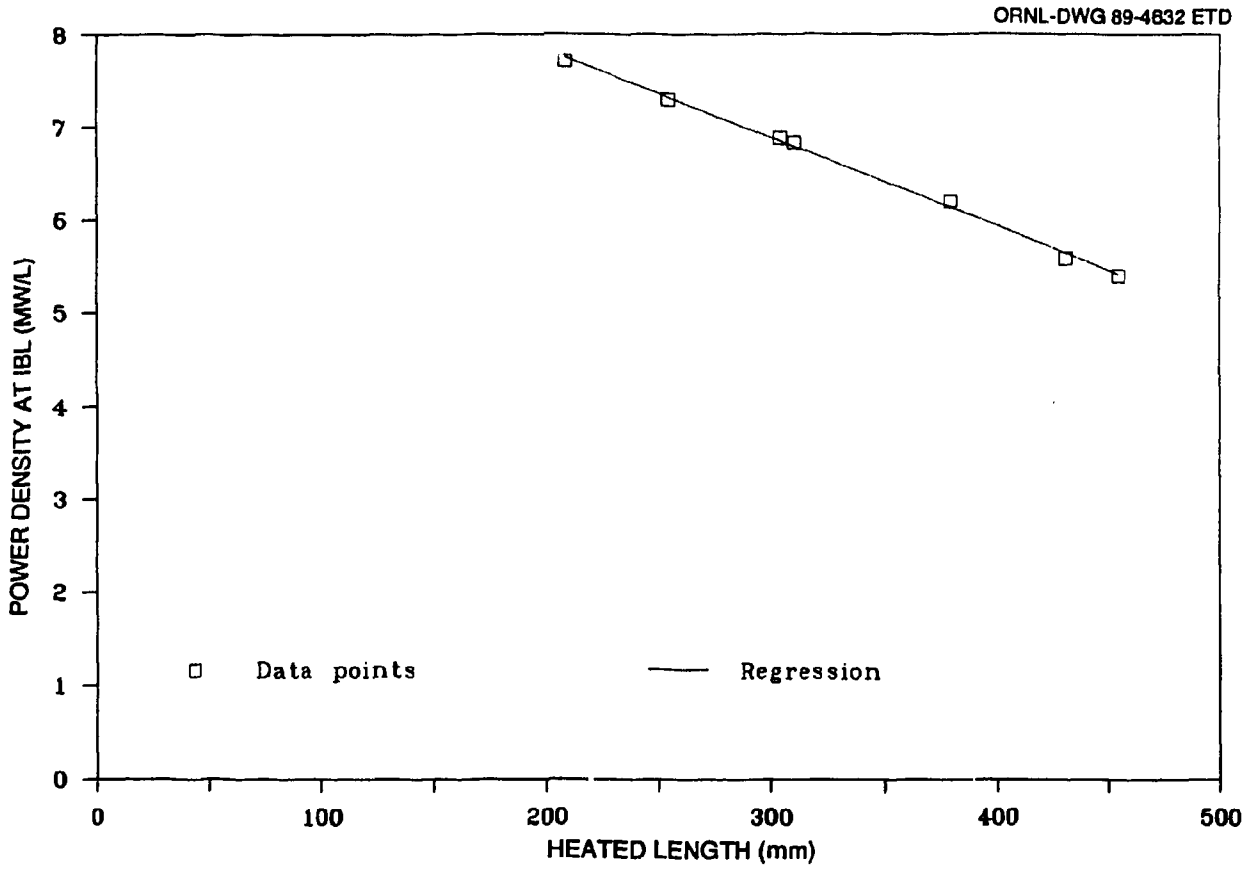

Fig. 10. IBL limit vs heated length.

by the data, and for small extrapolations outside that range. The equation of the line follows:

Power density at IBL = 9.72 − 0.00947 × heated length

or

$$\rho(\mathrm{IBL}) = 9.72 - 0.00947 \times H_L \ . \qquad (1)$$

If the heated length is expressed in millimetres, the power density will be in megawatts per litre. The correlation coefficient of the least-squares fit is 0.9988.

Equation (1) can be used to estimate the power density advantage to be gained by offsetting the two elements of a split core. In a typical case, the fueled region of each element might be 350 mm long. For in-line elements, the total heated length would be 700 mm, and the IBL would be 3.1 MW/L. For offset elements with separate coolant streams,

the heated length would be only 350 mm, and the IBL would be 6.4 MW/L, more than double the value for an in-line geometry without coolant mixing.

Note that incipient boiling puts a limit on the heat that can be transferred to the coolant from the fuel plates: the fission power in the core, which includes the energy carried away from the fuel element by gamma and other penetrating radiation, can be ~5% higher than the coolant power.

The straight-line relationship will break down when the heated length is so great that the outlet pressure begins to approach the saturation pressure. However, the linearity could be extended by increasing the inlet pressure.

4. NEUTRONIC COMPARISON OF TWO- AND THREE-ELEMENT CORES

To compare a large number of possible core geometries and dimensions without incurring excessive computing costs and schedule delays, the PS-2 Committee decided that for screening purposes, comparisons would be made on the basis of the beginning-of-cycle (BOC) parameters in cores with an ungraded fuel loading. Performance of a selected design would then be extrapolated to end-of-cycle (EOC), graded core conditions by comparison with results from fuel grading and burnup calculations on a typical design. Eventually, detailed burnup calculations would be carried out on the new reference core.

Early neutronics calculations were carried out separately by ORNL and INEL staff using different techniques, and the results were compared. Close agreement of the results (e.g., Table 2) gives some assurance that models, codes, and cross-section sets were fit for the purposes of the PS-2 Committee.

The key parameter for comparing core neutronic performance is the rendement (i.e., the peak thermal flux divided by the neutron production rate in the core). The three calculations in Table 2 all fall within ~1% of the mean value.

Table 2. 41-L In-line core (Appendix B, Fig. B.2)

Source of calculation	Code used	Number of energy groups	Cross-section set	Spatial weighting[a]	Results	
					K_{eff}	Rendement
R. T. Primm, ORNL	Venture	7	ANSL[b]	No	1.254	3.42
J. Ryskamp, INEL	PDQ	4	ANSL[b,c]	Full	1.251	3.39
F. C. Difilippo, ORNL	Venture	4	Older	Partial set	1.28	3.32

[a]Of cross sections within the core region.

[b]Ref. 2.

[c]For some key elements.

Table 3 shows results from several calculations by R. T. Primm. All of the cores had consistent, comparable geometries. Each was made up from 1.27-mm-thick fuel plates separated by 1.27-mm-wide heavy-water coolant channels. The central hole diameter was always 103 mm, and the radial thickness of the fueled zones was 60 mm (except for the outermost element of three-element designs, which was only 50 mm thick).

The BOC reactivity needed to provide the minimum core life specified for the ANS reactor (14 d) depends to some extent on the core geometry because the loss of reactivity for a given fuel burnup is not the same for all possible core designs. However, as an approximation for purposes of comparison only, it was decided that a nominal reactivity at BOC of 1.25 would be chosen: prior experience showed this to be a fairly typical value for the BOC reactivity of an unpoisoned 14-d core at 300 to 350 MW.

Appendix D summarizes many of the much larger set of calculations performed by Primm. Varying the core dimensions changes both the reactivity and the rendement. Therefore, direct comparisons of the rendement figures in Table 3 would be inappropriate because if the reactivity is high, fuel could be removed from the core, which would increase the rendement. The two calculations for different fuel loadings in otherwise identical 50-L two-element cores (Table 4) can be used to correct, approximately, for reactivity effects on rendement. The rendement rises from 3.082 to 3.139, an increase of 1.85%, when the reactivity falls from 1.273 to 1.262, that is, by 0.864%. Thus, it was assumed that in the cores of Table 3, a given percentage change in reactivity would lead to a 1.85/0.864 = 2.1 times greater change, of the opposite sign, in the rendement.

Suppose that a particular core in Table 3 has a beginning-of-life reactivity of K_{eff} and a rendement of E. If the fuel loading were adjusted to make $K_{eff} = 1.25$ (the number chosen as a basis for comparison), the rendement would change to E′, where

$$\frac{E - E'}{E} \approx -2.1 \times \frac{K_{eff} - 1.25}{K_{eff}} ,$$

Table 3. Neutronic data used to set up correlations of neutronic performance

Fueled volume (L)	Number of elements	Plenum gap (mm)	Fueled length per element (mm)	Fuel loading (kg)	Effective[a] height (mm)	Reactivity	Rendement (m^{-2})	Figure No.[b]
41	2	50	310	22	720	1.252	3.287	B.7
41	2	130	310	22	880	1.247	3.195	B.2
50	2	50	379	22	858	1.273	3.082	B.8
60	2	50	455	22	1010	1.292	2.887	B.9
60	2	130	455	22	1170	1.283	2.827	B.14
50	3		253.3	22	850	1.273	2.757	
60	3	50	304	22	1062	1.281	2.598	B.12
70	3	50	354	22	1212	1.291	2.465	B.13
50	2	50	379	19.5	858	1.262	3.139	B.8

[a]Number of elements × (fueled length + plenum gap).

[b]Appendix B.

Table 4. 50-L Cores—reactivity and rendement

Fuel loading (kg)	Reactivity K_{eff}	Rendement (m^{-2})
22	1.273	3.082
19.5	1.262	3.139

or

$$E' \approx E\left(3.1 - \frac{2.625}{K_{eff}}\right). \tag{2}$$

The correction to the rendement is generally small, as may be seen by comparing Tables 3 and 5, so that extreme accuracy in making the adjustment is unnecessary, which is fortunate, because in reality the relationships among fuel loading and depletion, reactivity, core life,

Table 5. Corrected rendements for the cores of Table 3

Fueled volume (L)	Number of elements	Plenum gap (mm)	Fueled length per element (mm)	Fuel loading (kg)	Effective[a] height (mm)	Corrected rendement[b] (m^{-2})	Figure No.[c]
41	2	50	310	22	720	3.30	B.7
41	2	130	310	22	880	3.18	B.2
50	2	50	379	22	858	3.20	B.8
60	2	50	455	22	1010	3.08	B.9
60	2	130	455	22	1170	2.98	B.14
50	3		253.3	22	850	2.86	
60	3	50	304	22	1062	2.73	B.12
70	3	50	354	22	1212	2.63	B.13
50	2	50	379	19.5	858	3.20	B.8

[a]Number of elements × (fueled length + plenum gap).

[b]Corrected to a BOC reactivity of 1.25.

[c]Appendix B.

and rendement are rather nonlinear and may equal or exceed the correction calculated from Eq. (2).

Plotting the height and rendement figures from Table 5 reveals a rather linear relationship (see Fig. 11). The TK SOLVER linear regression routine gives the following relationships:

Two-element corrected rendement

$$\approx 3.81 - 0.00072 \times \text{effective height}$$
$$= 3.81 - 0.00144 \times (\text{fueled length per element} + \text{axial gap}) \quad (3)$$

Three-element corrected rendement

$$\approx 3.40 - 0.00063 \times \text{effective height}$$
$$= 3.40 - 0.00189 \times (\text{fueled length per element} + \text{axial gap}) \quad (4)$$

Because the correlation for three-element cores was initially derived from only three data points, for one of which there was some uncertainty about the value used for the effective length (see Tables 3 and 5), the correlation was later confirmed with additional data points (see Appendix E).

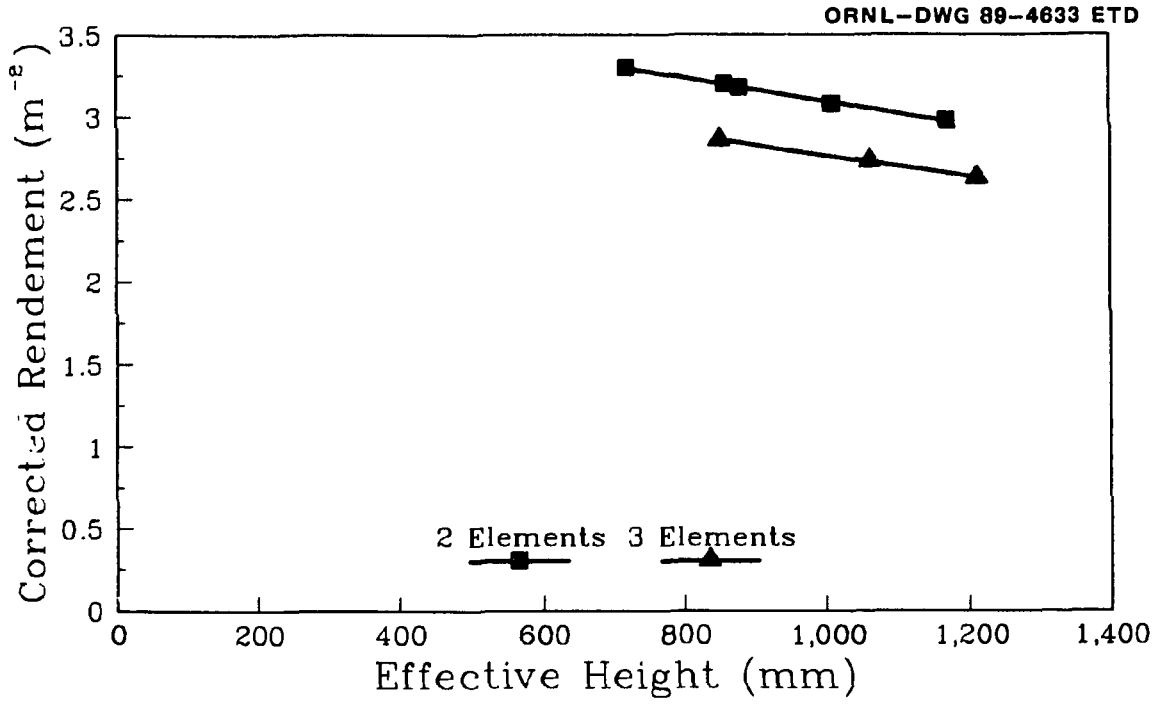

Fig. 11. Rendement vs effective height.

4.1 POWER, POWER DENSITY, AND FLUX FOR TWO- AND THREE-ELEMENT CORES

For a given element height, Eq. (1) calculates the power density that can be accommodated (under the stated assumptions) without exceeding the IBL.

For the geometry considered, the core volume is proportional to the element length. From inspection of the figures in Appendix B, the relationship between fueled length [heated length (H_L)] and volume of two-element cores is expressed as

$$\text{Volume (cm}^3\text{)} = \pi \times \text{fueled length} \times (24^2 - 18^2 + 17^2 - 11^2).$$

If the dimensions are expressed in millimetres, then

$$\text{Volume (L)} = 0.1319 \times \text{fueled length per element}$$

or

$$V2 = 0.1319 \times H_L \ . \tag{5}$$

Similarly, for the three-element cores,

$$V3 = 0.1976 \times H_L \ . \tag{6}$$

Note that these relationships are valid only for the radial fuel thicknesses shown in the figures of the Table 4 cores.

The product of permissible power density (Eq. 1) with core volume [Eq. (5) or (6)] gives the permissible power level. The product of power level and rendement [Eq. (3) or (4)] is proportional to the achievable flux; the relevant equations are listed in Table 6, and when plotted they give some very interesting curves.

As the length of each element is increased, the core volume increases and so, at first, does the permissible power. However, longer elements have lower IBLs; for cores longer than ~500 mm, the power density is falling more rapidly than the volume is increasing, so the allowable power decreases (Fig. 12). Of course, for any given element length, the volume (and, therefore, permissible power) of a three-element core is ~50% greater than that of the two-element one. No

Table 6. Volume, power density, power, rendement, and relative flux for two- and three-element cores with fueled length, H_L (mm) and 50-mm plenum gap

Parameter	Two-element core	Three-element core
Volume, L	0.1319 H_L[a]	0.1976 H_L
Power density, MW/L	9.72 − 0.00947 H_L	9.72 − 0.00947 H_L
Power,[b] MW	0.1319 H_L × (9.72 − 0.00947 H_L)	0.1976 H_L × (9.72 − 0.00947 H_L)
BOC rendement,[c] m^{-2}	3.81 − 0.00072 × 2 × (H_L + 50)	3.40 − 0.00063 × 3 × (H_L + 50)
Relative flux,[d] $mW \cdot m^{-2}$	0.1319 H_L × (9.2 − 0.00947 H_L) × (3.738 − 0.00144 H_L)	0.1976 H_L × (9.72 − 0.00947 H_L) × (3.306 − 0.00189 H_L)

[a]Fueled (heated) length in each element.

[b]Power = volume × power density.

[c]Corrected to K_{eff} = 1.25 (~14-d core life).

[d]Relative flux = power × rendement.

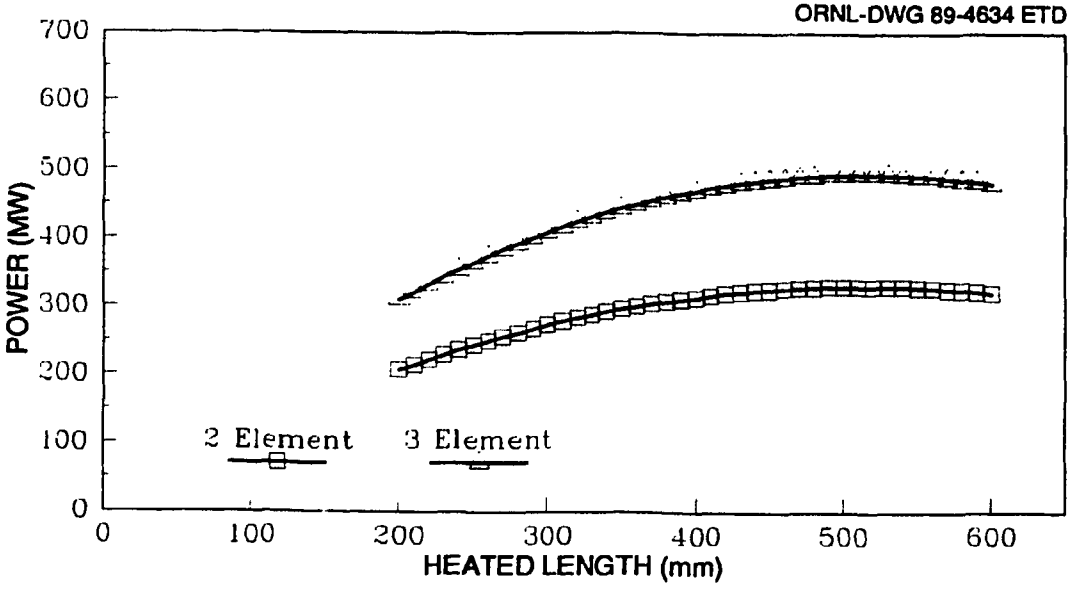

Fig. 12. Power vs heated length for two- and three-element cores.

points are plotted for two-element core volumes greater than ~80 L, because such cores would have heated lengths outside the range of data used to generate Eq. (1).

A somewhat similar relationship exists between core volume and power (Fig. 13), because the volume is linearly proportional to the element length, although with a different constant of proportionality for two- and three-element cores. Permissible power density decreases with increasing volume (Fig. 14) because cores with larger volume have greater heated lengths.

To compare the fluxes produced by two- and three-element cores, not only the power but also the rendement must be known. Figure 15 shows that the rendement steadily decreases as the core volume (and, therefore, height) is increased. The peak thermal flux is proportional to the product of rendement and power as shown in Fig. 16.

On the average, a fission releases ~2.5 neutrons and 32 pJ (200 MeV) of energy. Therefore, the neutron production rate per megawatt of reactor fission power is approximately $(10^6/32 \times 10^{-12}) \times 2.5 \approx 7.8 \times 10^{16}$/MW. To meet the design criterion for a peak thermal flux in the range 5 to 10 $\times 10^{19}$ $m^{-2} \cdot s^{-1}$, the product of power and rendement in the ANS core must exceed $(5 \times 10^{19})/(7.8 \times 10^{16}) \approx 650$ $MW \cdot m^{-2}$. In the

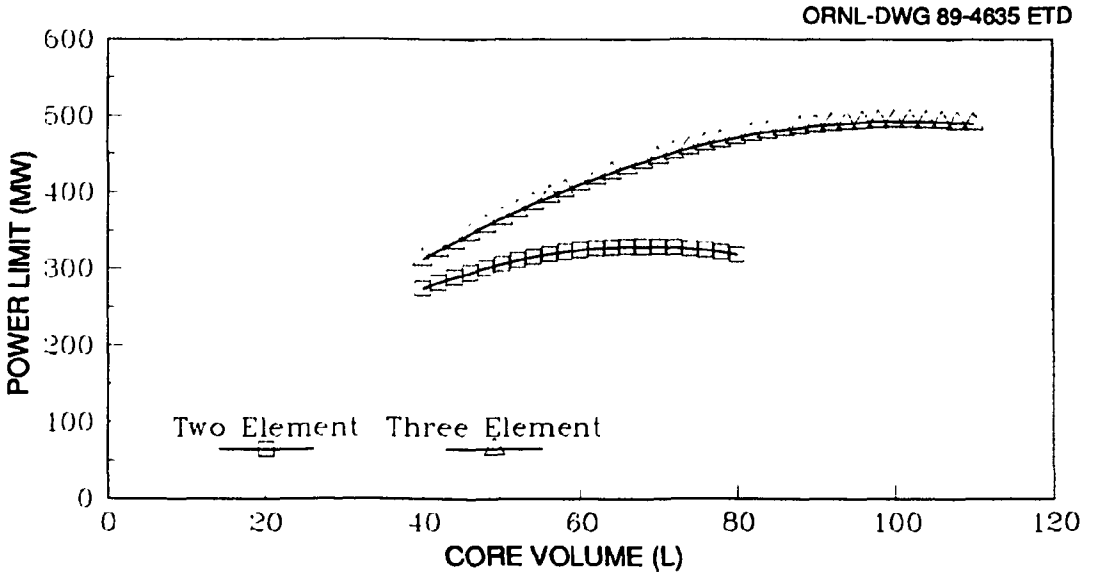

Fig. 13. Power vs core volume for two- and three-element cores.

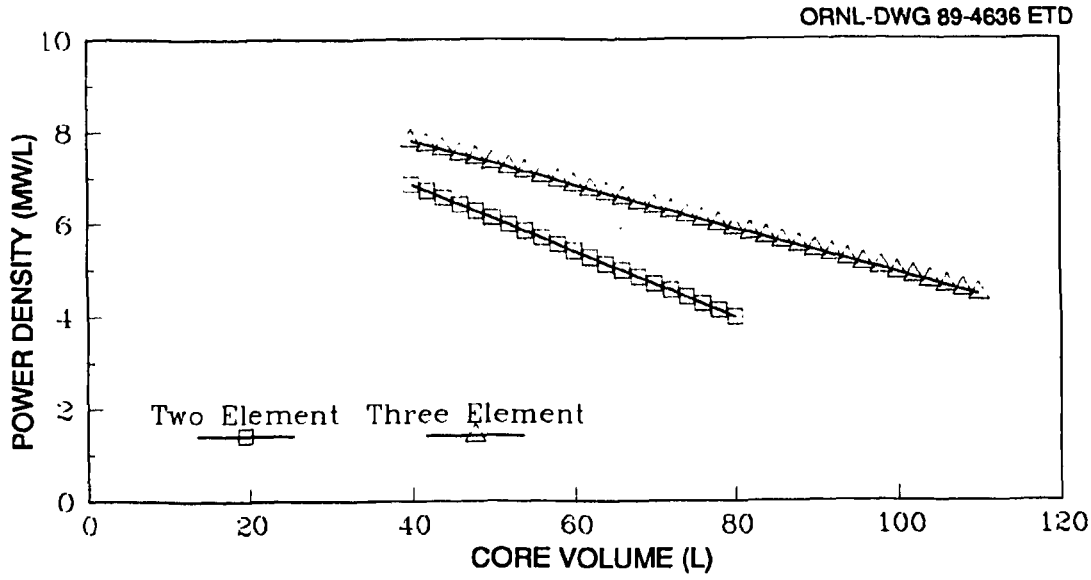

Fig. 14. Power density vs core volume for two- and three-element cores.

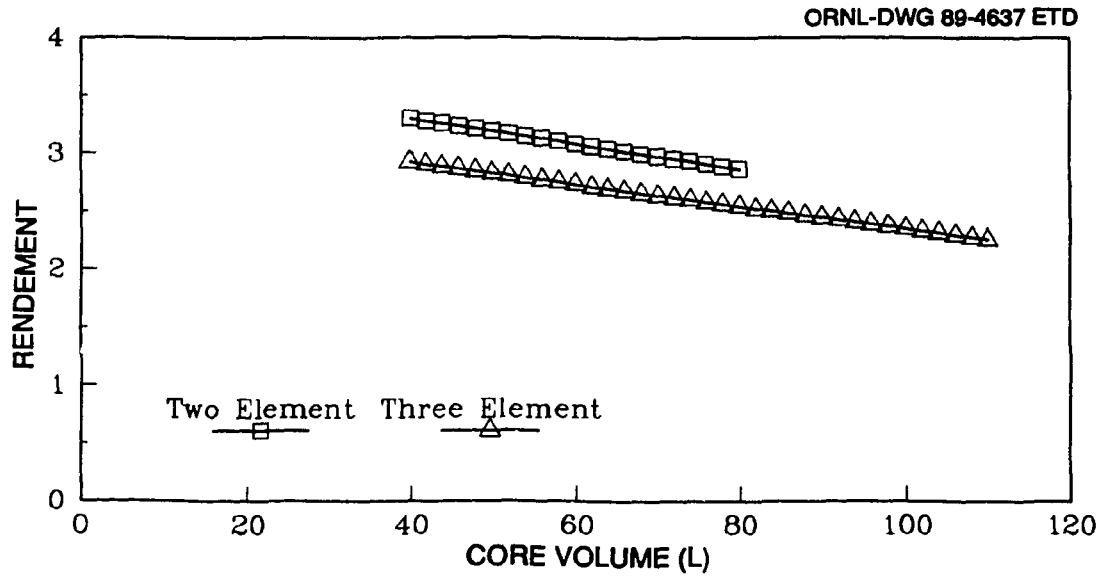

Fig. 15. Rendement vs core volume for two- and three-element cores.

range of power and volume covered by Fig. 16, all the cores easily exceed the minimum criterion.

Figure 16 shows that for core volumes greater than ~40 L, the three-element cores can give a higher flux, but they have a lower rendement (Fig. 15). Therefore, the higher flux is bought at the cost of higher power – actually, at a much higher power (Fig. 17).

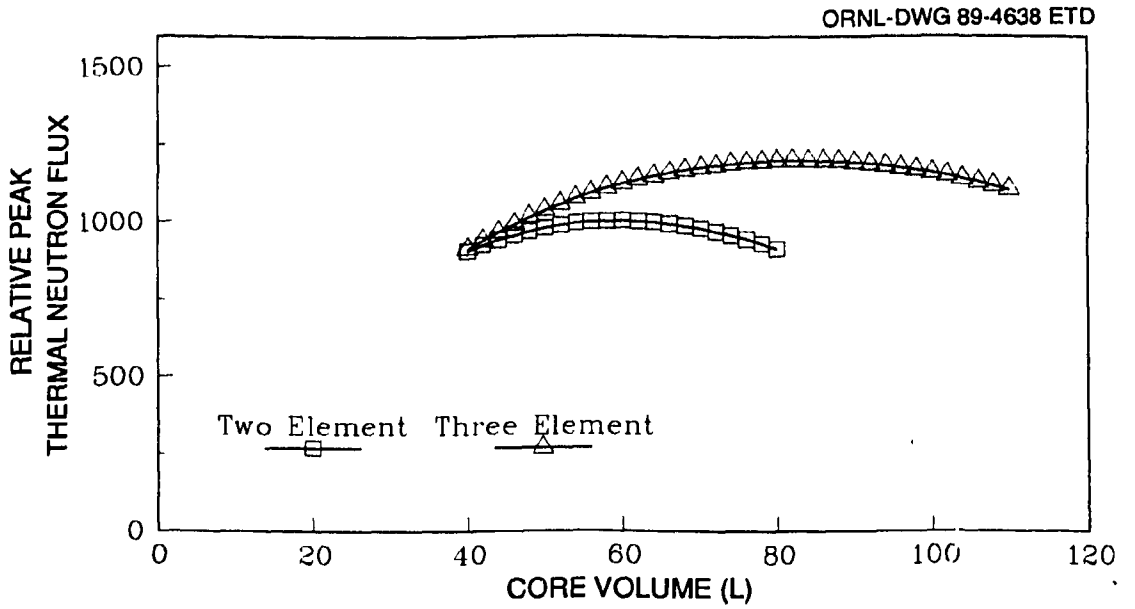

Fig. 16. Relative peak thermal neutron flux vs core volume for two- and three-element cores.

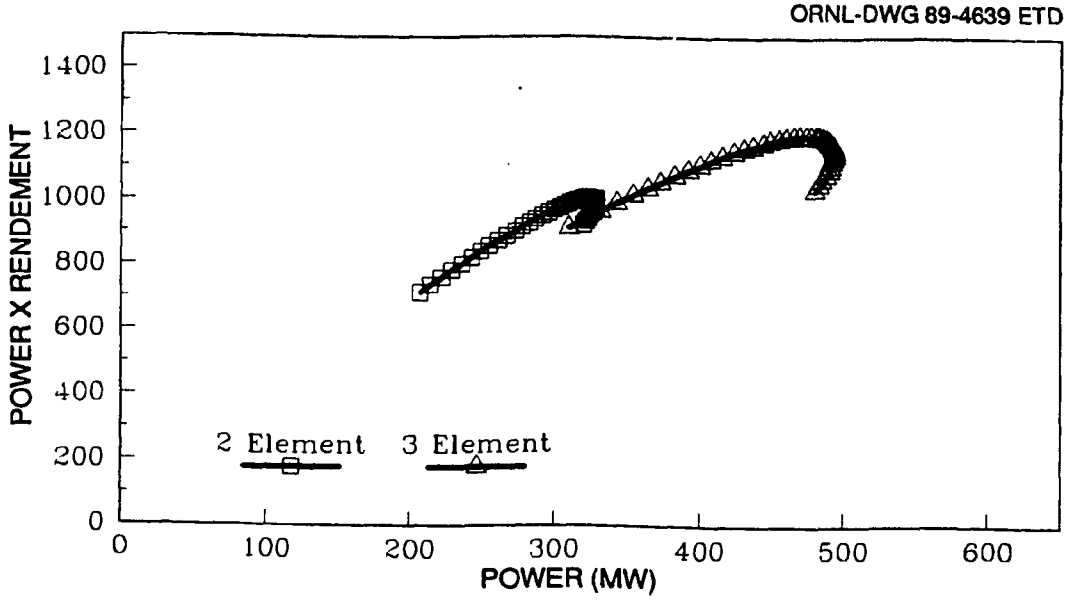

Fig. 17. Power vs power × rendement for two- and three-element cores.

The highest flux two-element core has a volume of ~60 L (Fig. 16) and a relative flux of just over 1000 at its maximum power of 324 MW (Fig. 17). The three-element core matches that flux in a volume of ~46 L, but requires 25 MW more power to do so. Moreover, to gain even a

10% advantage over the two-element core – that is, to give a relative flux of 1100 – the three-element core must have a volume of only 57 L but a power of 400 MW.

The increased power level associated with three-element cores would lead to larger fission product inventories, which will increase the source term to be accommodated by the containment and filtration systems. An increase from two elements to three would also add $1.5M to $2M to the annual fuel fabrication costs of the ANS.

An increase in power from 325 to 400 MW would increase construction costs for the facility by approximately $40M.

Furthermore, although meeting the same IBLs, the three-element core power density of 400 MW/57 L = 7 MW/L is 30% higher than in the optimum two-element core (324 MW/60 L = 5.4 MW/L): the higher power density might lead to faster oxide growth and lower critical heat flux limits.

The PS-2 Committee decided that these disadvantages of the three-element configuration definitely outweighed a 10% flux increase, and the two-element configuration was selected for further study.

Comparing the flux maxima of the curves in Fig. 16, the two-element design gives only 15% less flux than the three-element one, and it does so with 32% less power and 5% lower power density. The performance differences between the two geometries are surprisingly small (see Table 7).

Table 7. Summary comparison of selected two- and three-element designs

	Two-element[a]	Three-element[b]	Three-element[c]	Three-element[a]
Power × rendement	1001	1001	1102	1197
Power, MW	324	351	400	477
Core volume, L	59.4	46.9	57.3	83.0
Power density, MW/L	5.5	6.4	7.0	5.7

[a]Maximum achievable flux design – see Fig. 17.

[b]Selected to have the same flux as the optimum two-element core.

[c]Selected as the lowest power three-element design that exceeds the flux capability of a two-element core by 10% or more.

4.2 SELECTION OF ELEMENT THICKNESS

The cores just compared had the same radial thickness of the fuel region: 60 mm, except for the outer element of the three-element cores that was only 50 mm thick. The effect of increasing or decreasing the radial fuel thickness was also investigated.

Table 8 shows a significant advantage to making the radial thickness of the fuel region as large as possible. Over the range considered, the rendement falls only 3%, while the IBL rises by 25%: the net result would be an increase in flux, which is proportional to the product of power and rendement, of ~21%.

Table 8. Rendement, K_{eff}, and corrected rendement for 50-L two-element cores[a]

Radial fuel thickness (mm)	Heated length (mm)	Allowable power density[b] (MW/L)	K_{eff}	Rendement (m^{-2})	Corrected rendement[c] (m^{-2})	Figure No.[d]
52.3	455	5.41	1.286	3.045	3.22	B.15
60.0	379	6.13	1.273	3.082	3.20	B.8
69.5	310	6.78	1.259	3.071	3.12	B.18

[a]All cores have 50-mm plenum gap and 22 kg of ^{235}U.

[b]Calculated from Eq. (1).

[c]Corrected to K_{eff} = 1.25 by means of Eq. (2).

[d]In Appendix B.

One limit on the thickness of the fueled region is set by the stability of the thin fuel plates. As the fuel region is widened, the involute fuel plates must have a larger span and are therefore less stiff and less resistant to distortion or instability under the influence of the hydraulic forces exerted by the high-velocity coolant flow.

Calculations of the critical coolant velocity for fuel plate instability and collapse are difficult, and there are few experimental data for curved plates. Development of the analysis continues, and hydraulic

stability of the fuel elements will eventually be verified by full-scale experiments and demonstration. At the time of the PS-2 Committee's studies, calculations of critical velocity were based on an extension of the Miller correlation.[7] Figure 18 shows some results from those calculations. Inspection of the figure shows that a critical velocity of >41 m/s, representing a 50% margin over the proposed 27.4 m/s coolant velocity, can be achieved if the radial span of the fuel region is no greater than ~66 mm, but much work remains to be done in this area.

Further calculations were therefore carried out with a radial fuel thickness of 66 mm. Note, however, that the plates of the inner element are more strongly curved, and therefore stiffer, than the outer element plates. During conceptual design, further optimization studies will consider cores with inner and outer elements of different thickness to maximize the critical velocity of the overall core.

To make comparisons over a wide range of core volumes and heights, the incipient boiling power density correlation [Eq. (1)] was applied to elements of up to 600-mm heated length. Such a length is outside the range of data used to generate the correlation, and if such extended

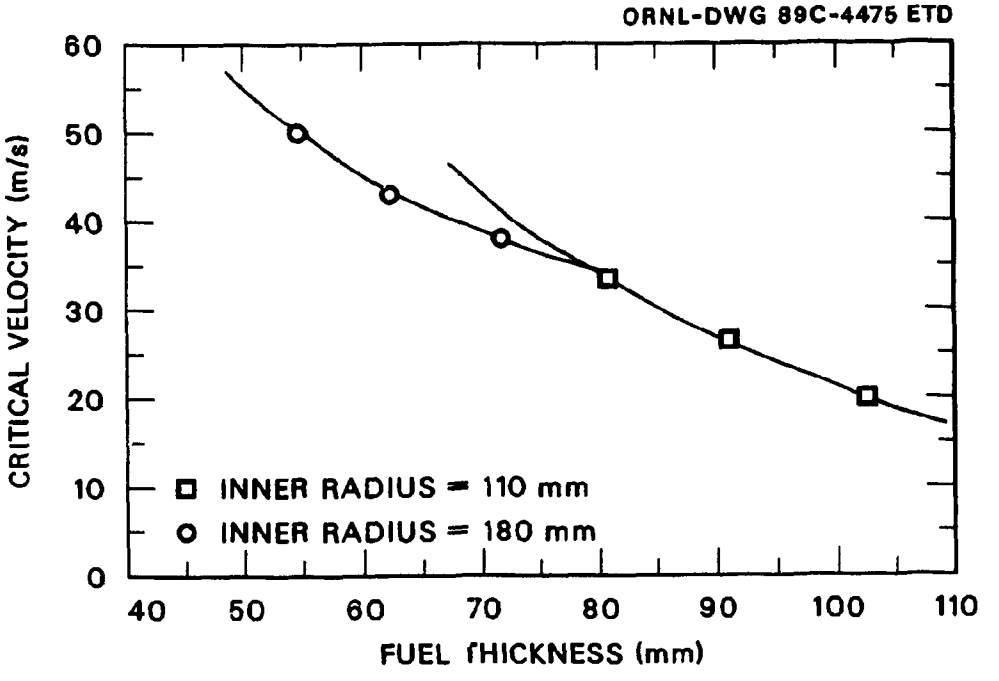

Fig. 18. Critical velocity and fuel radial thickness.

elements were to be adopted it might be necessary to raise the inlet pressure to suppress incipient boiling at the outlet.

The rendement correlation [Eq. (3)] was modified to account for the lower neutronic efficiency of the thicker cores. Assuming that the slope of the rendement vs effective height correlation is not significantly changed from the value of 0.00072 in Eq. (3) by the small (6-mm) increase in fuel thickness, the new constant can be be calculated from the results shown in Table 9.

$$\begin{aligned} \text{Corrected rendement} &= \text{constant} - 0.00072 \times \text{effective height} \\ 3.07 &= \text{constant} - 0.00072 \times 766 \\ \text{constant} &= 3.07 + 0.00072 \times 766 = 3.62 \\ \text{rendement (66 mm)} &= 3.62 - 2 \times 0.00072 \text{ (fueled length + plenum gap)} \end{aligned} \quad (7)$$

For any given fuel element length and plenum gap, the thicker elements are slightly less neutronically efficient, having a rendement that is lower by ~0.2. However, this lower rendement is more than compensated by the higher power that the thicker elements can accommodate.

Table 9. 50-L Two-element core with 22-kg fuel, 66-mm radial thickness of the fuel region, and 50-mm plenum gap

Figure No.[a]	B.19
BOC reactivity	1.252
BOC rendement, m^{-2}	3.064
Corrected rendement,[b] m^{-2}	3.07
Fueled length,[c] mm	333
Plenum gap, mm	50
Effective height, mm	766

[a]Appendix B.

[b]Corrected to $K_{eff} = 1.25$.

[c]Per element.

[d]Effective height = 2 × (fueled length + plenum gap).

The volume of these two-element cores with 66-mm-thick fuel regions may be found by inspection of the drawings in Appendix B.

$$\text{Volume } (cm^3) = \pi\,(25.2^2 - 18.6^2 + 17.6^2 - 11^2) \times H_L \ .$$

If the dimensions are expressed in millimetres, then

$$\text{Volume (L)} = 0.1501 \times \text{fueled length per element} \ . \qquad (8)$$

Figures 19 and 20 show that for any given volume, in the range considered, the 66-mm-thick elements can accommodate more power (because the heated length is shorter); but the thinner elements have higher rendement. The net result is that for volumes greater than ~37 L, the 66-mm cores can give a higher peak thermal flux in the reflector (Fig. 21).

The product of power and rendement, proportional to peak thermal flux, is plotted against incipient boiling power (Fig. 22), revealing that the thinner cores can give more flux at power levels below ~325 MW. Higher fluxes can be achieved by choosing a thicker (66-mm) design and operating at higher power: this was the course adopted by the PS-2 Committee.

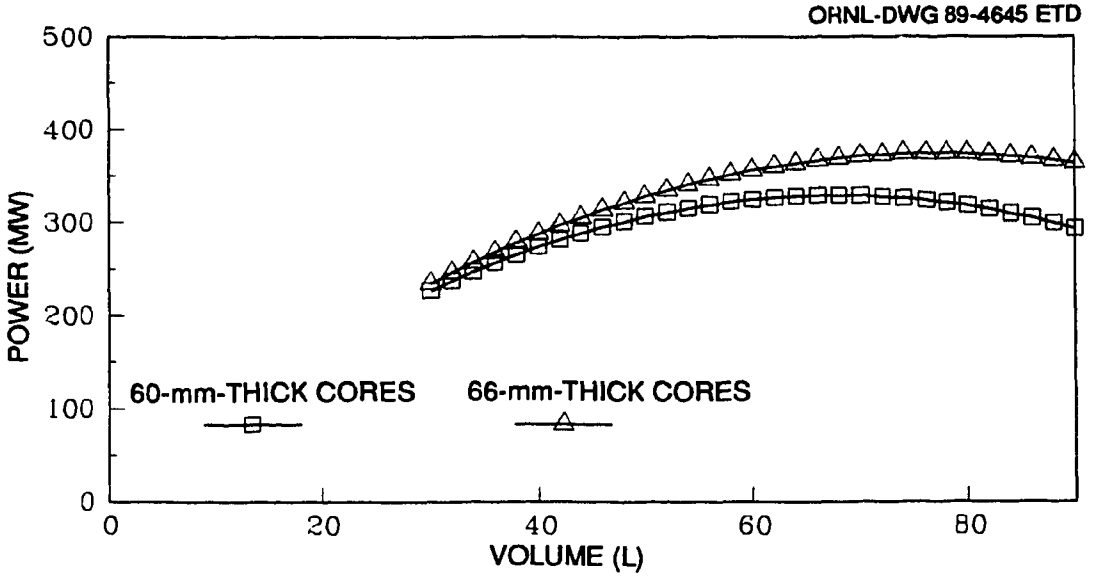

Fig. 19. Power vs core volume for 60- and 66-mm cores.

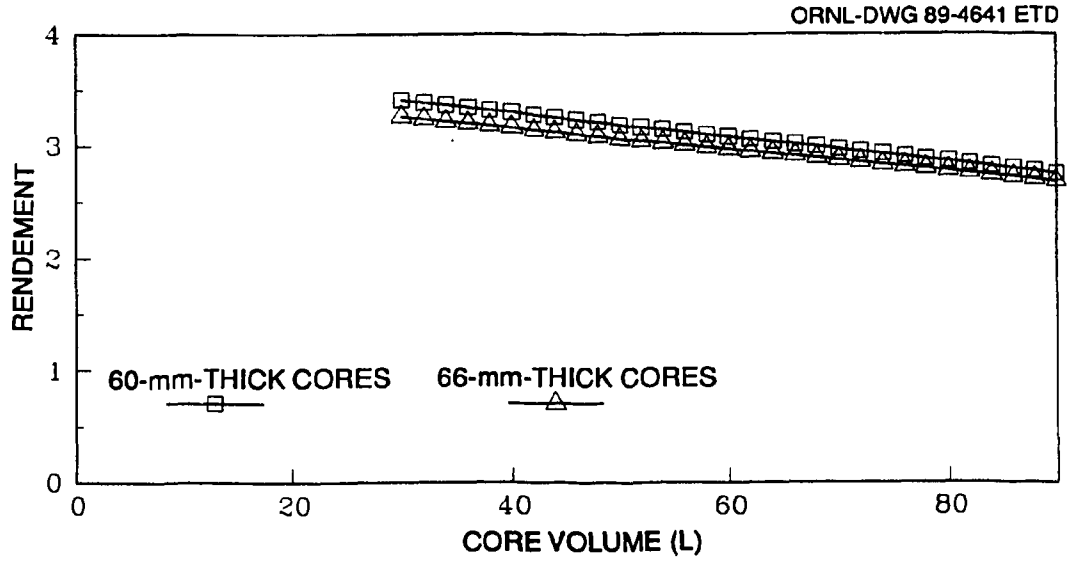

Fig. 20. Rendement vs core volume for 60- and 66-mm cores.

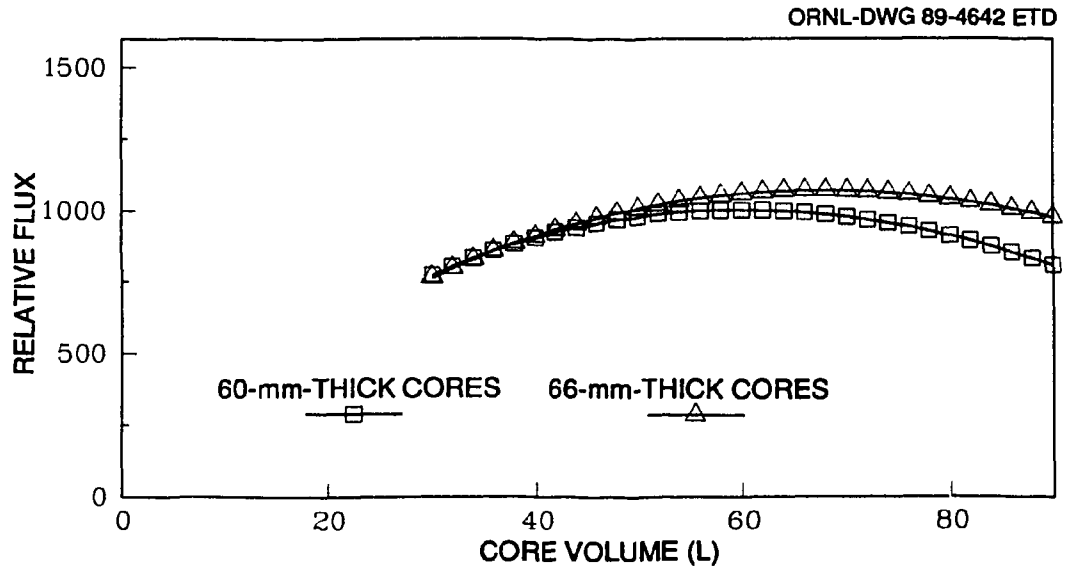

Fig. 21. Relative flux vs core volume for 60- and 66-mm cores.

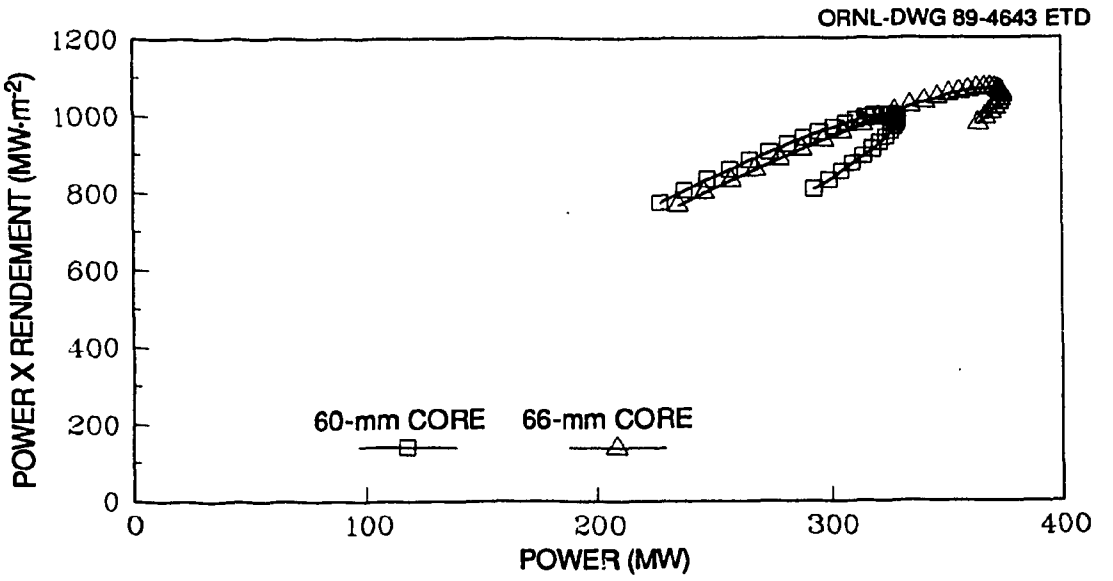

Fig. 22. Relative flux vs power for 60- and 66-mm cores.

4.3 SELECTION OF CORE VOLUME

Only one core volume, 67.4 L, maximizes the thermal flux attainable from two 66-mm fuel elements in the configuration discussed earlier. The IBL is 369 MW (power transferred into the coolant), corresponding to an average power density of 5.47 MW/L. However, as Fig. 21 shows, the maximum in the curve of flux vs core volume is a very flat one. This is further illustrated in Fig. 23, which shows the combinations of power and power density that could be chosen in return for a loss of only 5% or only 10% of the flux. Those curves too are very shallow; for a modest power increase, 90% of the peak thermal flux capability could be maintained while significantly reducing the power density and so achieving higher margins to critical heat flux and perhaps reducing the impact of oxide growth.

A core volume of 67.4 L is optimal, according to the correlation equations shown in Table 10. However, the correlations are based on models that are less than complete: for example, all the comparisons were based on BOC calculations, corrected by an approximate method to account for variations in reactivity and core life. Furthermore, the two methods employed to calculate the IBL — one analytical, the other

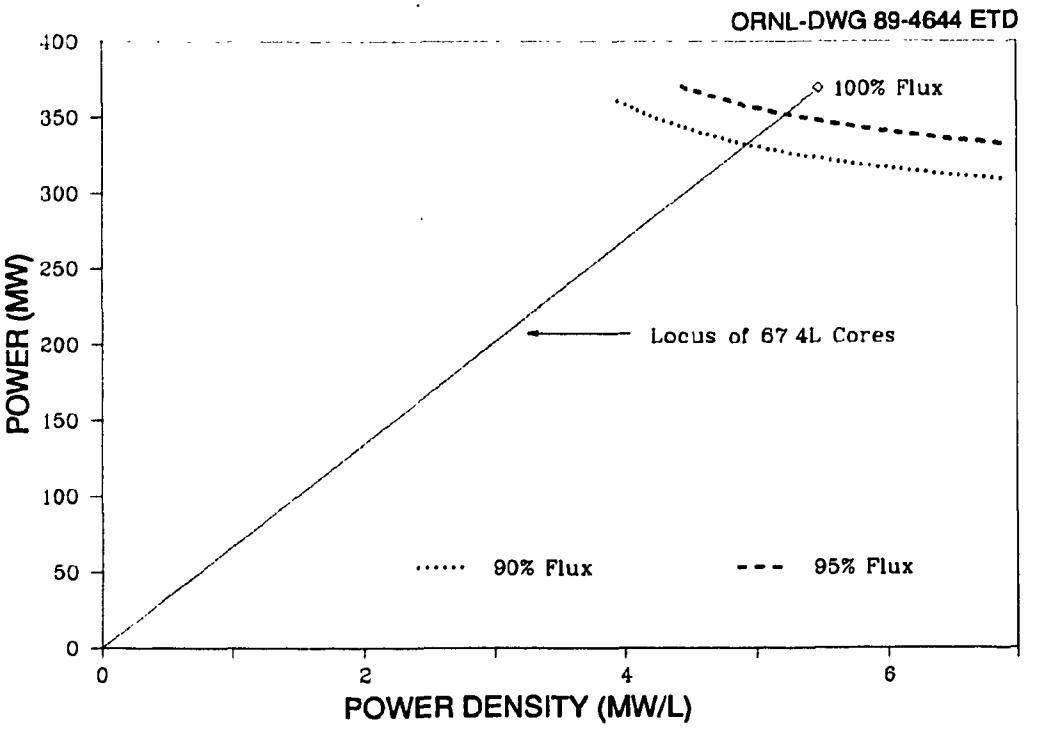

Fig. 23. Power vs power density at 90, 95, and 100% of maximum attainable nominal flux.

numerical — differed by a few percent. In addition, the uncertainties to be applied to the power limits were treated by an approximate, although conservative, method. Therefore, it is important to understand the degree to which the conclusions drawn from these calculations might be affected by inaccuracies or changes in the correlations. Consequently, calculations were made of the optimum core volume and relative flux that would be predicted if the coefficients of the correlations in Table 10 were changed by ±15% as shown in Table 11. Also, the relative flux that would be predicted at a fixed power level (332 MW or 90% of the permissible maximum for the 67.4-L core) was calculated. The results, shown in Table 12, indicate that even if the coefficients in the correlations were wrong by ±15%, the best core volume is still within ~13% of the 67.4-L baseline.

Table 13 shows the effect on the attainable performance of a 67.4-L core (the optimum core volume with the nominal correlations) of ±15%

Table 10. Volume, power density, power, rendement, and relative flux for two-element cores with 50-mm plenum gap

Parameter	60-mm-Thick elements	56-mm-Thick elements
Volume, L	$0.1319\ H_L$	$0.1501\ H_L$
Power density, MW/L	$9.72 - 0.00947\ H_L$	$9.72 - 0.00947\ H_L$
Power,[b] MW	$0.1319\ H_L \times (9.72 - 0.00947\ H_L)$	$0.1501\ H_L \times (9.72 - 0.00947\ H_L)$
BOC rendement,[c] m^{-2}	$3.81 - 0.00072 \times 2 \times (H_L + 50)$	$3.62 - 0.00072 \times 2 \times (H_L + 50)$
Relative flux,[d] $MW \cdot m^{-2}$	$0.1319\ H_L \times (9.72 - 0.00947\ H_L) \times (3.738 - 0.00144\ H_L)$	$0.1501\ H_L \times (9.72 - 0.00947\ H_L) \times (3.548 - 0.00144\ H_L)$

[a] H_L is the fueled (heated) length in each element.

[b] Power = power density × volume.

[c] Corrected to $K_{eff} = 1.25$ (~14-d core life).

[d] Relative flux = power × rendement.

Table 11. Changes in incipient boiling and rendement correlation constants

Case	Incipient boiling correlations		Rendement correlations	
1[a]	9.72	$-0.00947\ H_L$	3.548	$-0.00144\ H_L$
2	+15%			
3	-15%			
4		15%		
5		-15%		
6			+15%	
7			-15%	
8				+15%
9				-15%

[a] The nominal case.

Table 12. Effects of 15% changes in the coefficients of the incipient boiling and rendement correlations on the values of optimum volume, power, and relative flux

Case	Volume (L)	Power[a] (MW)	Relative flux ($MW \cdot m^{-2}$)	Relative flux at 332 MW
1	67.4	332	962	962
2	75.6	485	1368	936
3	59.0	268	799	799[b]
4	59.8	322	957	957[b]
5	76.9	431	1209	932
6	69.1	371	1270	1136
7	65.4	366	870	789
8	65.7	367	1030	904
9	69.1	371	1110	963

[a]10% margin to the IBL.

[b]332 MW exceeds 90% of IBL; flux is calculated at 90% IBL power level.

Table 13. Effects of 15% changes in the coefficients of the incipient boiling and rendement correlations on the performance of a 67.4-L core

Case	Maximum power density[a] (MW/L)	Power[a] (MW)	Relative flux	Relative flux at 332 MW	Optimum core relative flux[b]
1	5.48	369	1069	962	962
2	6.93	467	1354	962	936
3	4.02	271	784	784[c]	799
4	4.84	326	945	925[c]	957
5	6.11	412	1194	962	932
6	5.48	369	1269	1142	1136
7	5.48	369	869	782	789
8	5.48	369	1030	923	904
9	5.48	369	1109	997	963

[a]10% margin to the IBL.

[b]From column 5, Table 11.

[c]332 MW exceeds 90% of IBL; flux is calculated at 90% IBL power level.

changes in the correlation constants. Columns 5 and 6 of Table 13 show that the relative flux obtainable, at 90% of the IBL, from a 67.4-L core is reduced by only a few percent compared with the "optimum core"; in other words, the choice of 67.4 L and the performance expected of the core are rather robust against uncertainties or changes in the correlations used during this core comparison study. Accordingly, the 67.4-L volume, optimal for the nominal correlations used, was adopted for the new reference core.

Table 13 indicates that every effort should be made to avoid changes or constraints leading to cases 3 or 7 – for example, one should not relax the pressure or temperature conditions at the core inlet to a degree that degrades the IBL, nor add material in the core region that will substantially degrade the rendement. Indeed, one should work assiduously to increase the "basic" rendement (i.e., the zero length limit) of the design. The PS-2 team did, by minor changes in core dimensions, make progress in this direction (see Sect. 5).

5. FINAL ADJUSTMENTS TO THE SELECTED CORE DIMENSIONS

Inspection of previous results revealed a number of dimensional changes and other steps that, if practical, might be expected to increase the available flux by raising the rendement more than they reduce the IBL:

- Reduce the radius of the central hole from 103 to 95 mm.
- Reduce the fuel loading to give a 14-d core life at 350 MW(f), that is, 332 MW(th) transferred into the coolant.
- Reduce the support post thickness from 10 to 7 mm.
  - The pressure difference across the support post wall is ~2 MPa.
  - The support post radius is ~175 mm compared with 268 mm for the 16-mm-thick core pressure boundary tube (CPBT) that withstands a ΔP of 4.14 MPa.
  - Therefore, the approximate minimum thickness of the core support post is (175/268) × (2/4.14) × 16 ~5 mm.
- Reduce the CPBT thickness to correspond to the reduced diameter and an inlet pressure of 3.7 MPa.
- Reduce the cooling channel gap between the outer fuel sideplate and the CPBT to 5 mm.

The design resulting from these changes is the one shown in Fig. 3 and adopted as the final preconceptual core design. With an ungraded fuel loading of 14.9 kg, the BOC rendement of this core is 3.058 or 8% greater than the unmodified 67.4-L version.

6. CONCLUSION

6.1 FLUX POTENTIAL FOR THE REFERENCE CORE

By inspection of previous results and of calculations carried through to the EOC, the following estimates were made.

The number of neutrons produced per megawatt of fission power is ~7.5 × 10^{16}. Therefore, the expected flux for the reference core is

$$332 \times 3.058 \times 7.5 \times 10^{16} \times (1.26 \pm 0.1) = 9.6 \pm 0.8 \times 10^{19}\ m^{-2} \cdot s^{-1}\ ,$$

or coolant power × rendement × neutrons produced/MW(f) × expected gains (from Table 14). The pessimistic combination predicts a flux capability ~8 to 9 × 10^{19} $m^{-2} \cdot s^{-1}$.

Table 14. Assumptions made during the PS-2 study for the factors affecting calculated peak thermal flux

	Optimistic	Realistic?	Pessimistic
Fission power/power into coolant	1.06	1.05	1.04
Power limit gain from multiplicative to statistical uncertainty combinations	1.15	1.10	1.05
Rendement gain from BOC/ungraded fuel to EOC/graded fuel	1.12	1.09	1.06
Multiply	1.36	1.26	1.16

6.2 SPECIFICATIONS

Table 15, which contains an estimated allowance for the extra fuel that will be needed in a graded core, lists the major parameters of the final preconceptual core design. The IBL is not the only limit that may restrict the power that can be safely dissipated in this core. Other limits include the critical heat flux, which is probably less restrictive than incipient boiling even though, for safety reasons, a larger

Table 15. Completed preconceptual core design data

Configuration	
Number of elements	2
Geometry	Split core
Element alignment	Coaxial
Coolant flow	Upflow
Flow path	Diverted
Fuel plates	Involute
Core dimensions	
Fueled volume, L	67.4
Heated length per element, mm	474
Flow area in coolant channels, m^2	0.071
Span of outer element plates, mm	83
Span of inner element plates, mm	97
Fuel loading per element, kg	9
Thermal-hydraulic conditions	
Inlet pressure, MPa	3.7
Inlet temperature, °C	49
Flow velocity in element, m/s	27.4
Mass flow in core, kg/s	1950
Power removed by coolant at IBL, MW	369
Power received by coolant at nominal operating point, MW	332
Power at IBL,[a] MW	388
Bulk outlet temperature at IBL, °C	88
Core physics	
Reactivity at BOC	1.26
Rendement at 14 d	3.26
Peak thermal flux at IBL, 10^{19} neutrons/$m^2 \cdot s$	9
Average fuel burnup, %	30
Thermal/fast flux ratio at thermal peak	100
Control elements	
Control and shutdown	Central hole, 4 absorbers
Shutdown	Outside CPBT, 8 absorbers

Table 15 (continued)

Materials	
Fuel	U_3Si_2
Enrichment, %	93
Coolant	D_2O
Structure	6061-T6 Aluminum
Control elements	Hafnium
Burnable poisons	Boron carbide

[a]Recent experimental results from the ANS heated water loop imply that the Griess correlation and the INEL data from the ATR underestimate the rate of oxide growth under ANS-like conditions: the ANS loop was constructed to check this very possibility. If these results are confirmed, the power in this core design may be limited to ~300 MW, a reduction of 14%; however, in that case the core emerging from the conceptual design would be reoptimized (e.g., by reducing fuel loading) so that the reduction in thermal neutron flux would be <14%.

margin will be required. Oxide formation on the fuel clad may be a more restrictive phenomenon than either IBL or critical heat flux and is discussed in Appendix E.

The reference core selected at the end of the ANS Project preconceptual design phase has a lower power density and greater margins to the IBL than previous designs, while meeting the performance criteria of the project.

REFERENCES

1. J. A. Lake et al., "Ultrahigh Flux Reactor Design Probing the Limits of Plate Fuel Technology," *Proceedings of the Workshop on an Advanced Steady-State Neutron Facility, Gaithersburg, MD, December 16–18, 1985.*

2. C. D. West et al., *Advanced Neutron Source (ANS) Project Annual Report, April 1987–March 1988*, ORNL/TM-10860, Martin Marietta Energy Systems, Inc., Oak Ridge Natl. Lab., February 1989.

3. D. L. Selby and J. A. Lake, "Appendix B. ANS Core Comparison Workshop Summary," *Advanced Neutron Source (ANS) Project Annual Report April 1987–March 1988*, ORNL/TM-10860, Martin Marietta Energy Systems Inc., Oak Ridge Natl. Lab., February 1989.

4. G. H. Hanson et al., *Report of the ANS Aluminum Cladding Corrosion Workshops*, ORNL/CONF-88-11203, Martin Marietta Energy Systems, Inc., Oak Ridge Natl. Lab.

5. Joseph M. Hendrie (BNL), letter to J. M. Rowe (NIST), Appendix to *1988 Review of the Basic Energy Sciences Program of the Department of Energy*, Nov. 30, 1988.

6. H. A. McLain, *HFIR Fuel Element Steady State Heat Transfer Analysis, Revised Version,* ORNL/TM-1904, Union Carbide Corp. Nuclear Div., Oak Ridge Natl. Lab., December 1967.

7. C. D. West et al., *Report of the Advanced Neutron Source (ANS) Safety Workshop*, ORNL/CONF-88-10193, Martin Marietta Energy Systems, Inc., Oak Ridge Natl. Lab., December 1988.

Appendix A

CORRESPONDENCE

MARTIN MARIETTA

Internal Correspondence

April 19, 1988

MARTIN MARIETTA ENERGY SYSTEMS, INC.

Distribution

Here are some of the ideas proposed during and subsequent to our recent meeting on the feasibility of the coolant flow divertor. Presumably combinations of these ideas, and any new ones that arise, should be analyzed when we are able to allocate resources to that task.

Figure	Concept	Notes
1	Flow straightners in plenum	Can give a uniform flow distribution over the inlet to the second fuel element, at the cost of an increased pressure drop
2	Increased separation of the fuel elements	Can prevent flow separation, but reduces reactivity and, possibly, flux
3	Vary internal diameter of CPBT	Can give an accelerating flow in the divertor, reducing the tendency for flow separation
4	Offset upper and lower elements	Can give the two elements a different coolant stream without the need to change flow direction
5	Convergent section where flow direction is changed	Same as 3 above

Colin D. West, FEDC (4-0370)

CDW:kfr

Distribution

R. G. Alsmiller
N. C. J. Chen
W. R. Gambill
R. C. Gwaltney
R. M. Harrington
B. S. Maxon
F. J. Peretz
D. L. Selby
P. B. Thompson
G. T. Yahr
G. L. Yoder

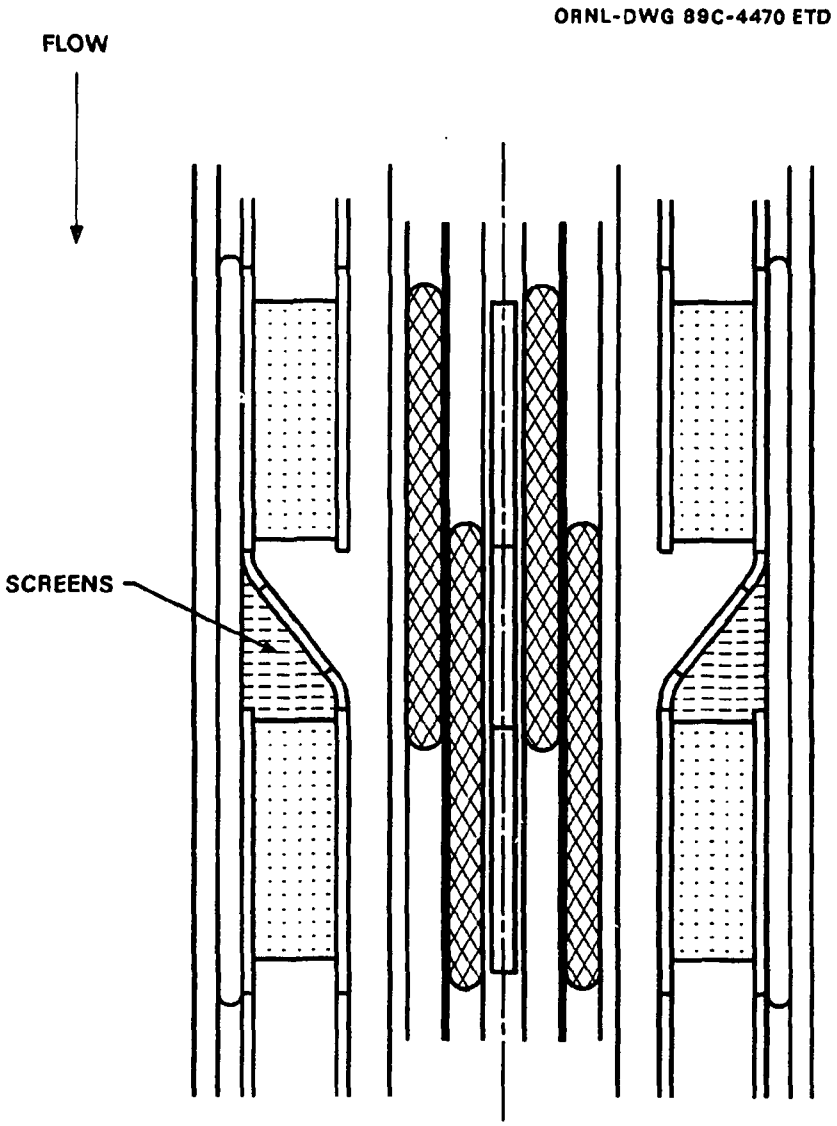

Fig. 1

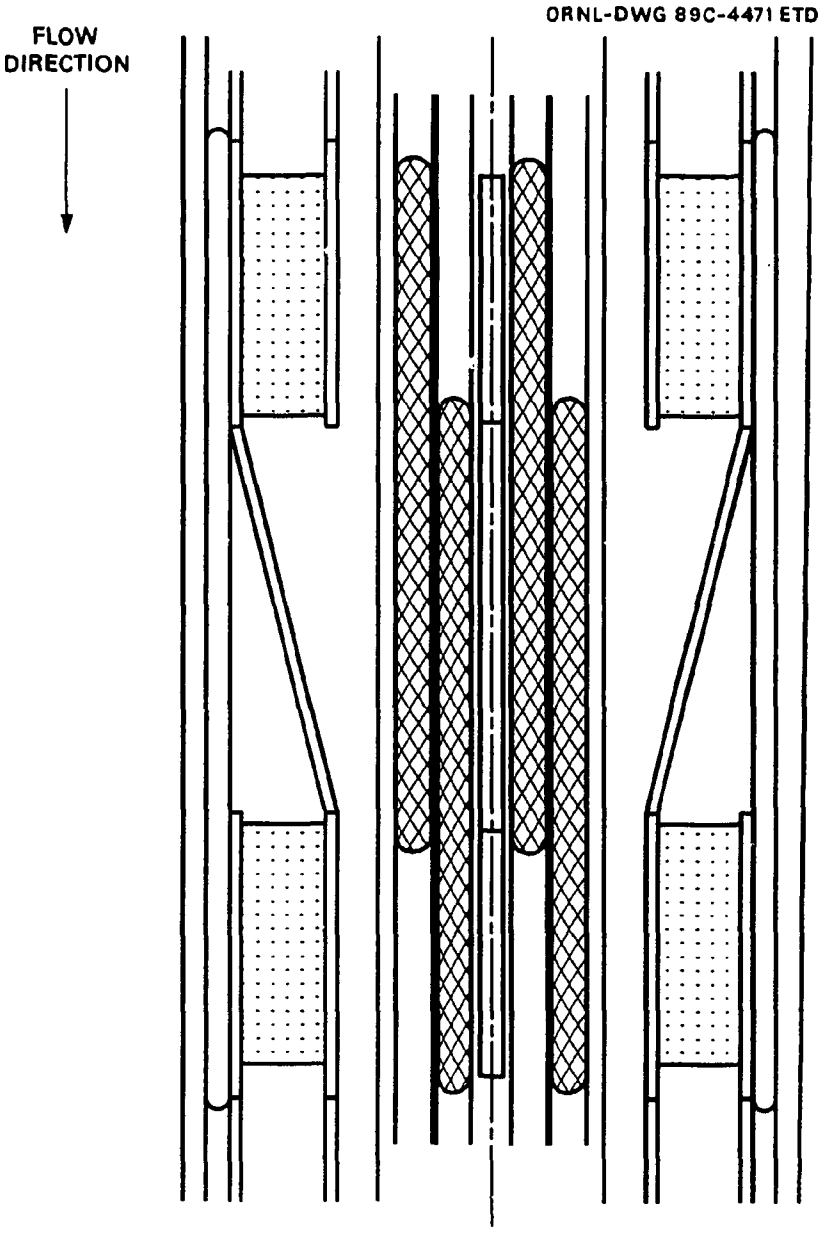

Fig. 2

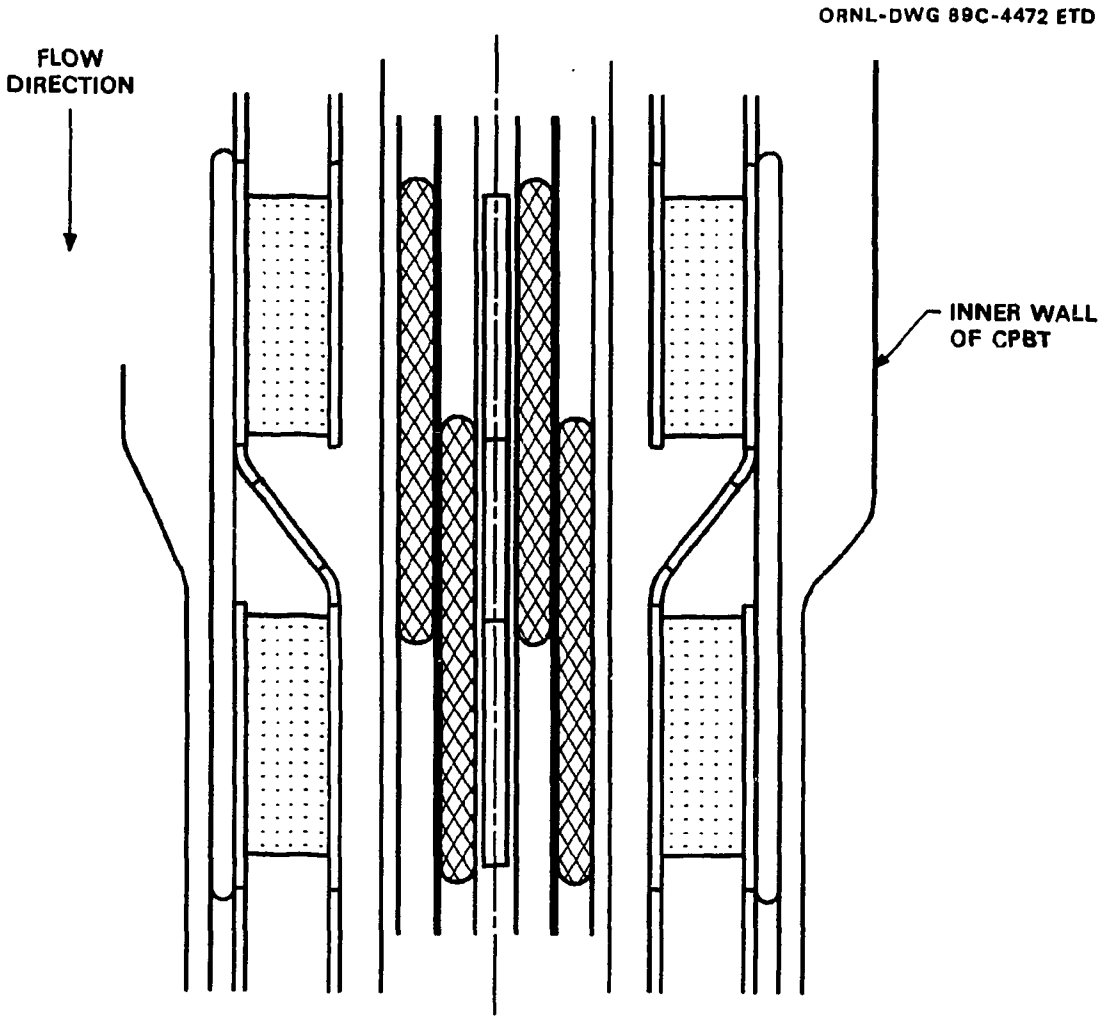

Fig. 3

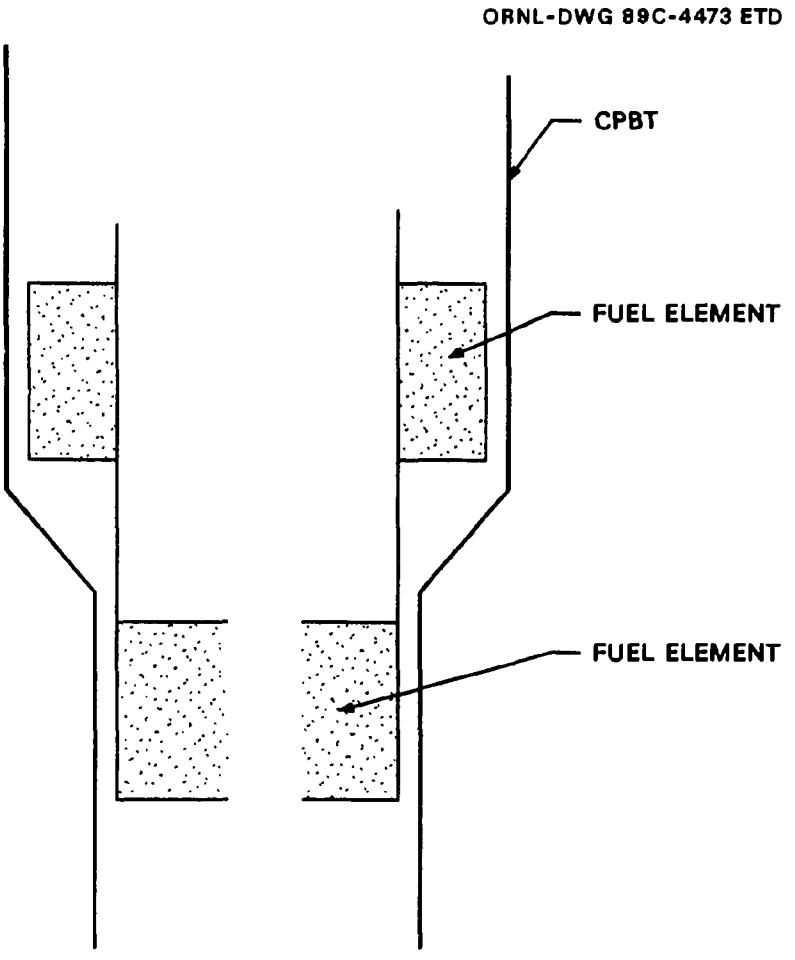

Fig. 4

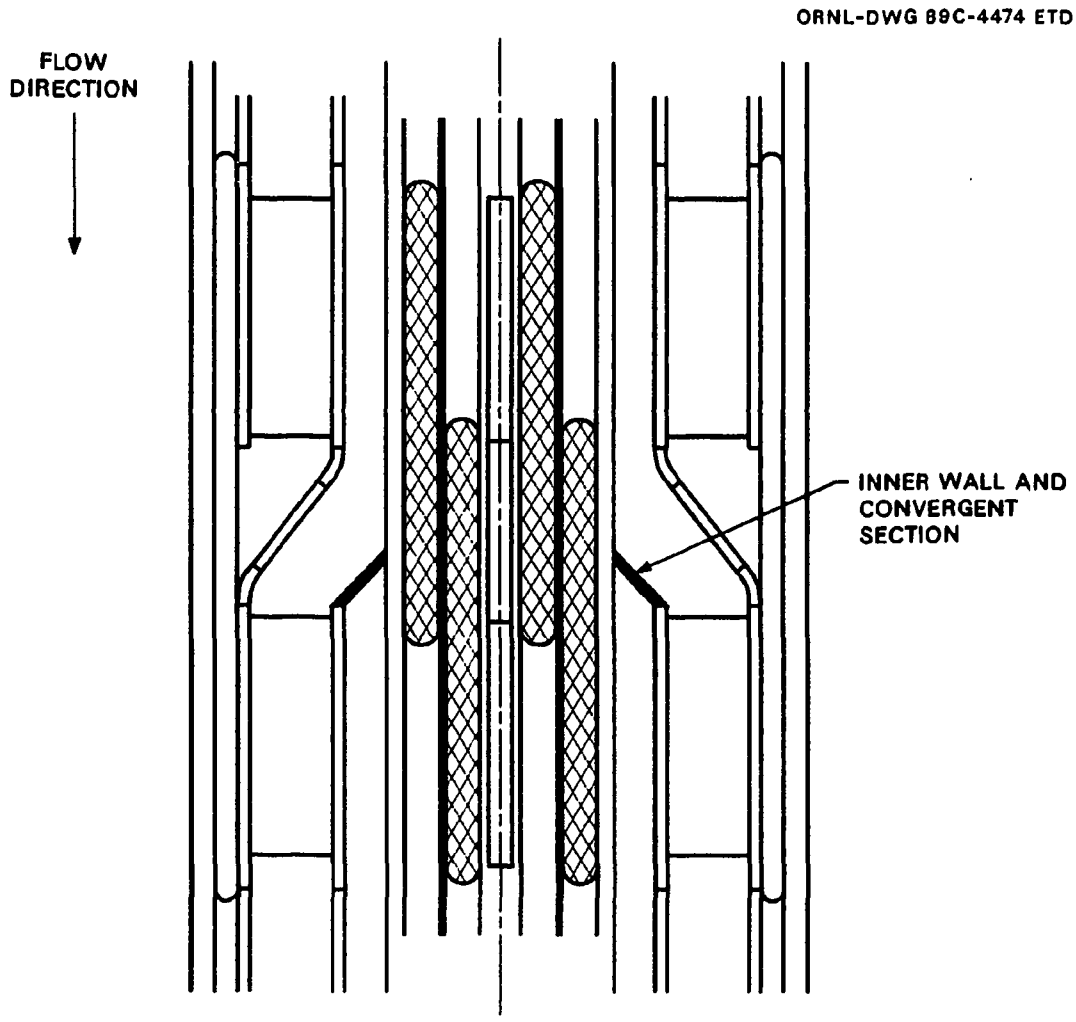
ORNL-DWG 89C-4474 ETD
FLOW DIRECTION
INNER WALL AND CONVERGENT SECTION

Fig. 5

Appendix B

SUMMARY OF CORE DIMENSIONS CONSIDERED TO DATE

This appendix presents a series of figures giving dimensions of the core options evaluated as part of the PS-2 effort. All of these options initially grew out of the split involute core concept recommended at the February 1988 core comparison workshop.[1] At the time of the workshop, a split core with involute plates and a volume of ~30 L was recommended.

As core analyses progressed, there was a feeling that lower power densities were required, and a core volume of 41 L was proposed. Sensitivity studies also indicated that the maximum reactivity was attained with a gap between the fuel of ~150 mm (a gap between the ends of the plates of 130 mm if each has a 10-mm end cap). These considerations led to the core shown in Fig. B.1 being proposed.

At the same time, efforts continued on the "enhanced" core concept, in which each core segment is cooled with a separate stream of coolant, near the temperature of the primary coolant leaving the primary heat exchangers. Because hydraulic considerations indicated that excessive gap distances would be required for aligned fuel elements, attention was given to offset elements with essentially straight inlet and outlet flow paths. Figure B.2 depicts a two-element offset core roughly equivalent to the 41-L aligned core, and Fig. B.3 depicts a three-element core with similar gaps between elements.

Review of the design optimization of the ILL reactor indicated that taller cores might further reduce the power density with minimal impact on the neutronic efficiency. Thus, 50- and 60-L versions of the three-element offset cores were proposed neutronic (Figs. B.4 and B.5), in which only the lengths of the fuel elements and gaps were altered. These five proposals served as the initial five cases for the PS-2 evaluations.

As the PS-2 evaluations progressed, it was suggested that parametric comparisons of the five basic cases were skewed by the different gap sizes in the various cases. It was particularly felt that large gaps

were a penalty for the three-element proposals. Because the optimization of reactivity that led to the original gap size was not considered applicable to the offset core geometries, an alternative approach based on the smallest gap size considered mechanically achievable was proposed. A vertical gap of 50 mm between the fueled regions of the elements was agreed upon, and a wide range of aligned, two- and three-element offset cores was evaluated. These cores are depicted in Figs. B.6–B.13. An additional two-element offset, 60-L core with a 130-mm gap was evaluated for comparison with the original case 2 core (Fig. B.14).

Several other perturbations in the basic core geometries were considered. A two-element offset core, with a volume of 50 L but the vertical dimensions of the 60-L core (Fig. B.15), was considered to assess the relative importance of core height and fuel element thickness. A three-element, 60-L core with the fuel elements transposed was also considered (Fig. B.16), to determine whether this arrangement produced a "flux trap" effect near the beam tube mouths. A two-element offset, 60-L core with the overall aspect ratio of the HFIR core was considered (Fig. B.17), as a gross check on the desirability of using tall, narrow cores. Following this case, a more moderate "thick" core, a 50-L core with the height of the 41-L core, was calculated (Fig. B.18).

A review of data on critical velocity calculations led to fuel thickness (the difference between the outer and inner radius of the free fuel plate zone) being limited to 66 mm. Figures B.19–B.22 considered a number of two-element core variants with 66-mm-thick fuel zones. These variants include 50- and 70-L cores with a 50-mm gap between elements, a 50-L core with a 250-mm gap (to investigate the impact of a larger gap on beam tubes), and a 50-L core with a 100-mm gap, and the central post tapered at 3.5.

A further check of the evaluation process was accomplished by calculating the ILL core (Fig. B.23), and a model of the HFIR core immersed in heavy water (Fig. B.24). The HFIR core was also calculated in the two-element offset configuration, by separating the two HFIR elements to provide a 50-mm gap between the elements (Fig. B.25). Care must be used

in comparing these results with the other cases, because the ILL and HFIR cases as initially defined do not include a CPBT.

Two 80-L cores were proposed, as shown in Figs. B.26 and B.27. The first is a two-element core in the standard configuration, with 66-mm-thick fuel zones and a 50-mm gap. The second is a three-element core, also typical of other three-element cases. However, the inlet pressure of this core was assumed to be lower, and a 10-mm CPBT was used.

Finally, various optimization curves were used to define a "baseline" core for final evaluations (Fig. B.28). The baseline core is a 67.4-L, two-element offset configuration, with 66-mm-thick fuel zones and a 50-mm gap between the fuel zones of the elements. "Modified baseline" proposals are shown in Figs. B.29–B.34. These modifications include central hole radii of 95 and 112 mm, as opposed to a baseline radius of 103 mm, a 5-mm bypass between the outer fuel element and the CPBT, and a 7-mm-thick central support post, as opposed to a baseline of 10 mm. Some of the "modified baseline" cores also include a 12.5-mm-thick CPBT, corresponding to a design pressure (not operating inlet pressure) of 3.7 MPa.

A summary table of the cases considered is attached, followed by the referenced figures.

REFERENCE

1. D. L. Selby and J. A. Lake, "Appendix B. ANS Core Comparison Workshop Summary," *Advanced Neutron Source (ANS) Project Annual Report April 1987–March 1988*, ORNL/TM-10860, Martin Marietta Energy Systems, Inc., Oak Ridge Natl. Lab., February 1989.

Original cases:

Fig. B.1. Case 1(130), two-element, aligned, 41-L, 130-mm gap.

Fig. B.2. Case 2(130), two-element, offset, 41-L, 130-mm gap.

Fig. B.3. Case 3(138), three-element, offset, 41-L, 138-mm gap.

Fig. B.4. Case 4(120), three-element, offset, 50-L, 120-mm gap.

Fig. B.5. Case 5(144), three-element, offset, 60-L, 144-mm gap.

Comparison cases with 50-mm gap:

Fig. B.6. Case 12(50), two-element, aligned, 50-L, 50-mm gap.

Fig. B.7. Case 2(50), two-element, offset, 41-L, 50-mm gap.

Fig. B.8. Case 6(50), two-element, offset, 50-L, 50-mm gap.

Fig. B.9. Case 7(50), two-element, offset, 60-L, 50-mm gap.

Fig. B.10. Case 3(50), three-element, offset, 41-L, 50-mm gap.

Fig. B.11. Case 4(50), three-element, offset, 50-L, 50-mm gap.

Fig. B.12. Case 5(50), three-element, offset, 60-L, 50-mm gap.

Fig. B.13. Case 10(50), three-element, offset, 70-L, 50-mm gap.

Comparison case with 130-mm gap:

Fig. B.14. Case 7(130), two-element, offset, 60-L, 130-mm gap.

Special cases:

Fig. B.15. Case 8(50), two-element, offset, 50-L, 50-mm gap, narrow elements.

Fig. B.16. Case 9(50), three-element, offset, 60-L, 50-mm gap, inverted elements.

Fig. B.17. Case 11(50), two-element, offset, 60-L, 50-mm gap, squat core.

Fig. B.18. Case 13(50), two-element, offset, 50-L, 50-mm gap, 69.5-mm-wide fuel.

Cases with 66-mm-thick fuel elements:

Fig. B.19. Case 14(50), two-element, offset, 50-L, 50-mm gap, 66-mm-wide fuel.

Fig. B.20. Case 14(150), two-element, offset, 50-L, 150-mm gap, 66-mm-wide fuel.

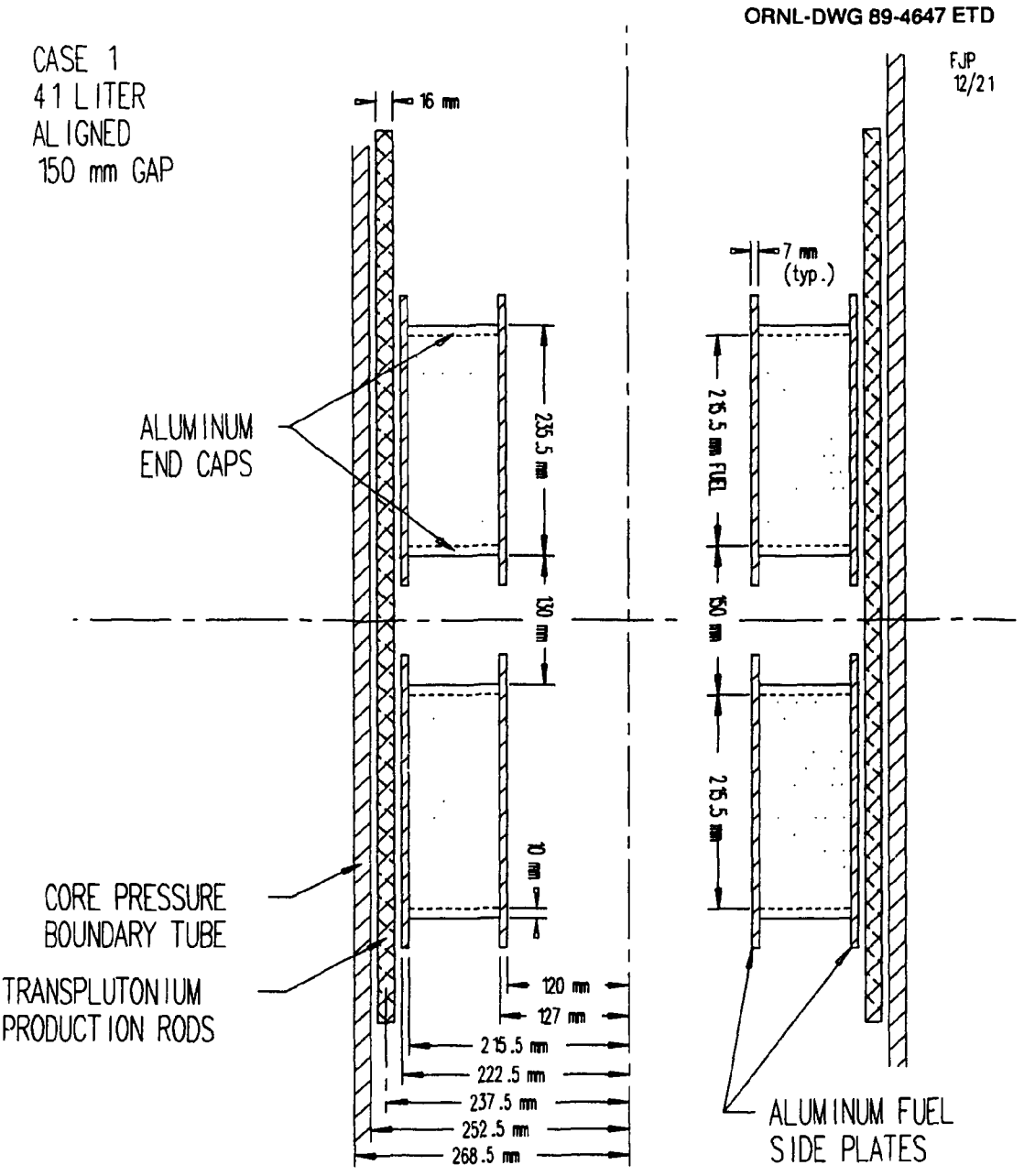

Fig. B.1. Case 1(130), two-element, aligned, 41-L, 130-mm gap.

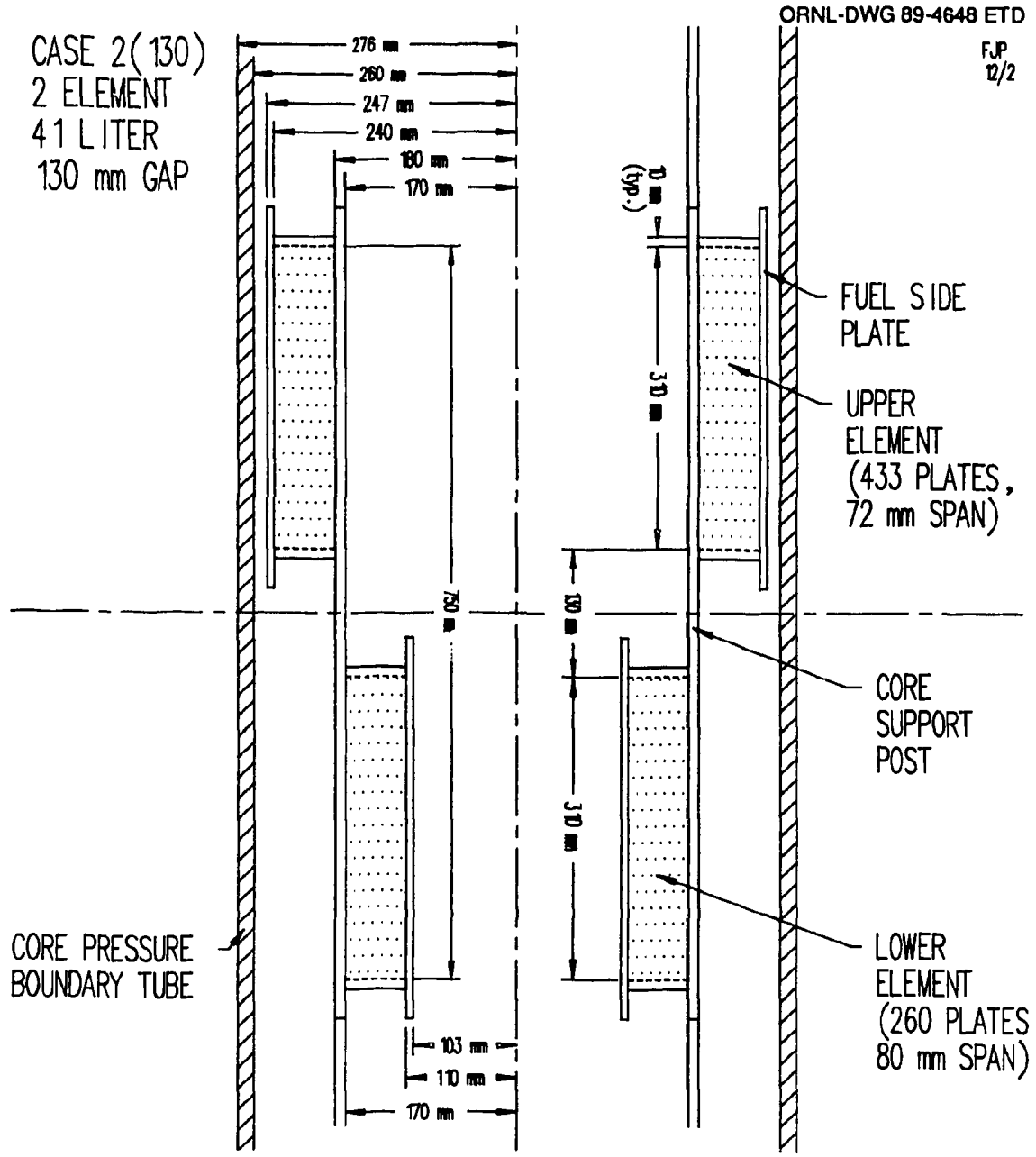

Fig. B.2. Case 2(130), two-element, offset, 41-L, 130-mm gap.

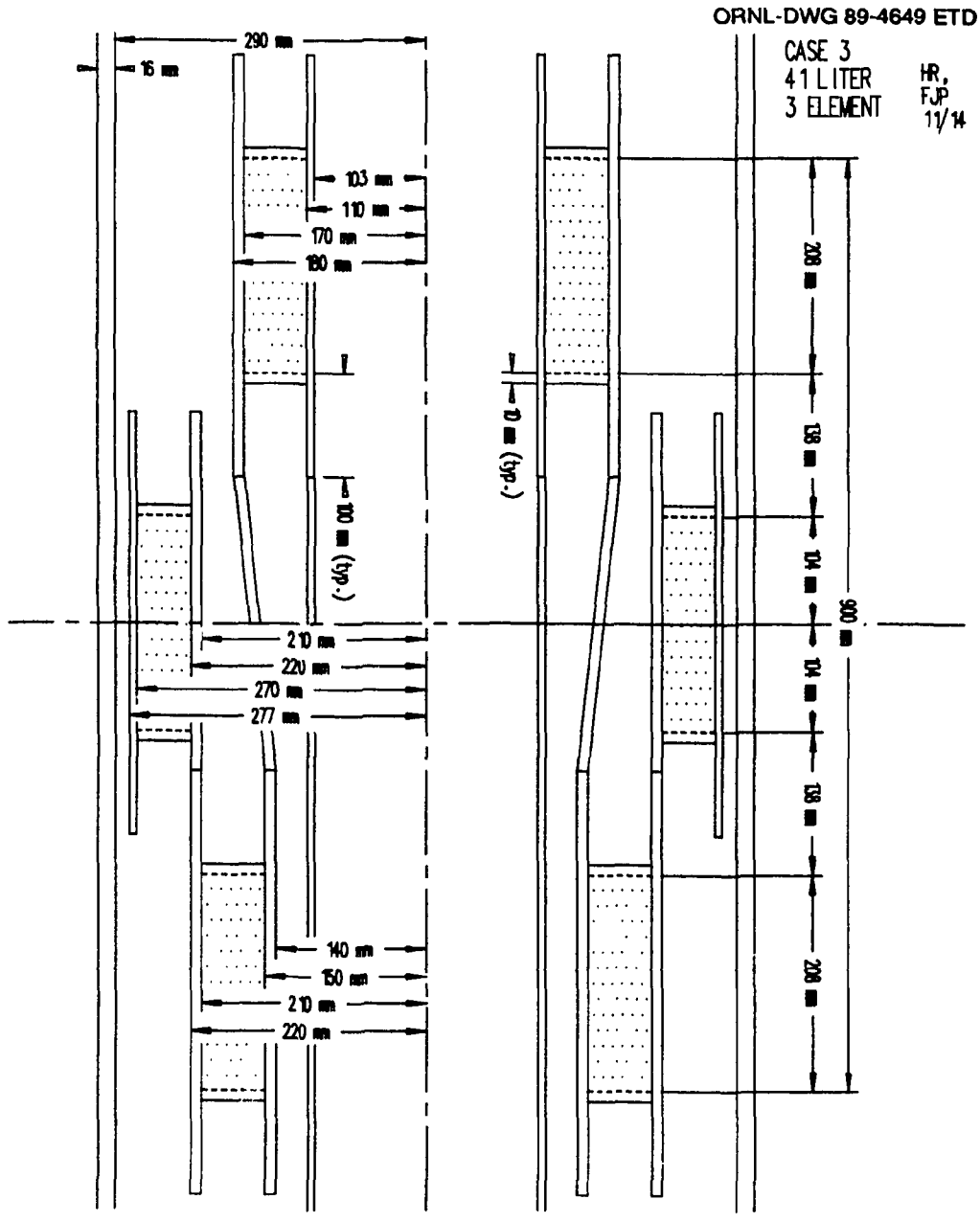

Fig. B.3. Case 3(138), three-element, offset, 41-L, 138-mm gap.

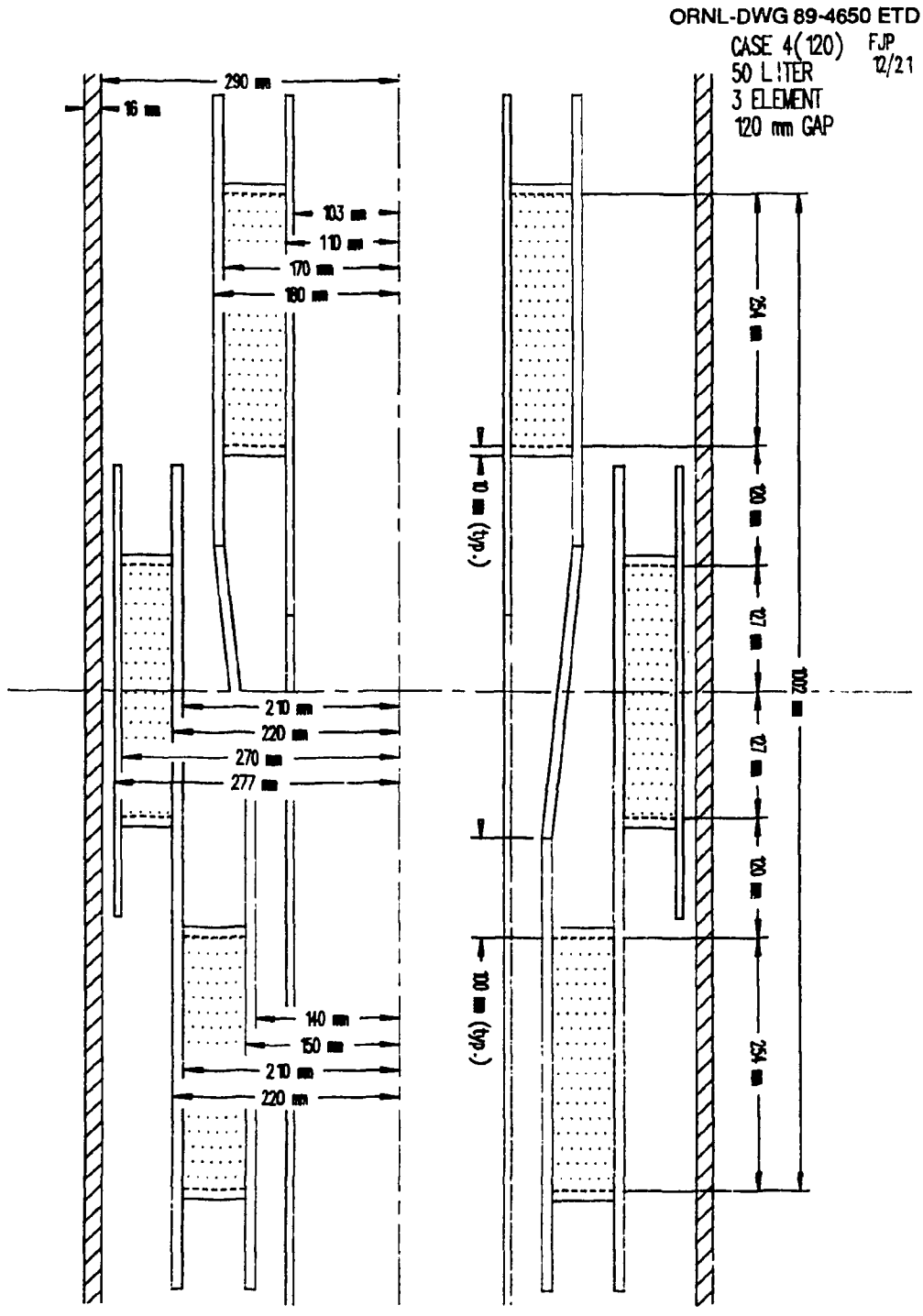

Fig. B.4. Case 4(120), three-element, offset, 50-L, 120-mm gap.

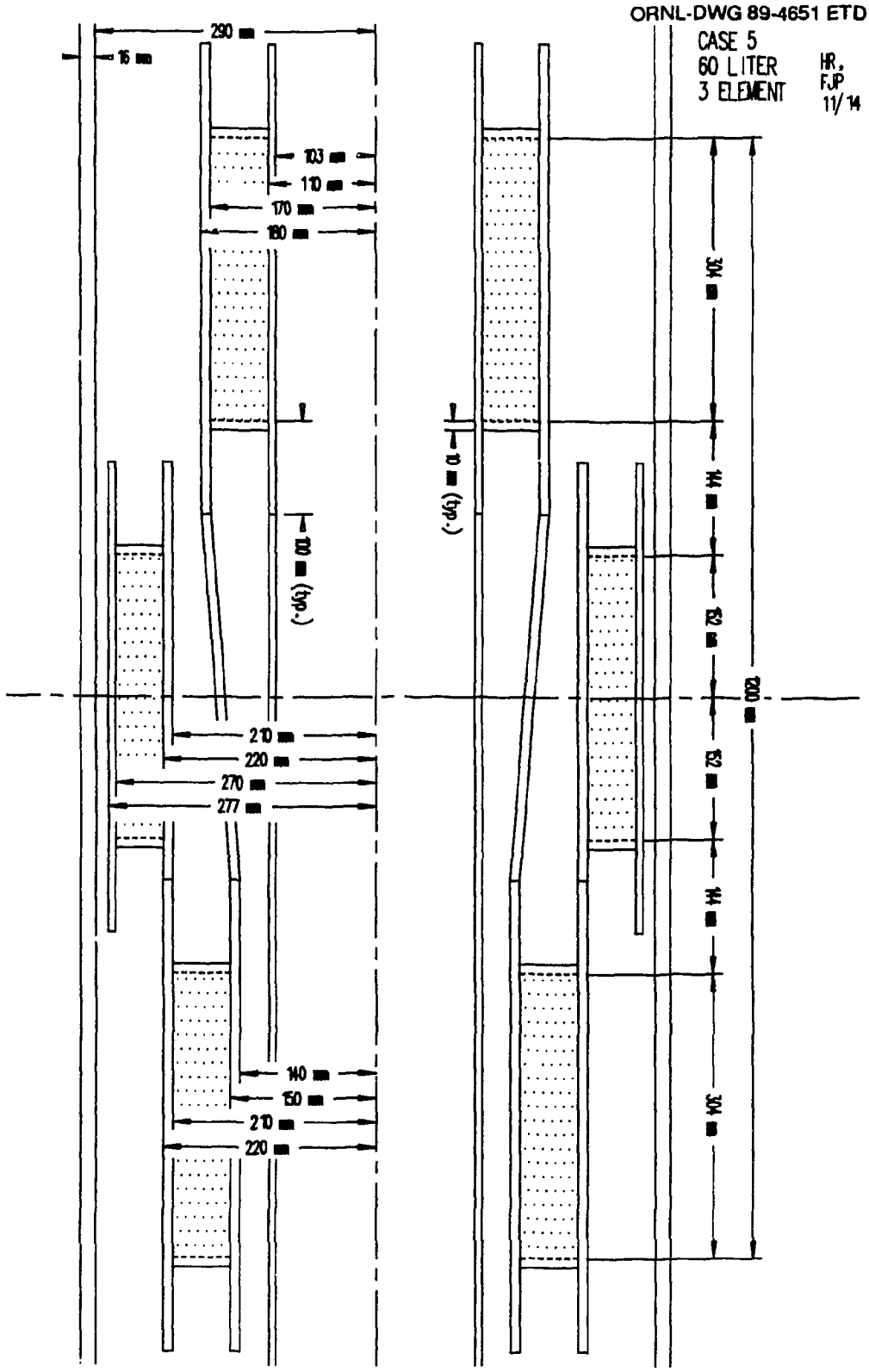

Fig. B.5. Case 5(144), three-element, offset, 60-L, 144-mm gap.

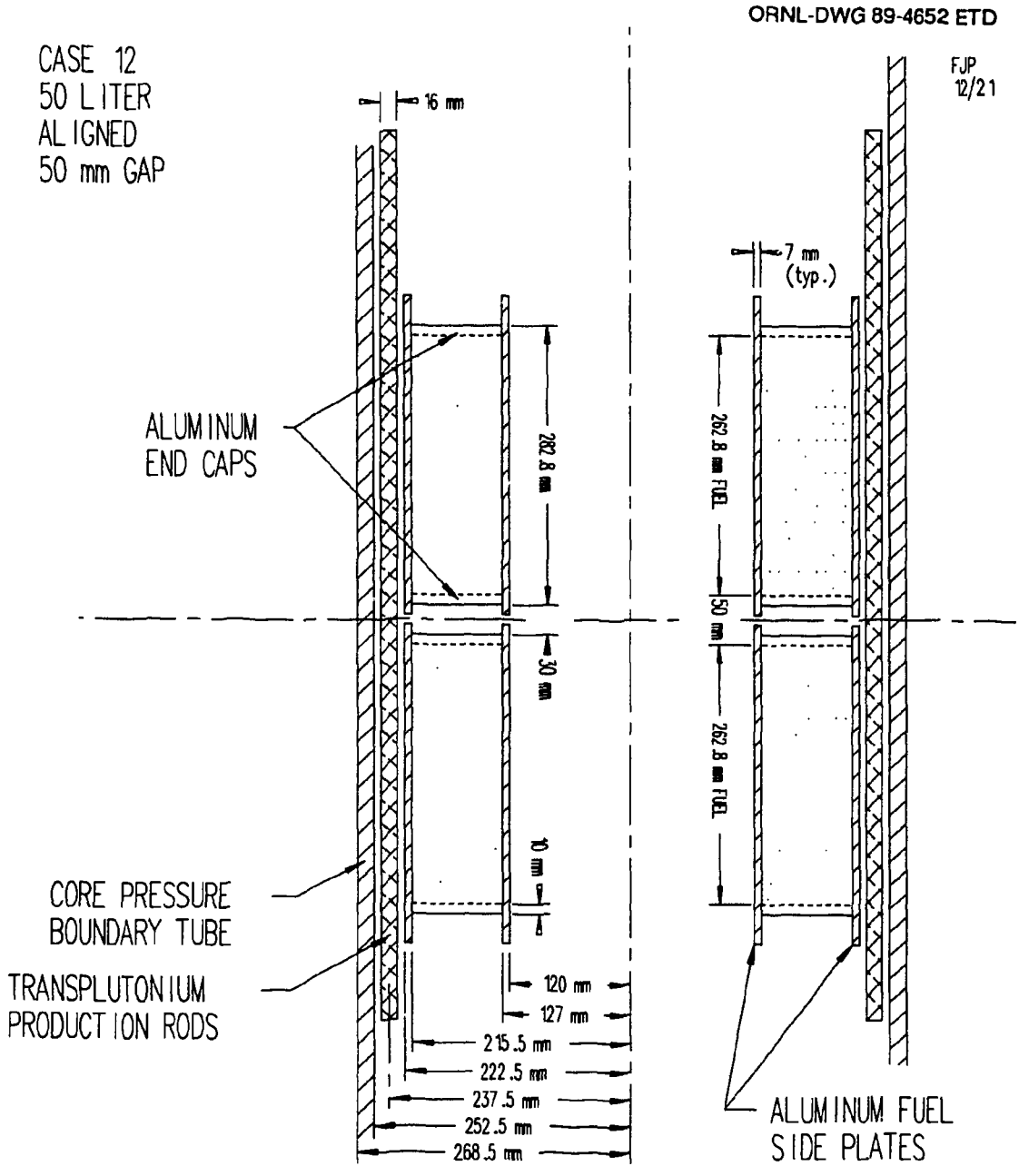

Fig. B.6. Case 12(50), two-element, aligned, 50-L, 50-mm gap.

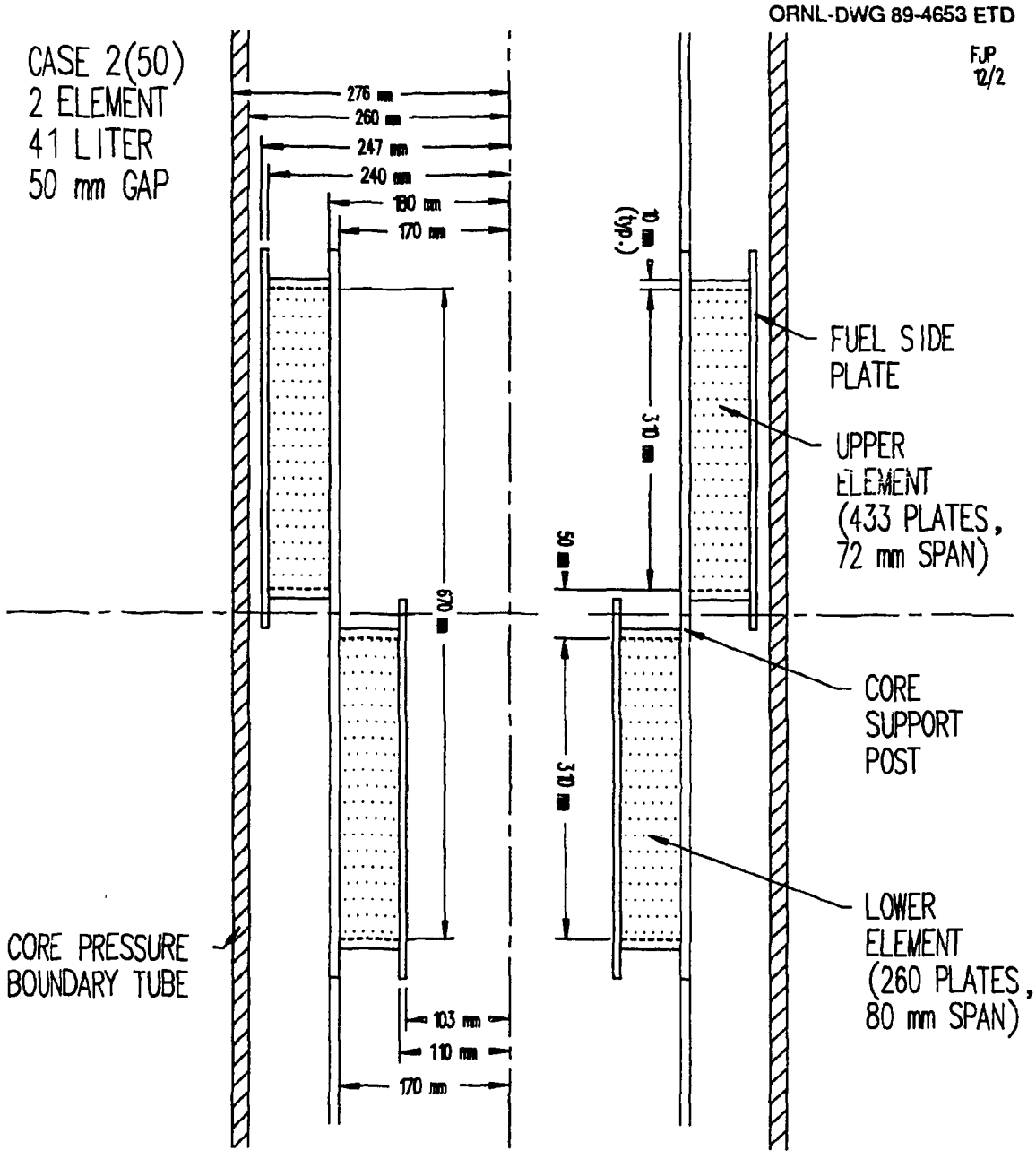

Fig. B.7. Case 2(50), two-element, offset, 41-L, 50-mm gap.

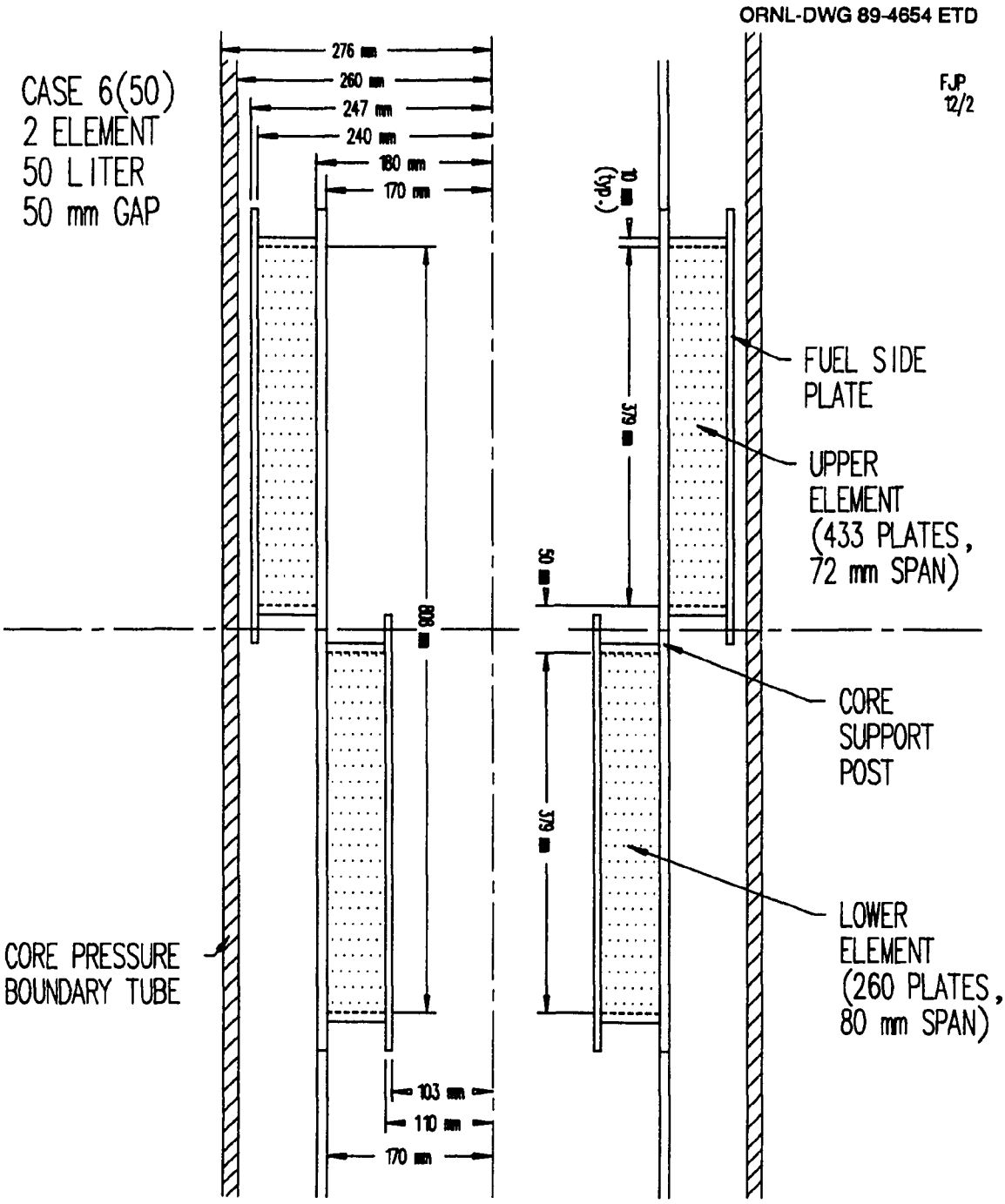

Fig. B.8. Case 6(50), two-element, offset, 50-L, 50-mm gap.

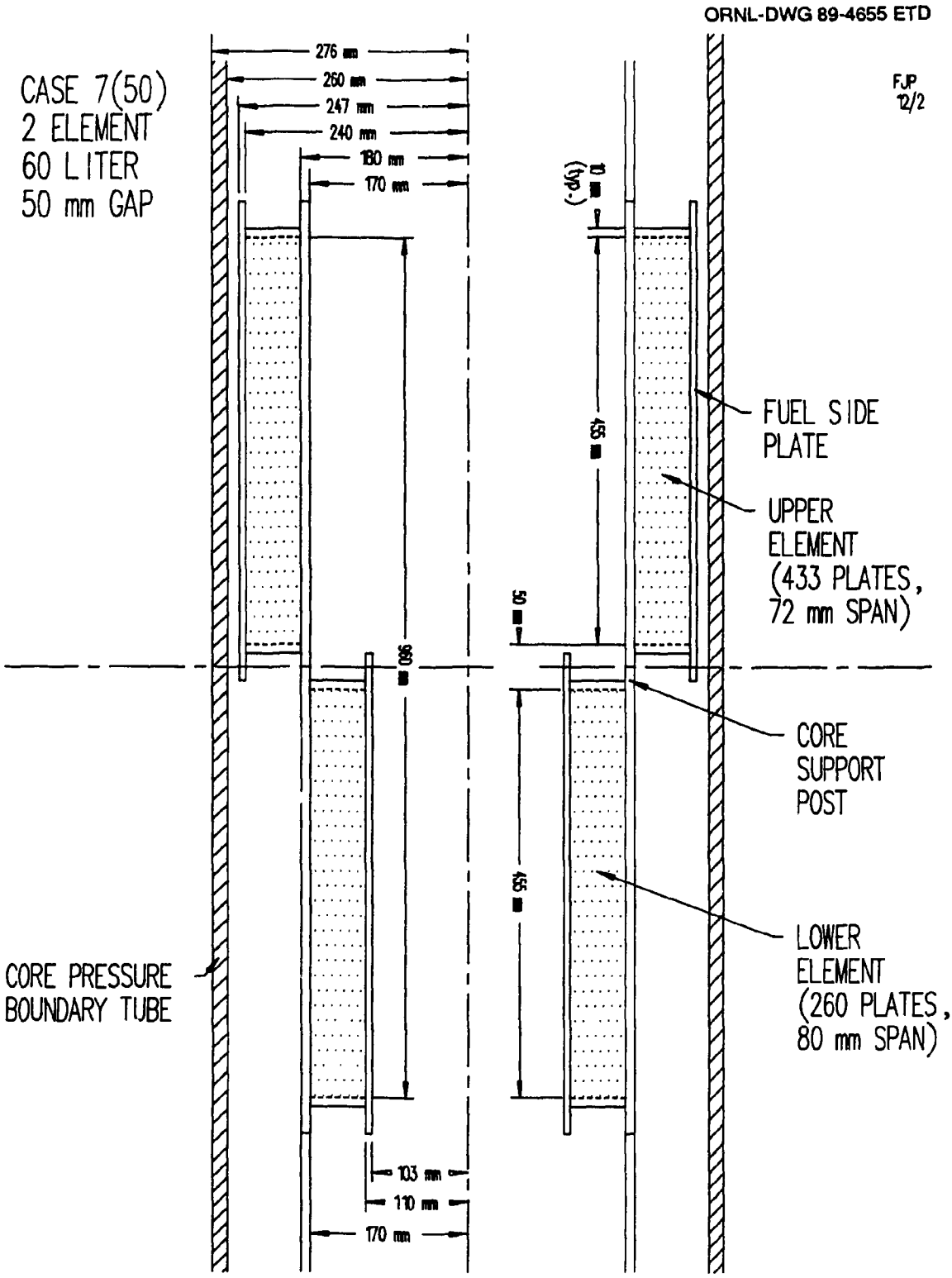

Fig. B.9. Case 7(50), two-element, offset, 60-L, 50-mm gap.

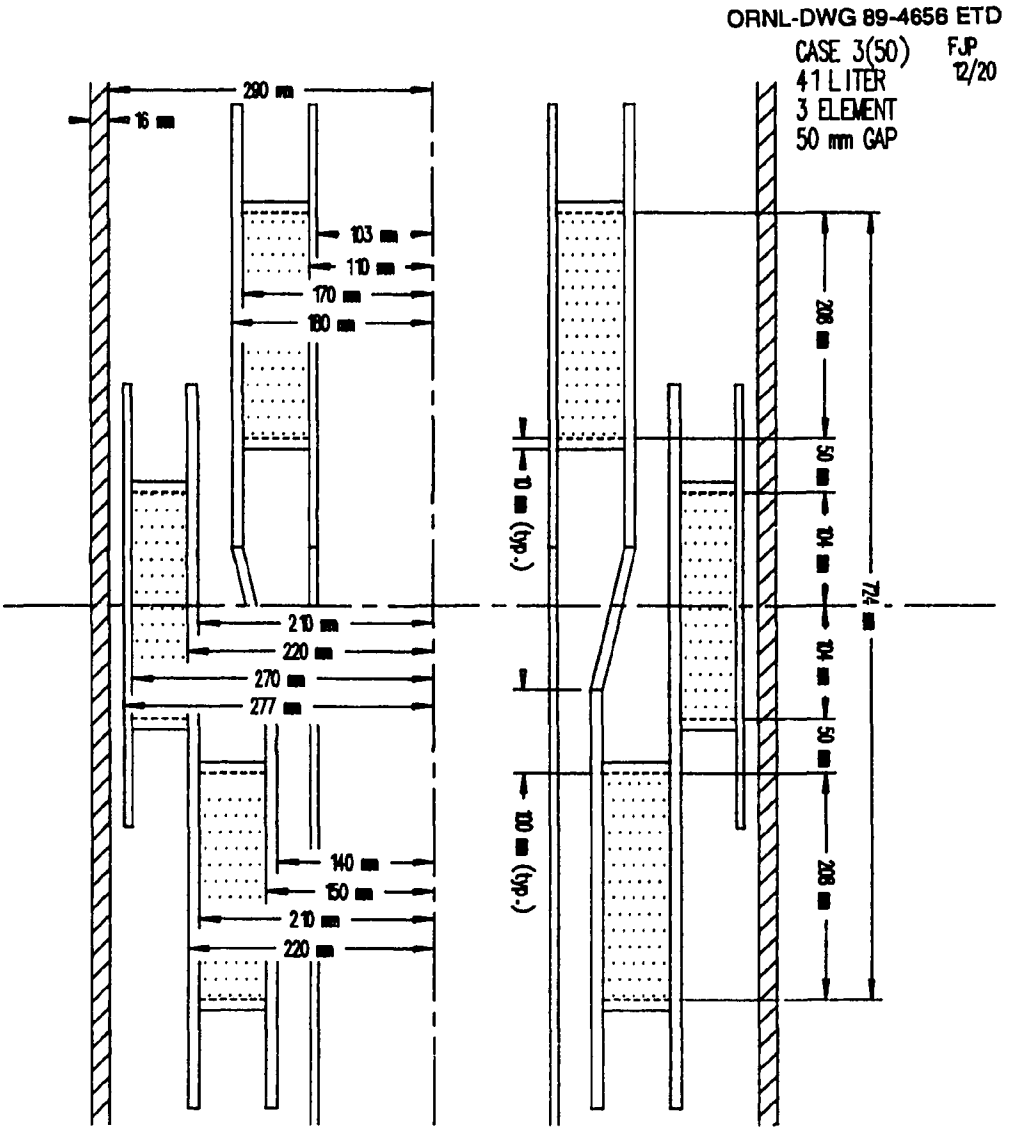

Fig. B.10. Case 3(50), three-element, offset, 41-L, 50-mm gap.

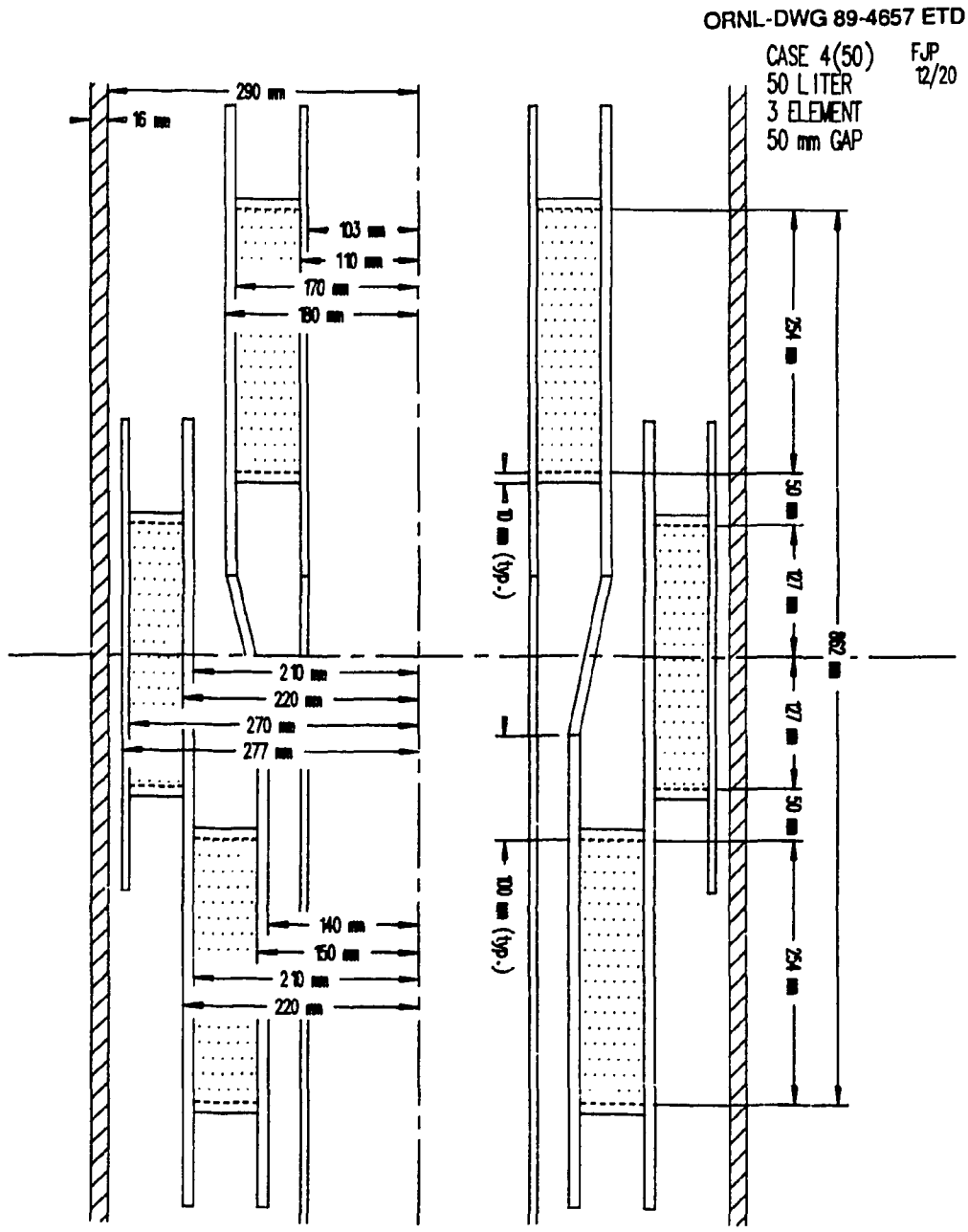

Fig. B.11. Case 4(50), three-element, offset, 50-L, 50-mm gap.

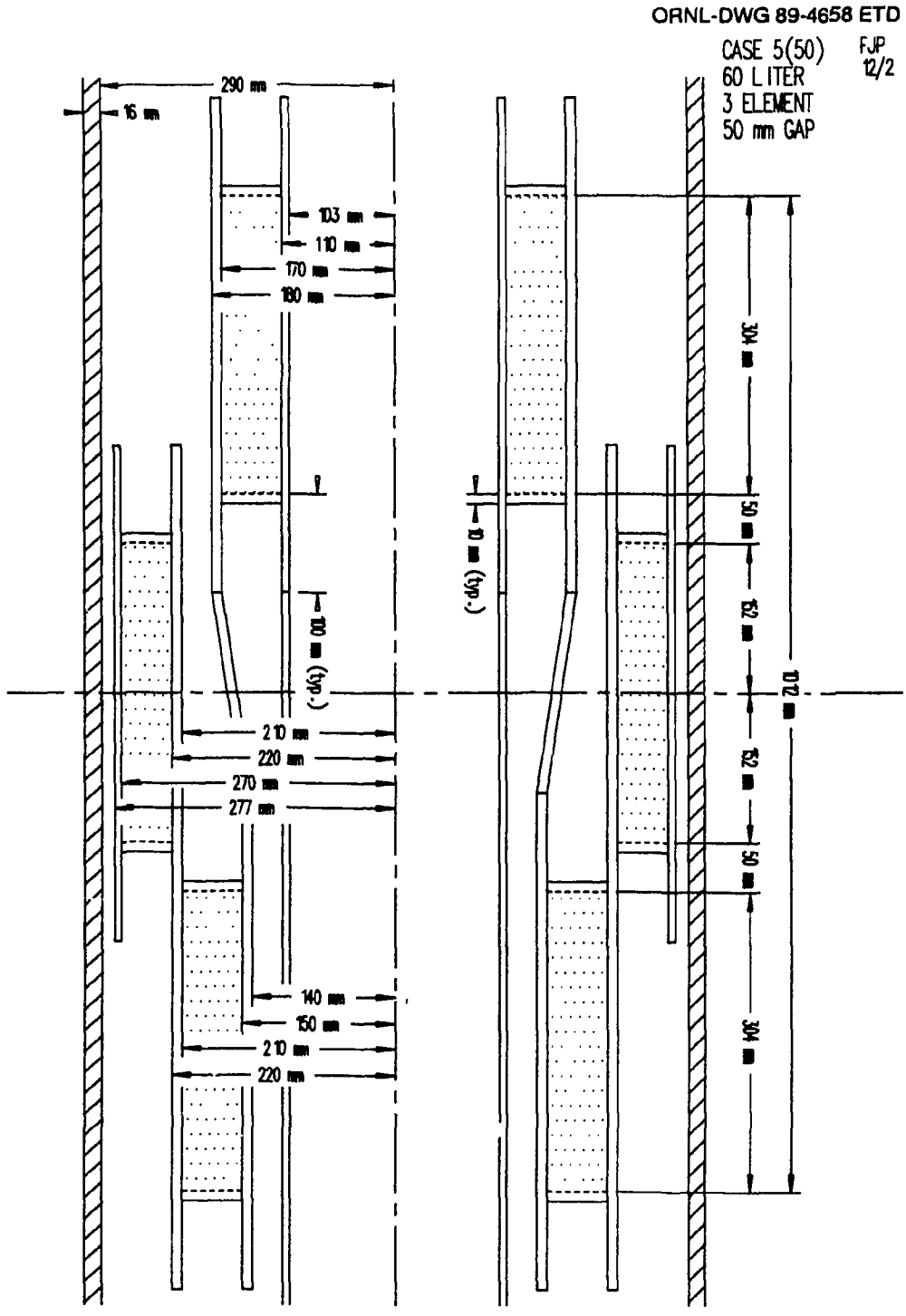

Fig. B.12. Case 5(50), three-element, offset, 60-L, 50-mm gap.

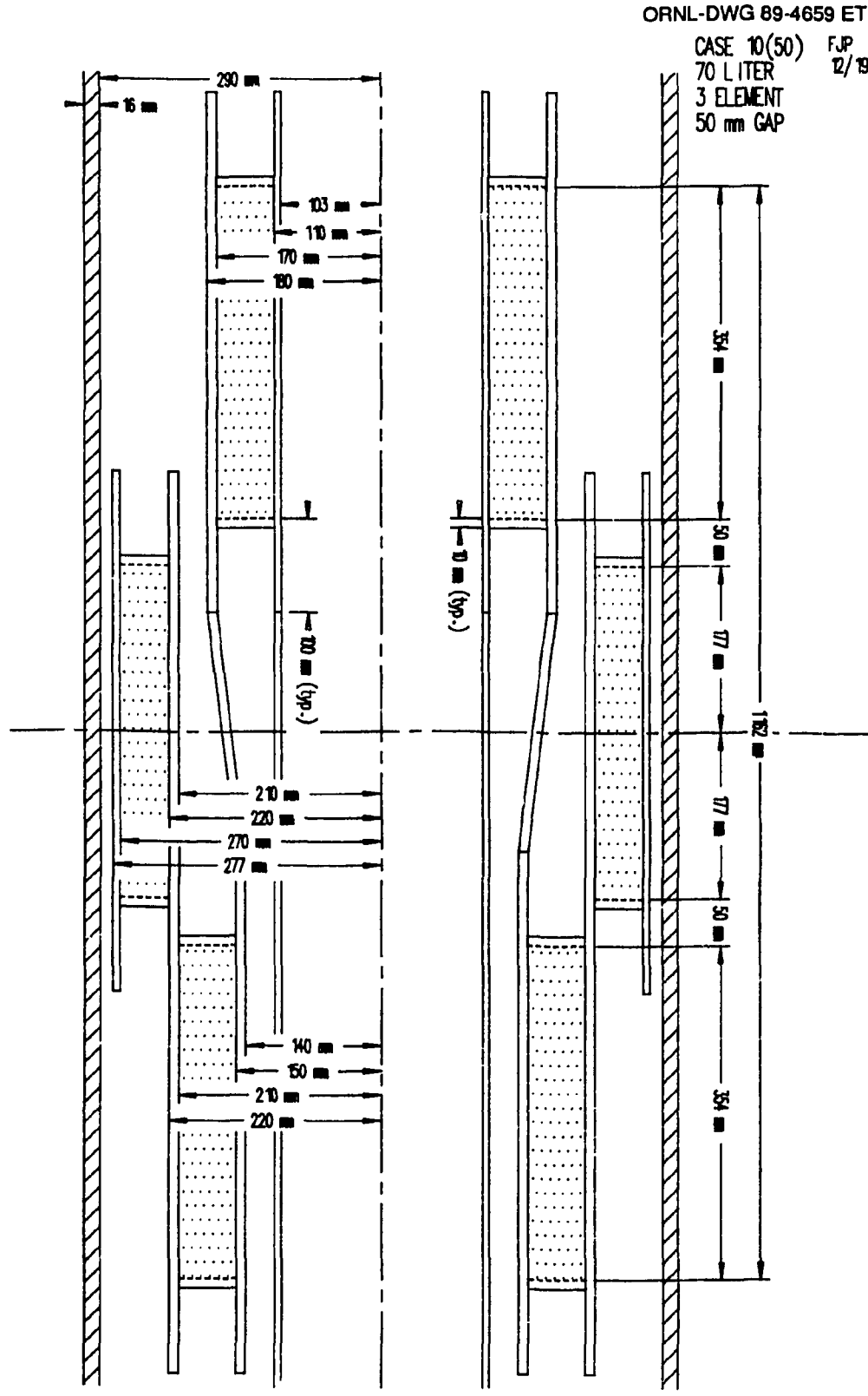

Fig. B.13. Case 10(50), three-element, offset, 70-L, 50-mm gap.

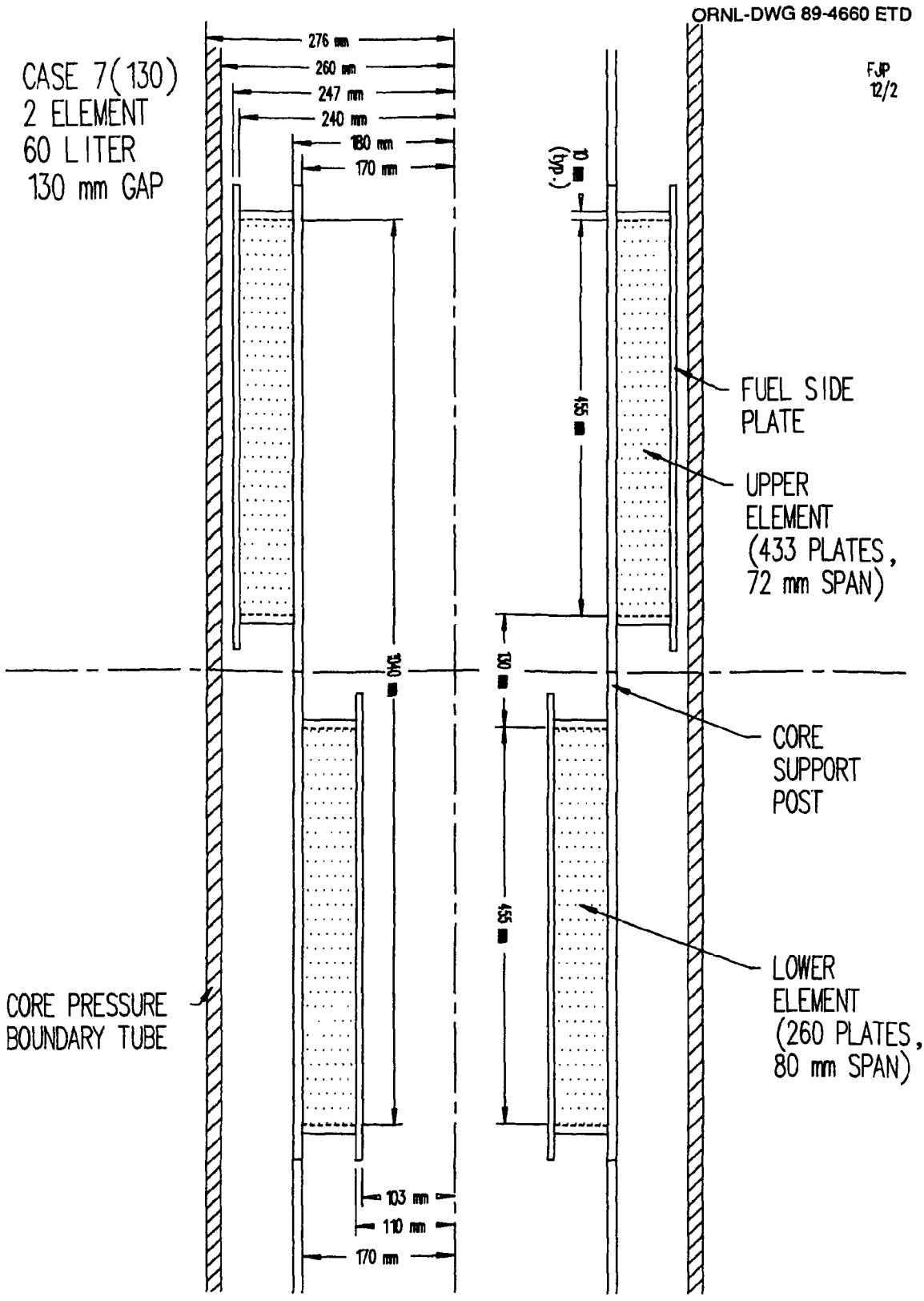

Fig. B.14. Case 7(130), two-element, offset, 60-L, 130-mm gap.

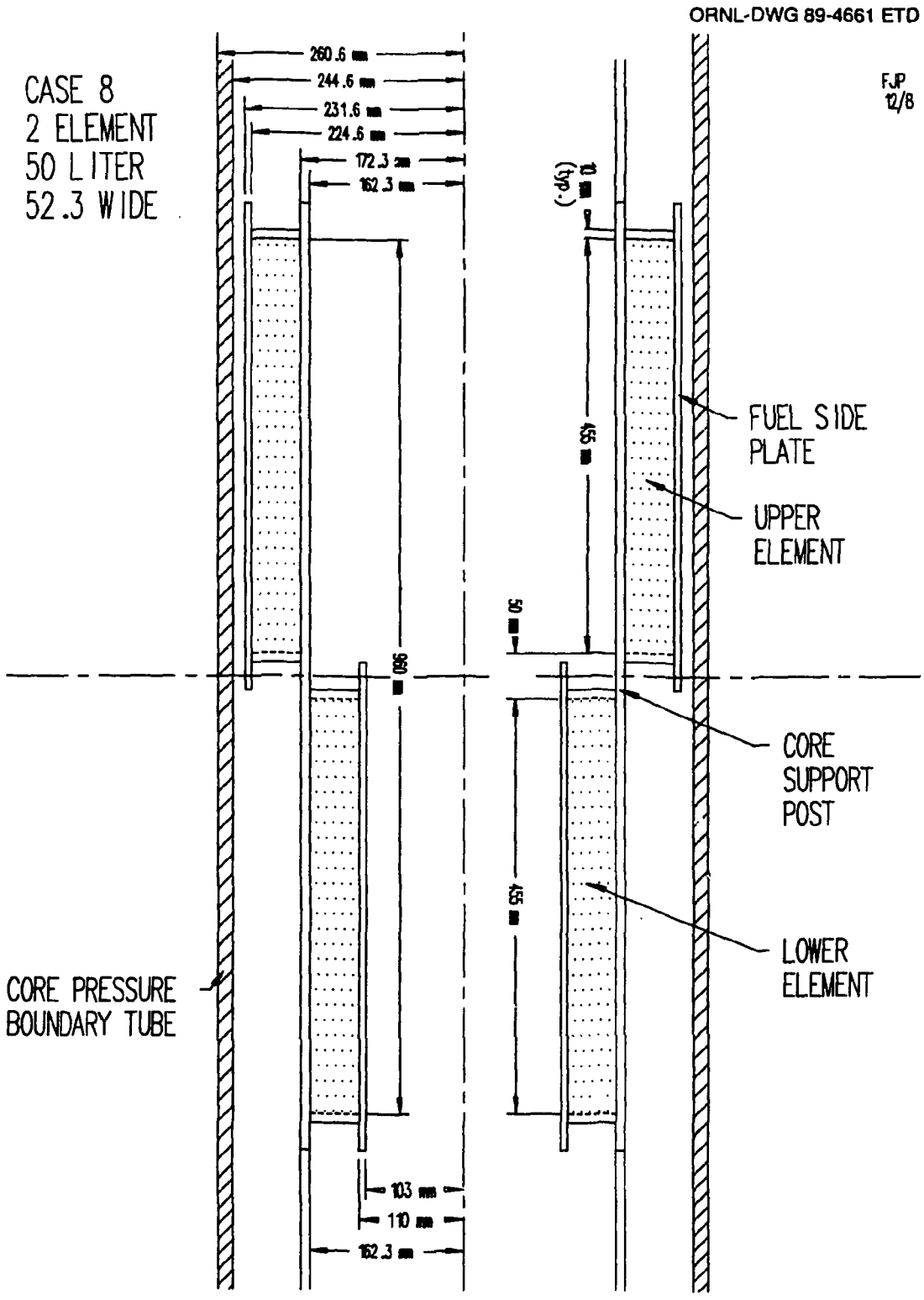

Fig. B.15. Case 8(50), two-element, offset, 50-L, 50-mm gap, narrow elements.

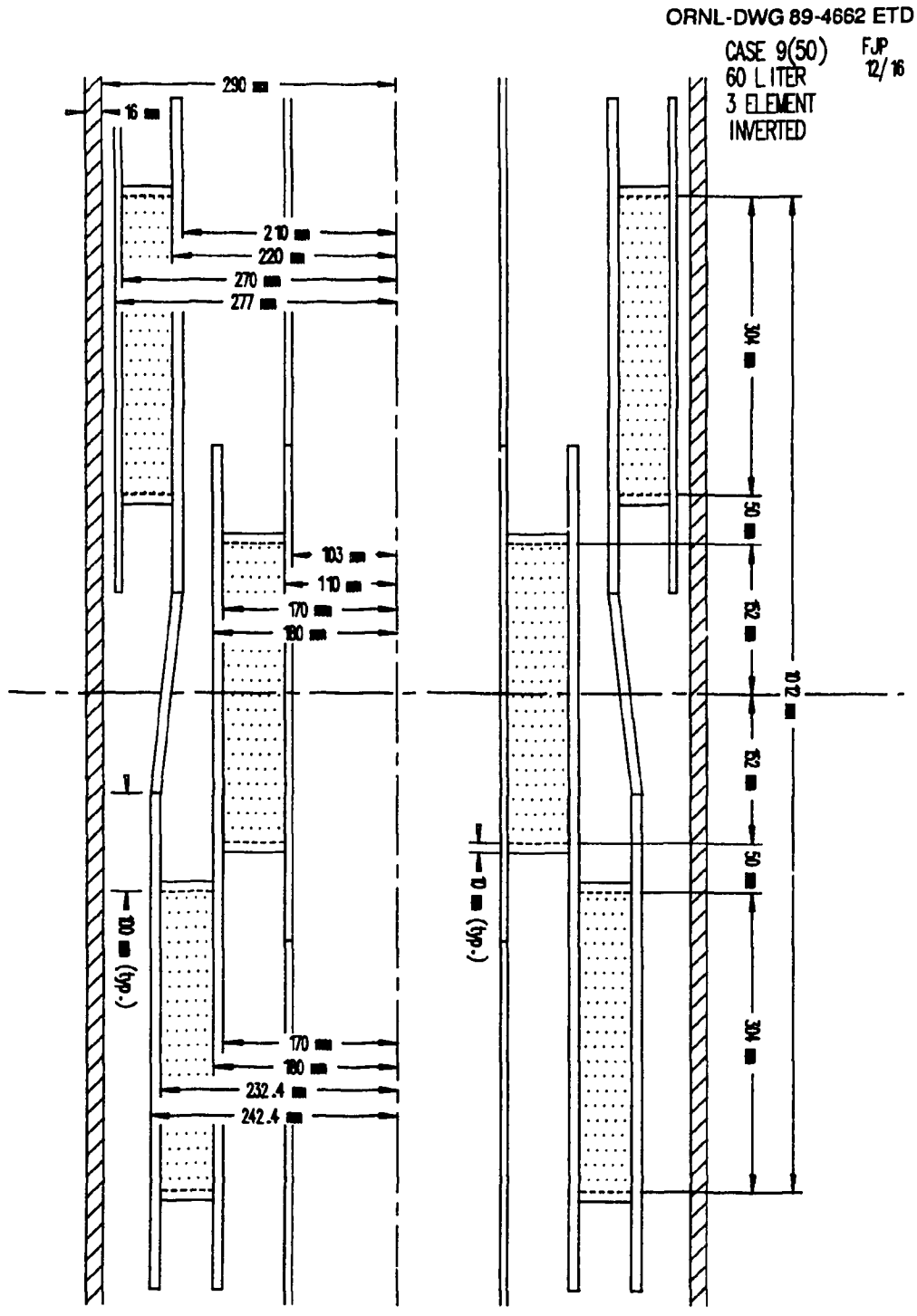

Fig. B.16. Case 9(50), three-element, offset, 60-L, 50-mm gap, inverted elements.

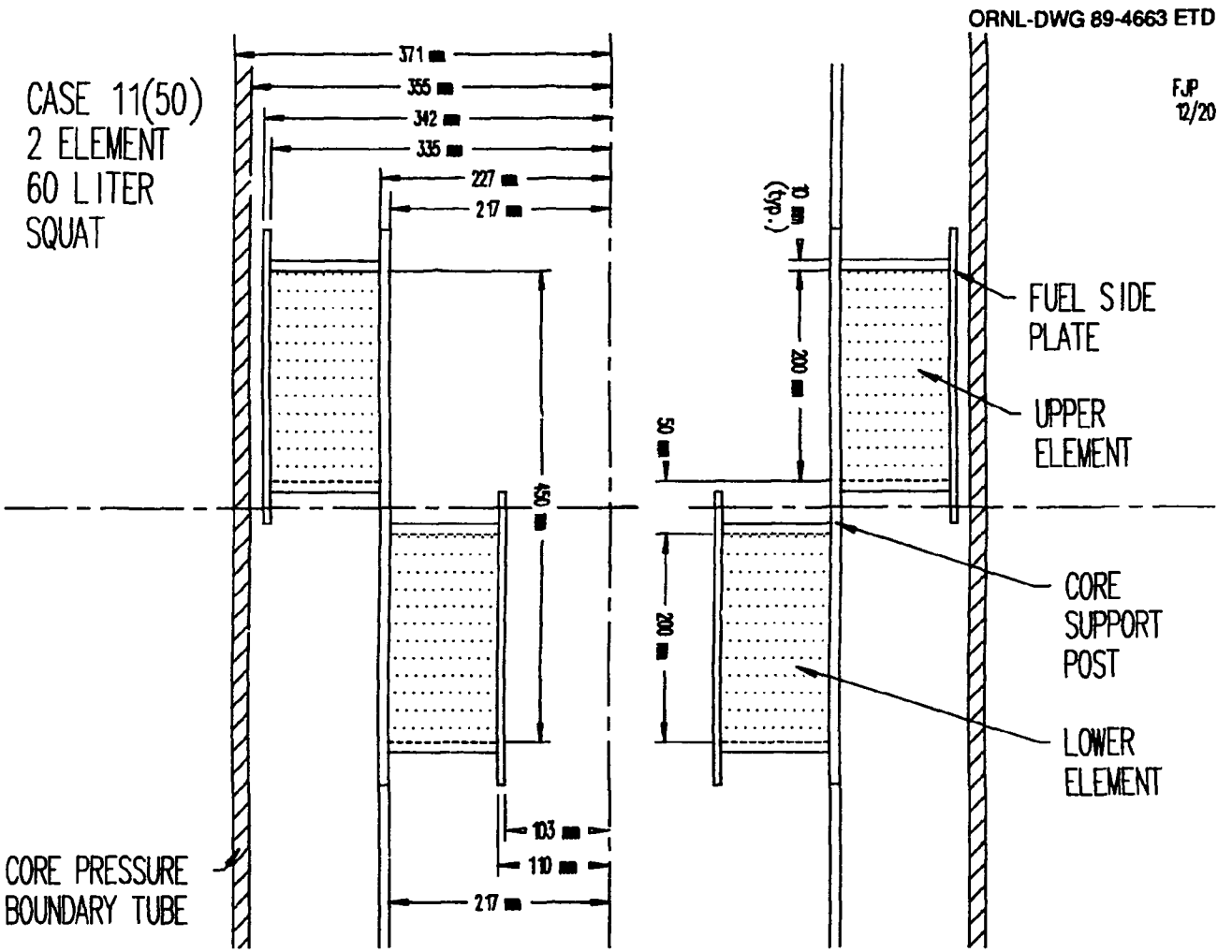

Fig. B.17. Case 11(50), two-element, offset, 60-L, 50-mm gap, squat core.

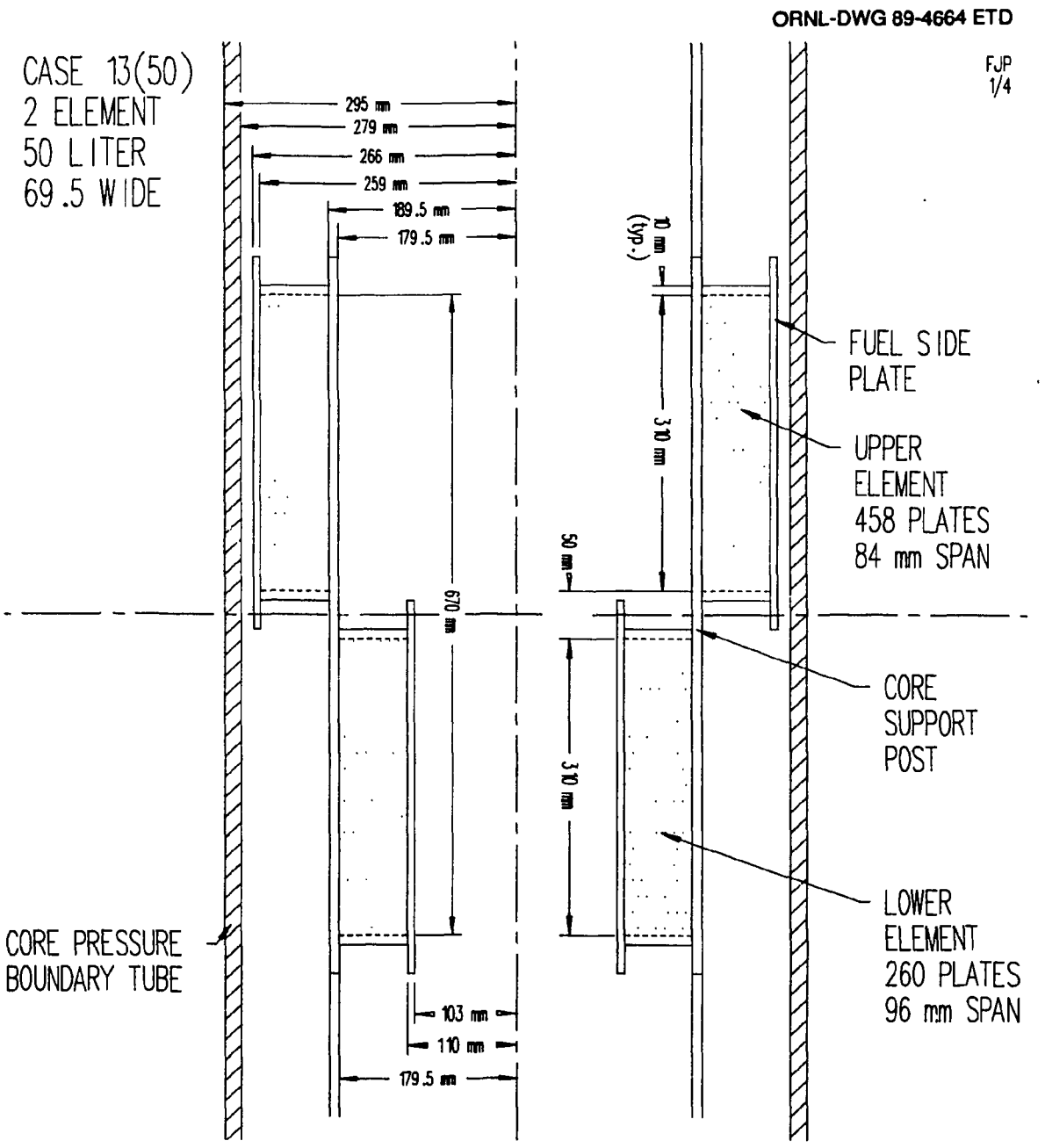

Fig. B.18. Case 13(50), two-element, offset, 50-L, 50-mm gap, 69.5-mm-wide fuel.

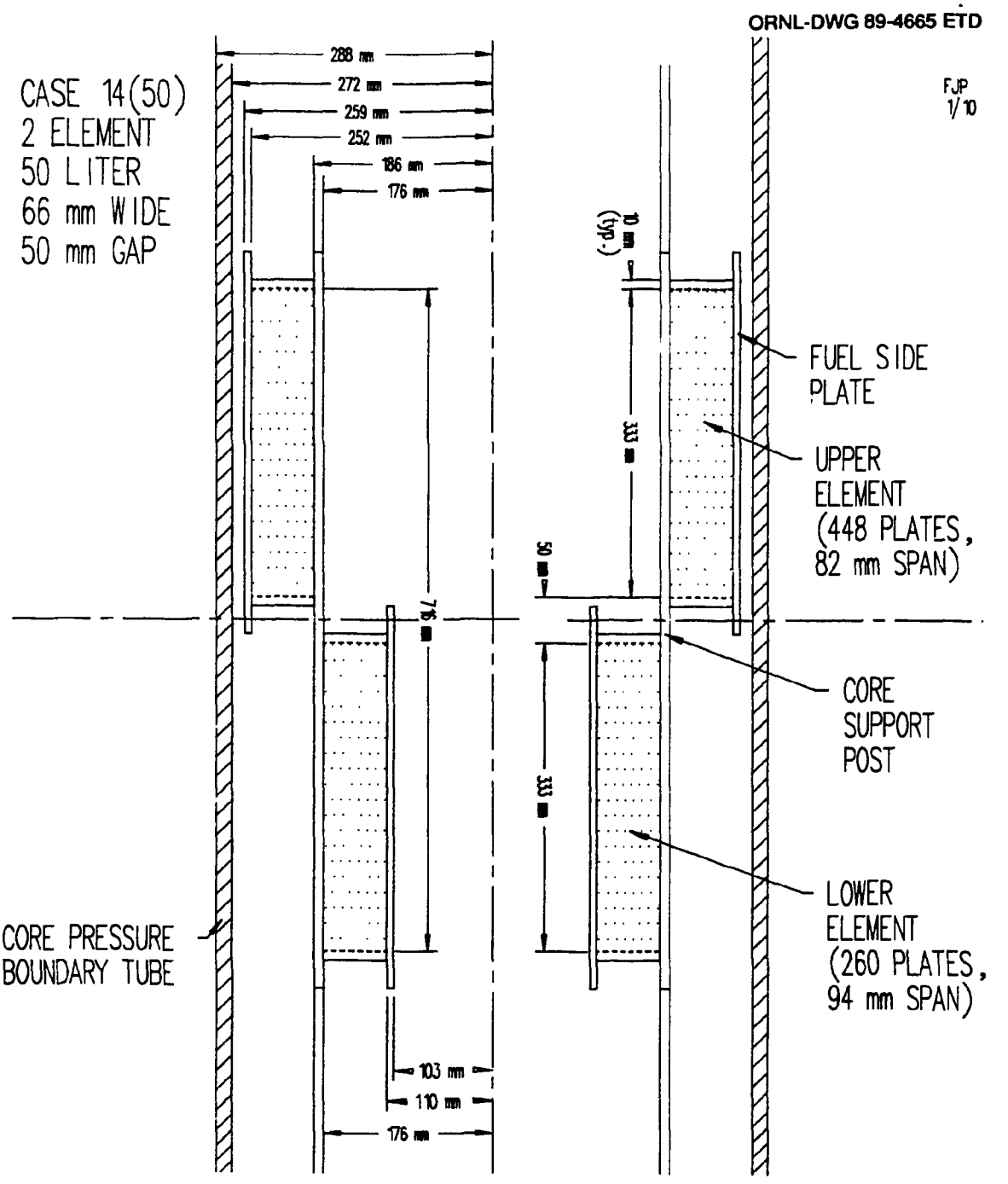

Fig. B.19. Case 14(50), two-element, offset, 50-L, 50-mm gap, 66-mm-wide fuel.

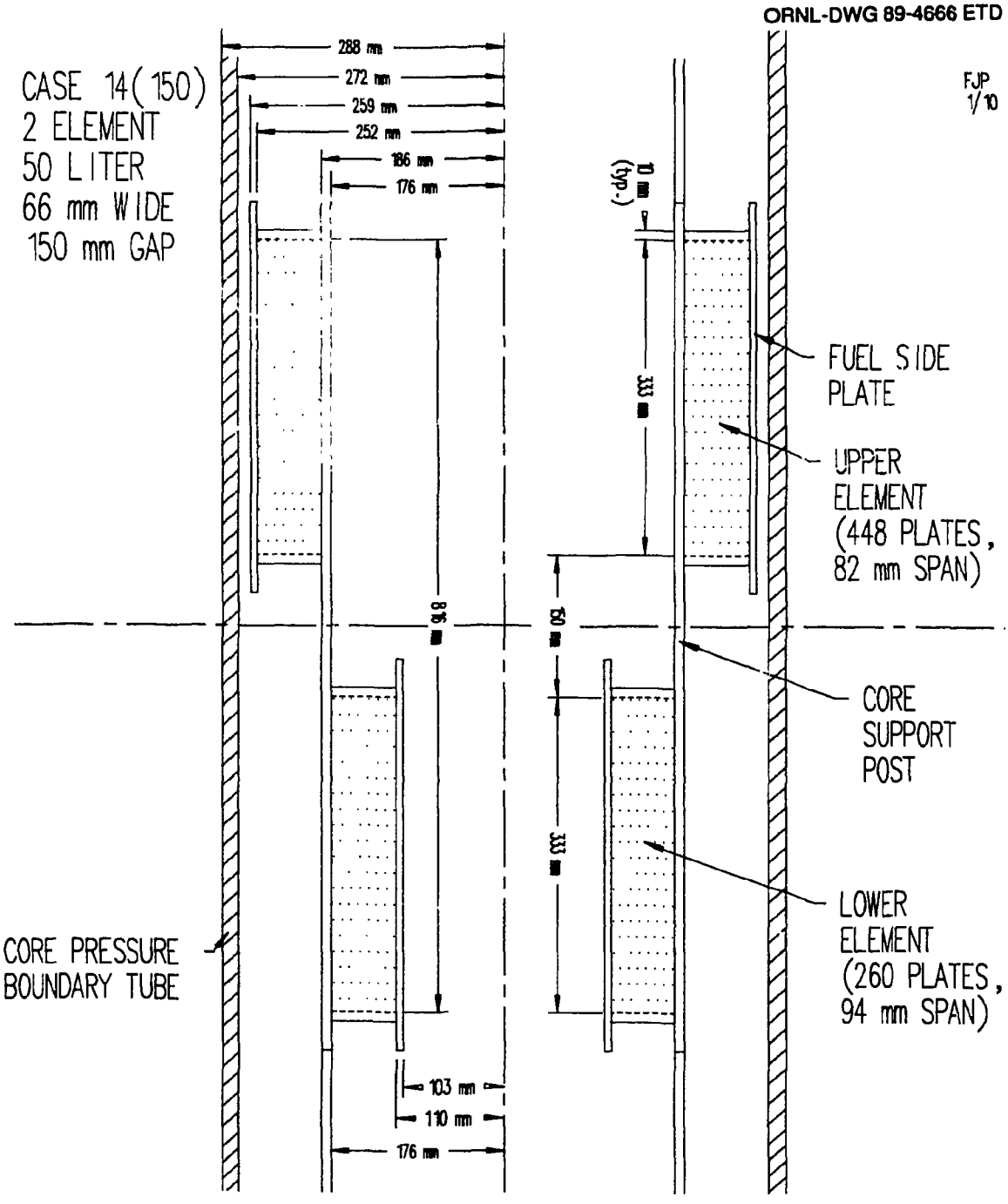

Fig. B.20. Case 14(150), two-element, offset, 50-L, 150-mm gap, 66-mm-wide fuel.

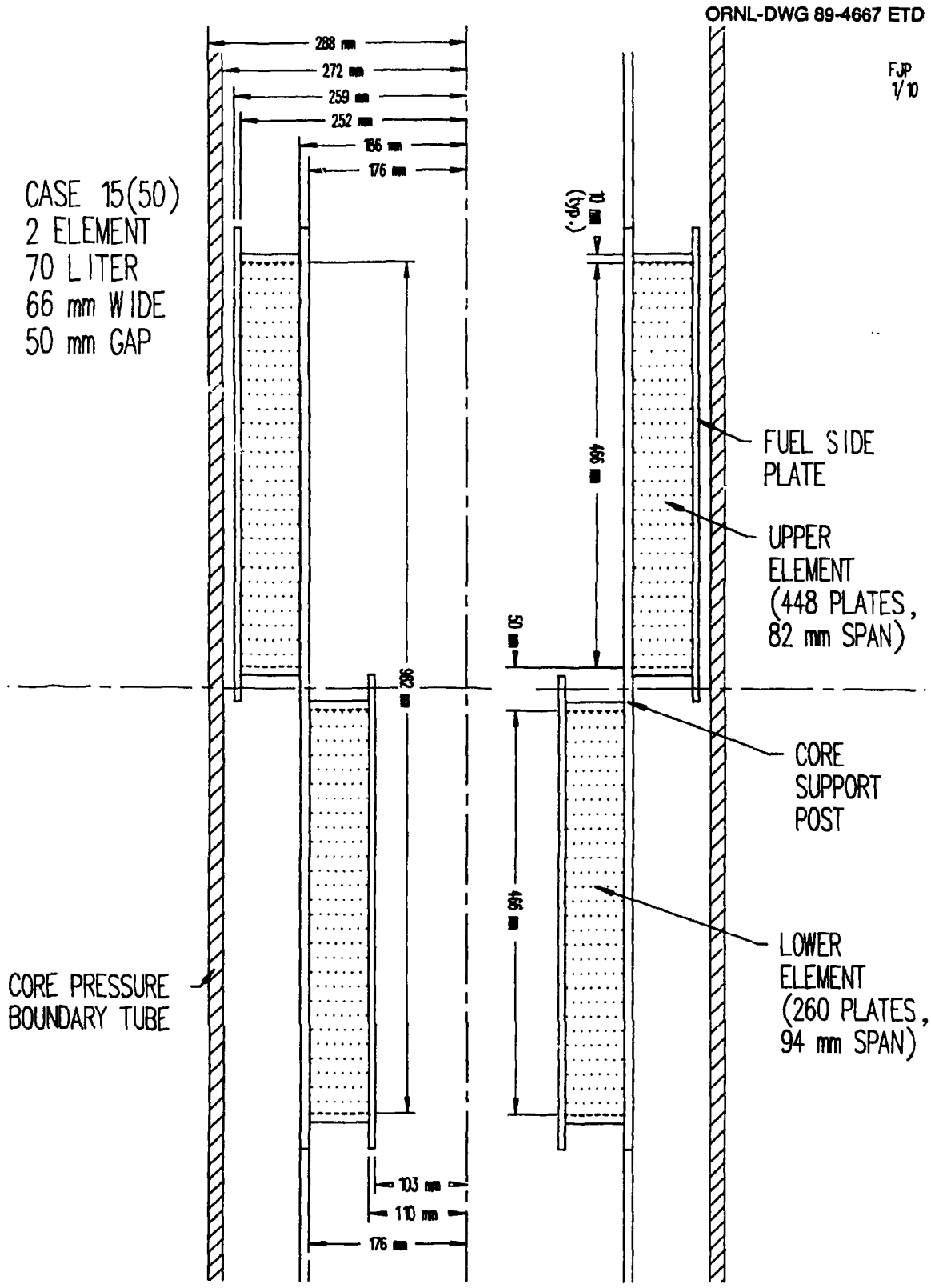

Fig. B.21. Case 15(50), two-element, offset, 70-L, 50-mm gap, 66-mm-wide fuel.

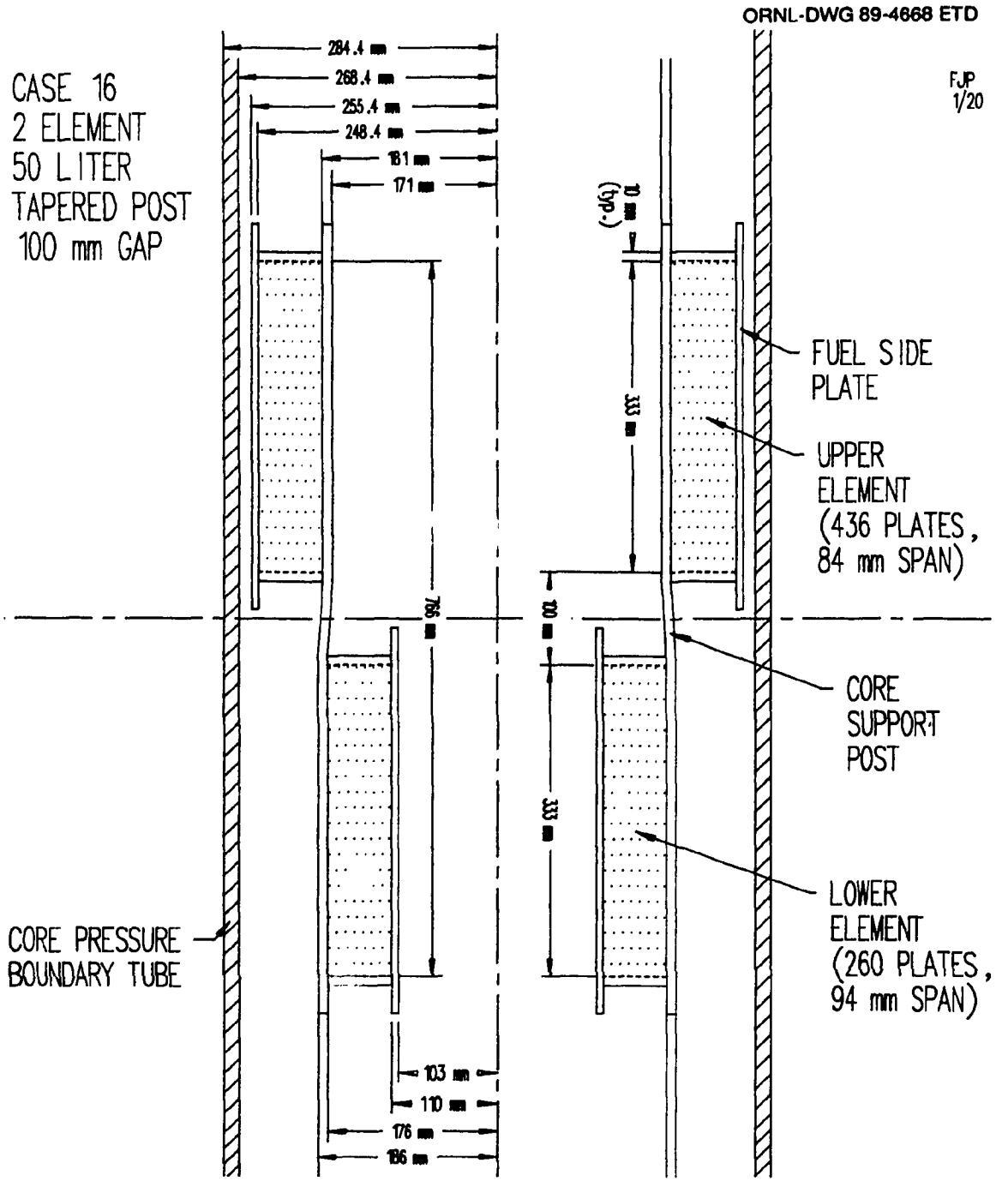

Fig. B.22. Case 16(50), two-element, offset, 50-L, 100-mm gap, tapered central post.

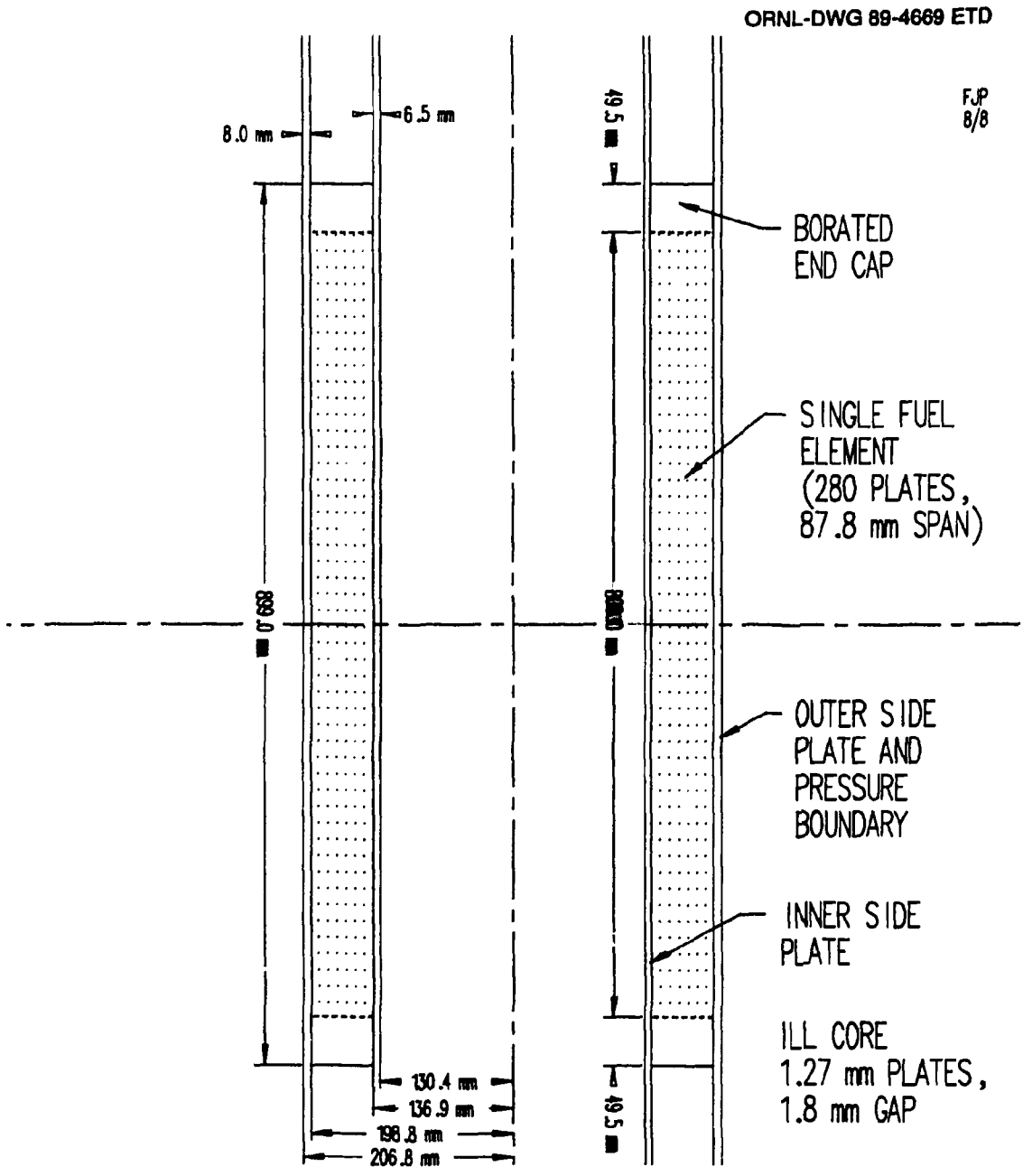

Fig. B.23. ILL reactor core.

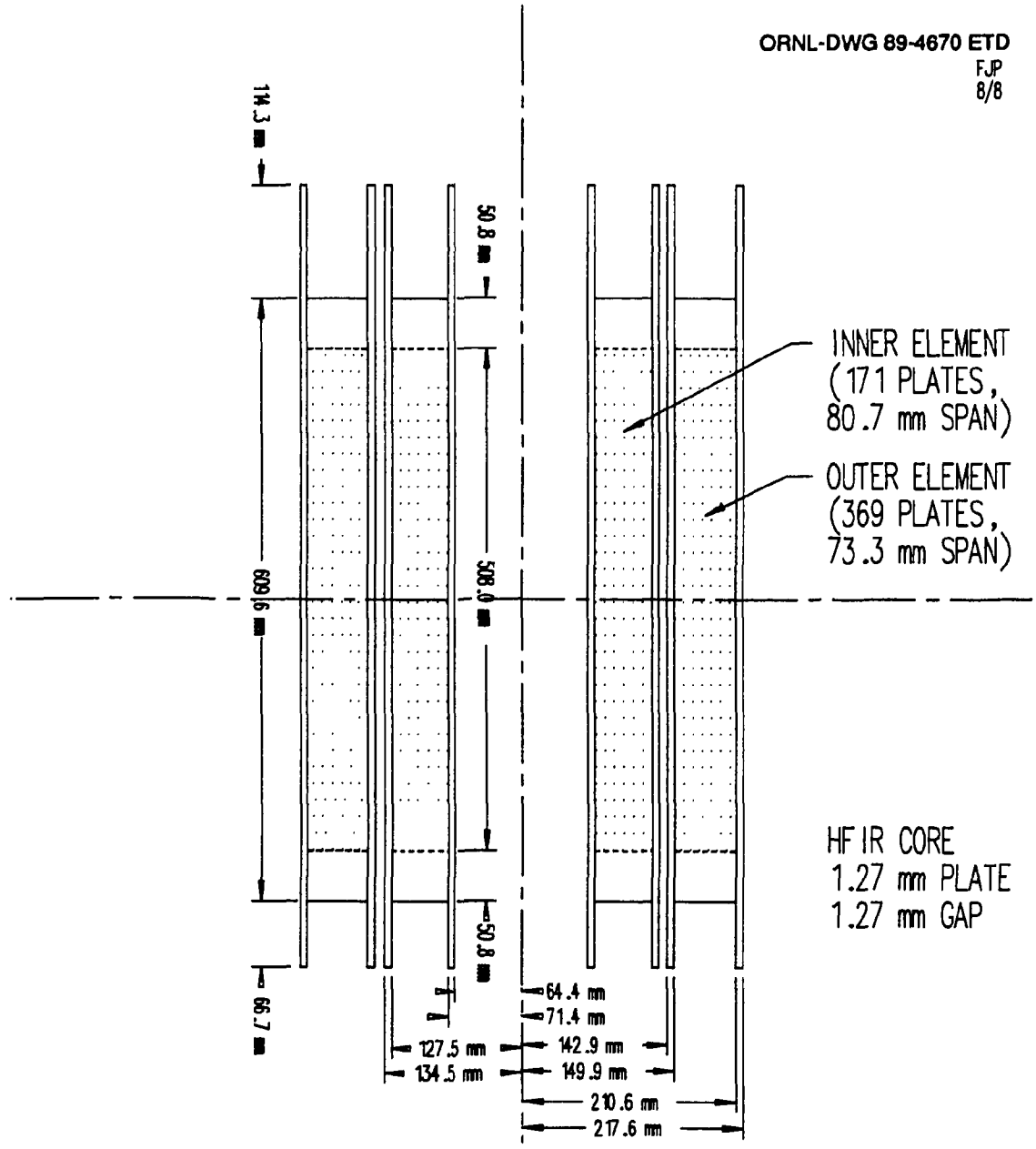

Fig. B.24. HFIR reactor core (immersed in heavy water).

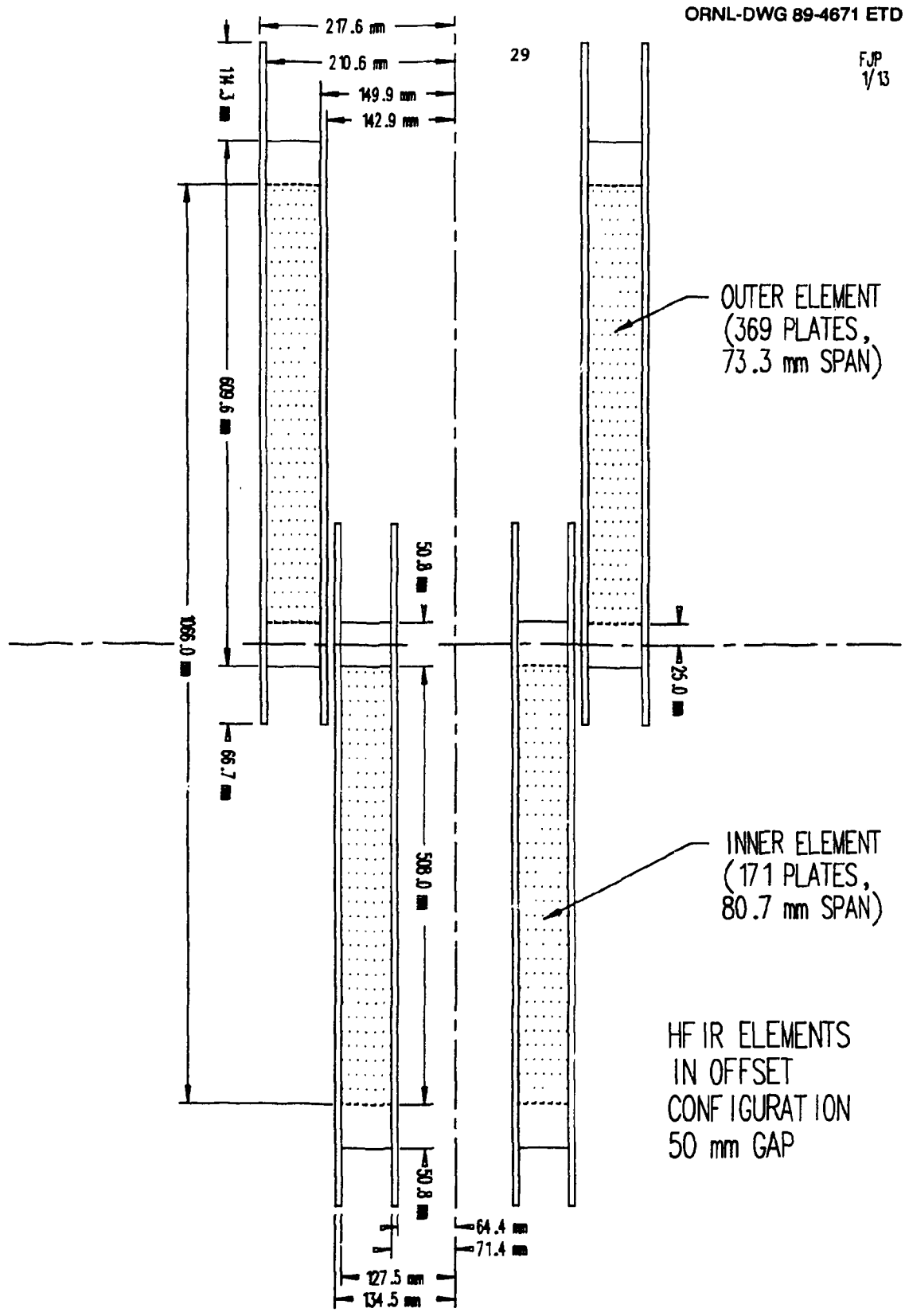

Fig. B.25. HFIR fuel elements, arranged in two-element offset configuration.

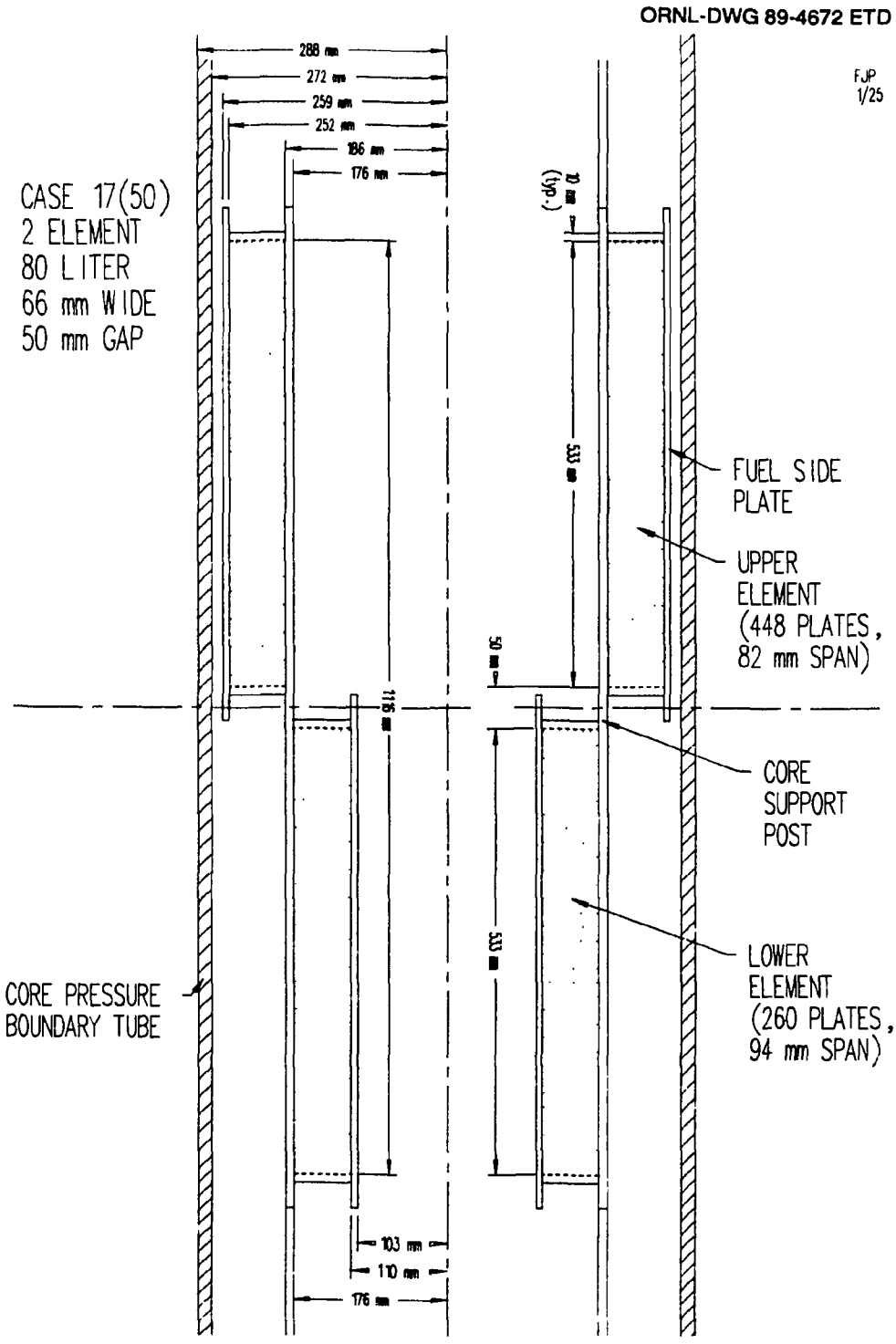

Fig. B.26. Case 17(50), two-element, offset, 80-L, 50-mm gap.

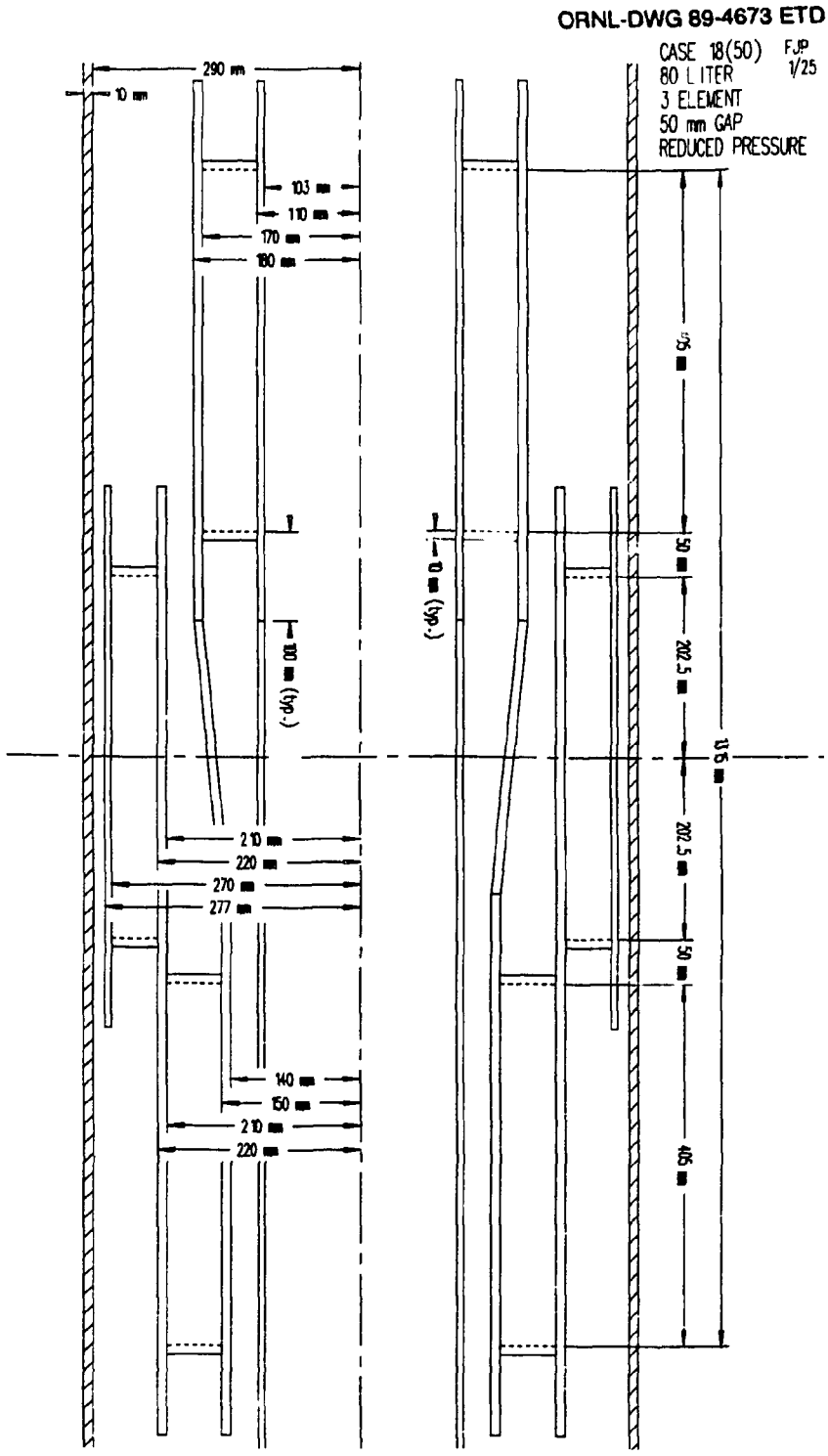

Fig. B.27. Case 18(50), three-element, offset, 80-L, 500-mm gap, reduced pressure.

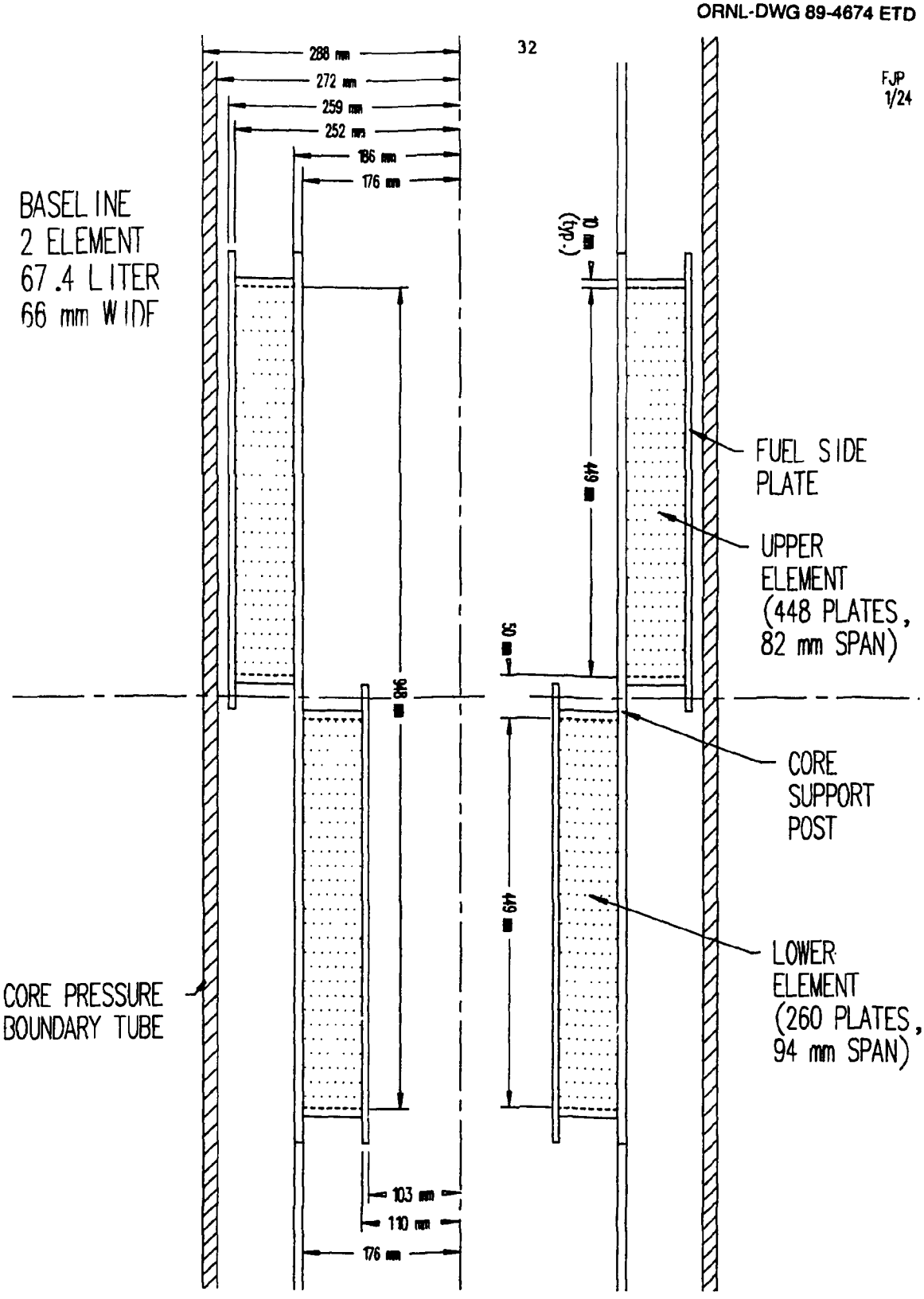

Fig. B.28. Baseline, two-element, offset, 67.4-L, 50-mm gap, 66-mm-wide fuel.

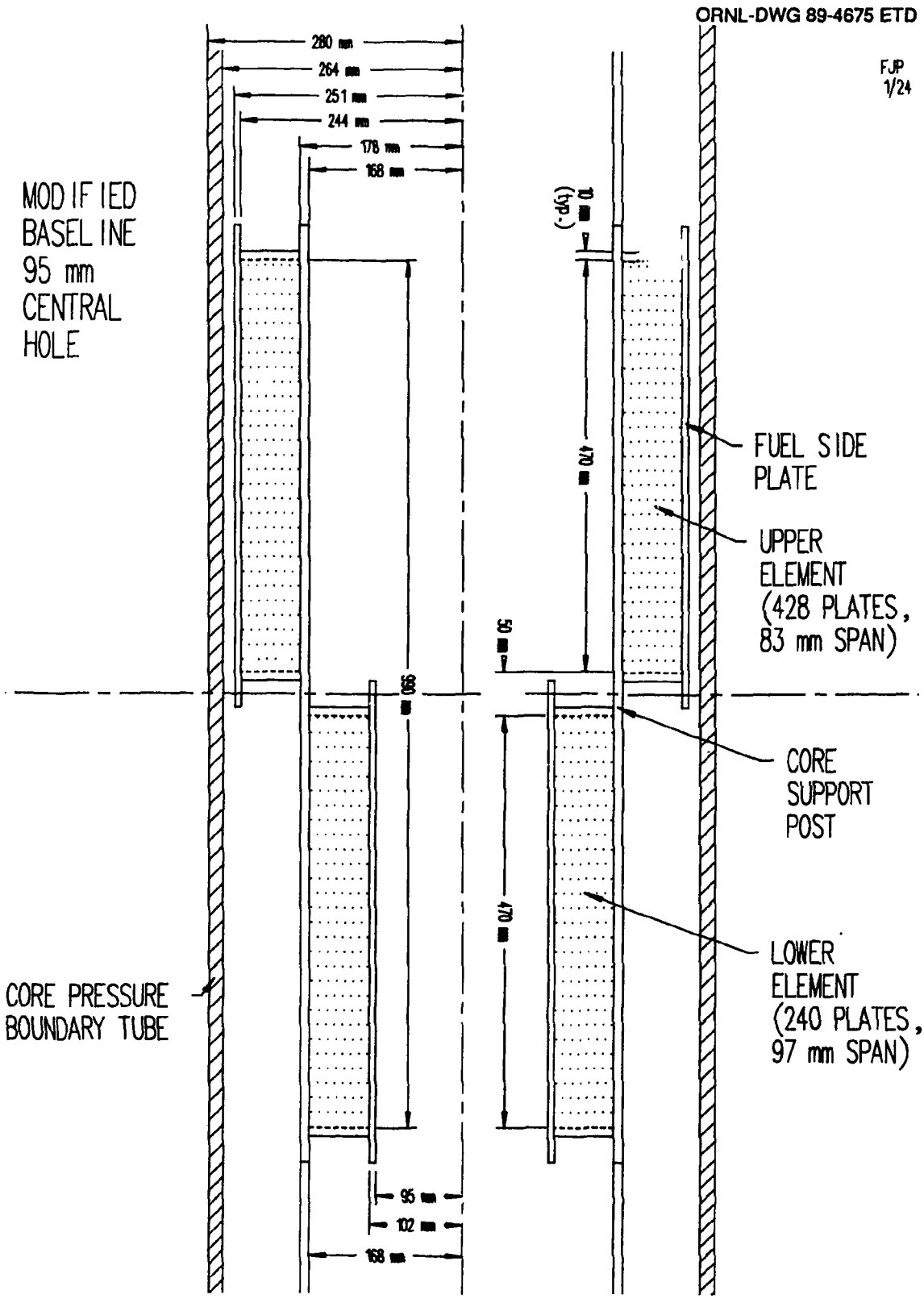

Fig. B.29. Modified baseline, 95-mm central hole.

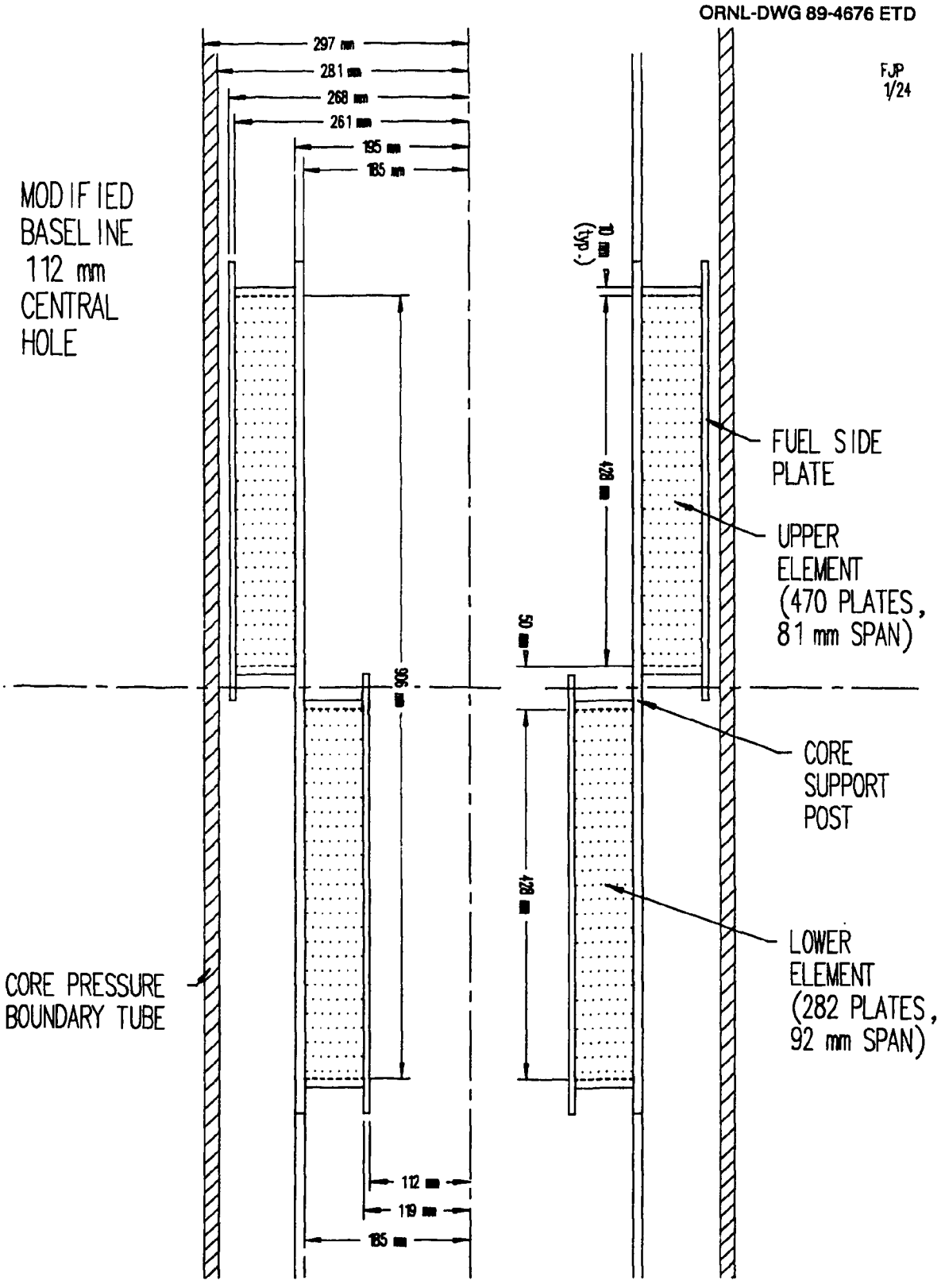

Fig. B.30. Modified baseline, 112-mm central hole.

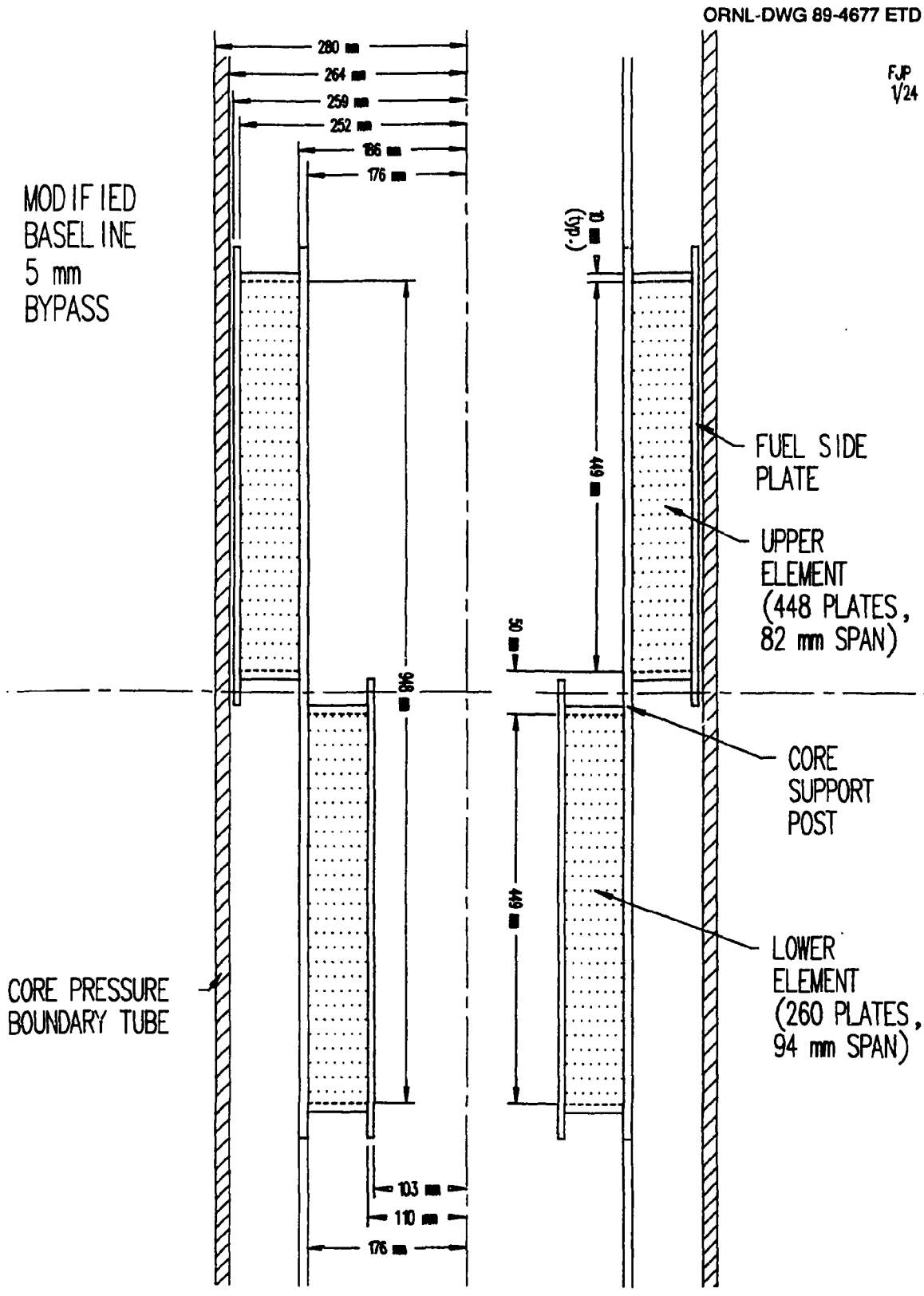

Fig. B.31. Modified baseline, 5-mm outer bypass.

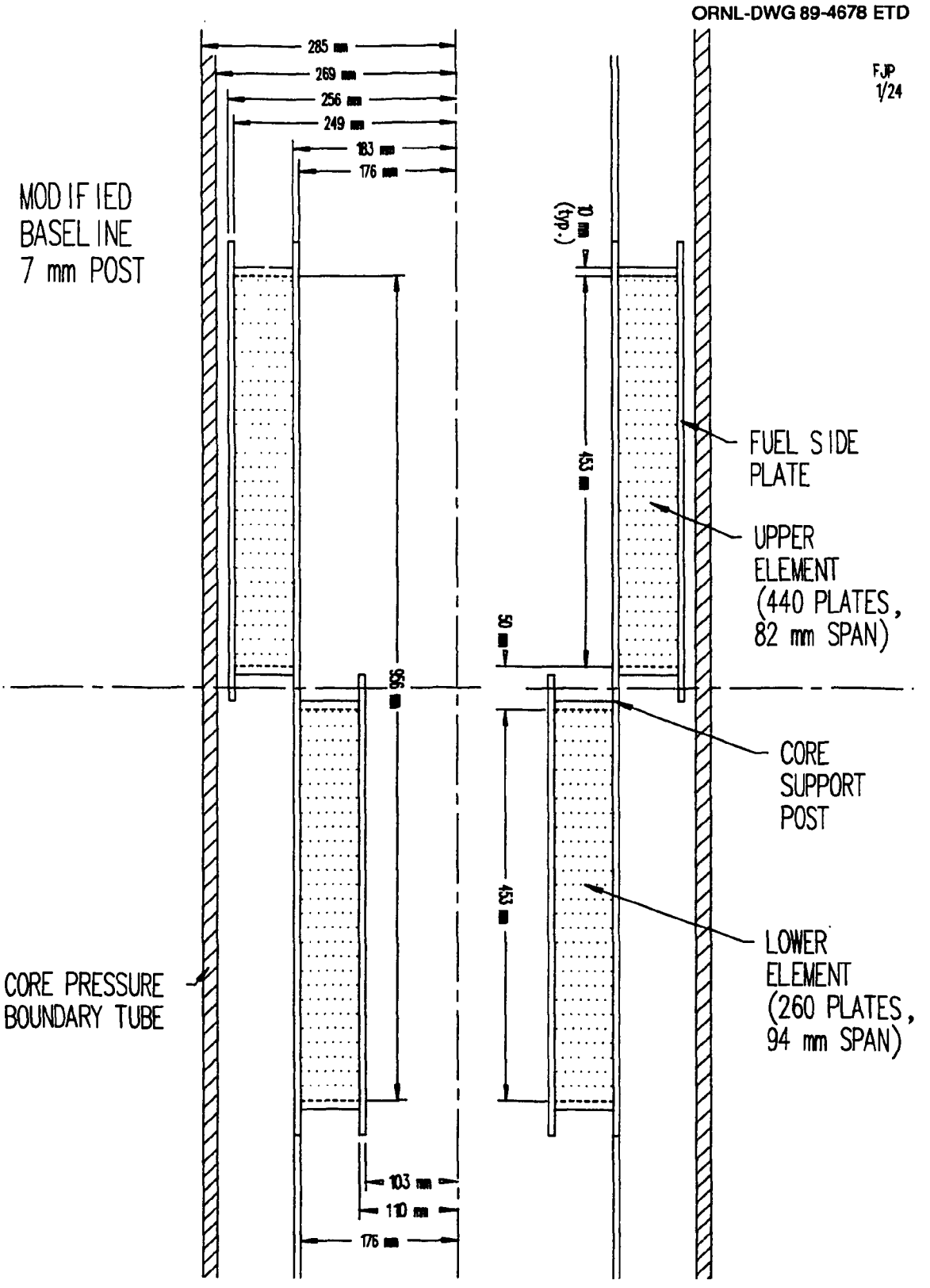

Fig. B.32. Modified baseline, 7-mm core support post.

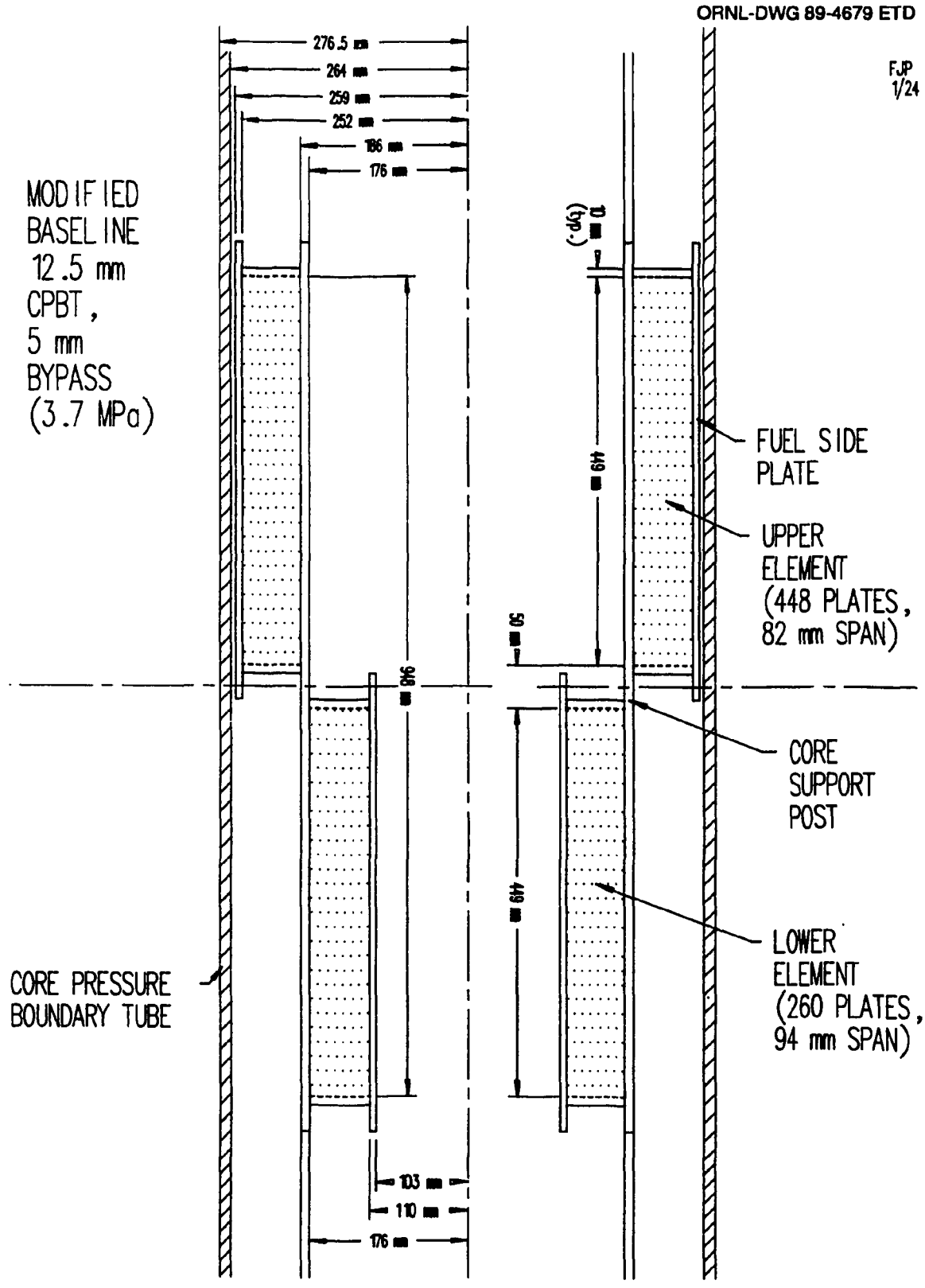

Fig. B.33. Modified baseline, 12.5-mm CPBT, 5-mm bypass.

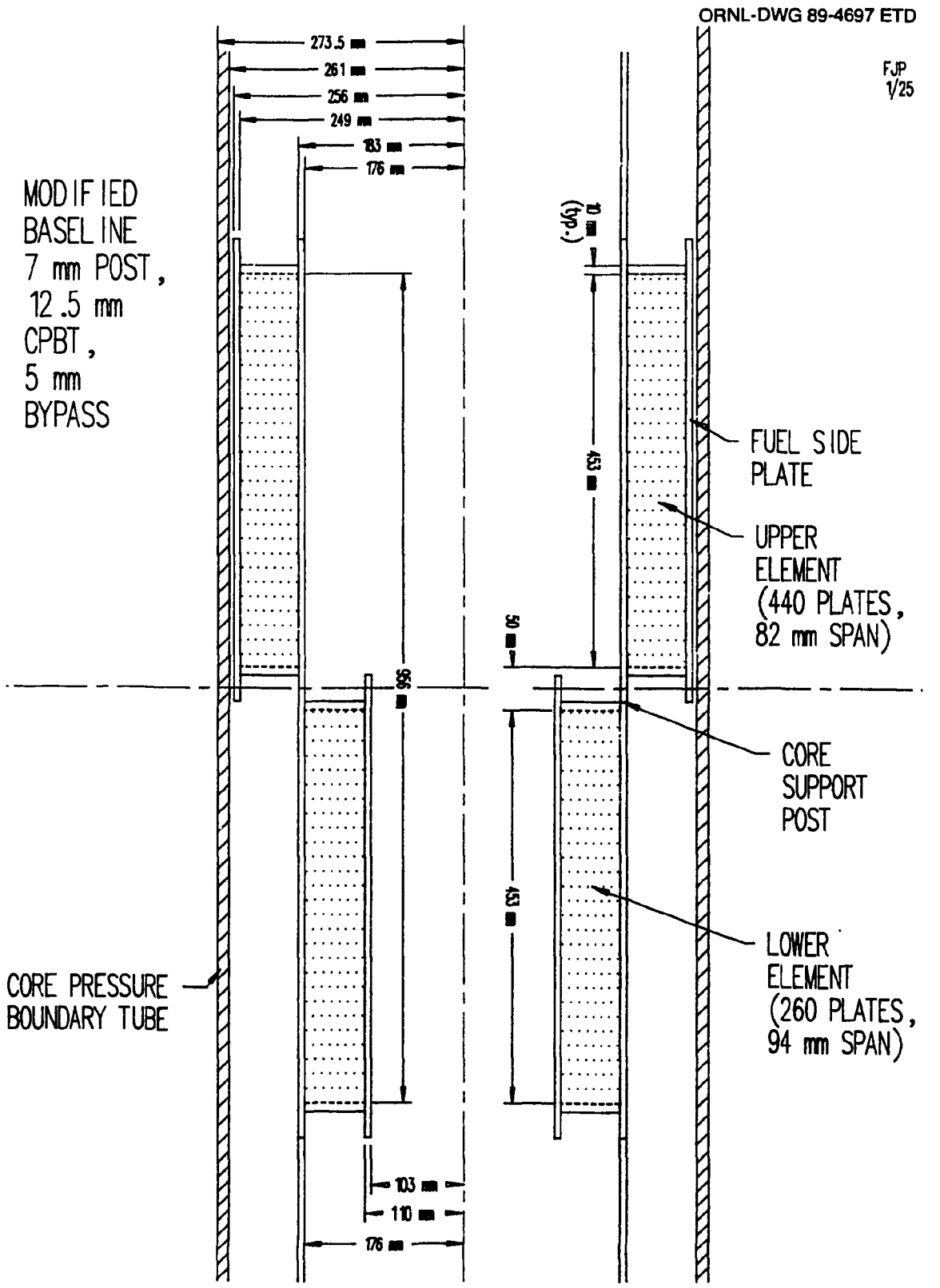

Fig. B.34. Modified baseline, 12.5-mm CPBT, 5-mm bypass, 7-mm core support post.

Appendix C

IBL CALCULATIONS

The following summarizes the method used to calculate the incipient-boiling power levels of the various cores. The thermal-hydraulic ground rules adopted by the PS-2 Committee in October 1988 and used through January 1989 corresponded to these initial factors:

a. $(\delta_c)_{hc,avg} = 1.143$ mm (10.0% less than nominal).
b. $(V_{hc})_i = 25.54$ m/s (6.9% less than nominal).
c. The nuclear hot streak factor of 1.3 combined with multiplied engineering uncertainty factors for the hot streak gave $(dt_b)_{max} = 1.9508\ (dt_b)_{avg}$.
d. The nuclear hot spot factor of 1.7 combined with multiplied engineering uncertainty factors for the hot spot gave $\phi_{max} = 2.480\ \phi_{avg}$.
e. Coolant physical properties are those of D_2O.

The calculation is iterative and consists of these steps:

1. For each fuel element, calculate the active volume = $(A_x)_{core}\ L_h$, the active surface area A_s = (Vol) (A_s/Vol), and the cross-sectional flow area $A_{xf} = (A_x)_{core}/2$.
2. Choose one fuel element for the computations to follow.
3 Assume a core thermal power (q).
4. Reference element q = core of (element vol./core vol.).
5. $W_{core} = \rho_i\ A_{xf}\ V_i$.
6. $(dt_b)_{avg} = q/W\ Cp$.
7. $(t_{b,o})_{avg} = t_{b,i} + (dt_b)_{avg} = 49°C + (dt_b)_{avg}$.
8. $\phi_{avg} = q/A_s$.
9. $\phi_{max} = 2.480\ \phi_{avg}$.
10. $(t_{b,o})_{max,hst} = 49.5°C + 1.9508\ (dt_b)_{avg}$.

11. Calculate h_{nom}, with the Petukhov correlation, at $t_b = (t_{b,o})_{max}$.*

12. $h_{des} = 0.94\ h_{nom}$.

13. $(\Delta t_{b\ell})_{max} = \phi_{max}/h_{des}$.

14. $(\Delta t_{ox})_{max} = \dfrac{\phi_{max}\ \delta_{ox}}{k_{ox}}$. [Taken as zero at BOC.]

15. $(\Delta t_{clad})_{max} = \dfrac{\phi_{max}\ \delta_{clad}}{k_{clad}}$.

16. $(\Delta t_{fuel})_{max} = \dfrac{\phi_{max}\ \delta_{fuel}}{4\ (k_{fuel})_{min}}$. [Volumetric heat generation.]

17. $(t_{fuel})_{max} = (t_{b,o})_{max} + (\Delta t_{b\ell})_{max} + (\Delta t_{ox})_{max}$
$+ (\Delta t_{clad})_{max} + (\Delta t_{fuel})_{max}$.

18. If $(t_{fuel})_{max}$ [step 17] is $\leq$400°C, continue; if >400°C, the hot plate is temperature, not incipient boiling, limited.

19. $\Delta P_{core} = (P_i - P_o)_{core}$.

20. $P_{ib} = (P_o)_{hc} = P_i - \Delta P_{core} - (\Delta P_o)_{hc}$.

21. Look up t_{sat} at P_{ib}.

22. $(\Delta t_{sub,o})_{min} = t_{sat} - (t_{b,o})_{max}$.

23. Calculate $\phi_{ib} = h_{des}\ [\Delta t_{sat} + (\Delta t_{sub,o})_{min}]_{ib}$.

---

*Optional addition to step 11:

The dimensionless Petukhov correlation for turbulent flow is

$$(Nu_b)_x = \frac{(f/8)Re_b Pr_b (\mu_b/\mu_w)^{0.11}[1 + 1/3(D/L)^{2/3}]}{(1 + 3.4f) + \left(11.7 + \dfrac{1.8}{Pr^{1/3}}\right)(f/8)^{1/2}\ (Pr_b^{2/3} - 1)}$$

in which $f = [1.82 \log Re_b - 1.64]^{-2}$.

24. Calculate the incipient-boiling locus value from the correlation of Bergles and Rohsenow:

$$(\phi_{ib})_{\ell} = 15.29\ P^{1.156}\ (\Delta tsat)^{2.30}/P^{0.0234}\ ,$$

in which the lead coefficient of 15.6 for H_2O has been reduced by 2% by W. R. Gambill based on two-point calculations for D_2O.

25. Simultaneously solve the equations from steps 23 and 24; this gives $(\Delta t_{sat})_{ib}$ and ϕ_{ib}.

26. Calculate ϕ_{max}/ϕ_{ib}; if this ratio is within $\pm$0.8% of unity (typically within $\pm$0.3% for these core cases), the power assumed in step 3 is taken as the ib power. If not, reiterate from step 3. The typical number of trials was three.

Notation for Appendix C

A	area
C_p	coolant heat capacity
dt_b	increase of t_b
h	heat transfer coefficient
k	thermal conductivity
L	length
P	pressure
ΔP	pressure change
q	thermal power
t_b	bulk coolant temperature
t_{sat}	coolant saturation temperature
Δt	temperature difference
Δt_{sat}	surface superheat
Δt_{sub}	coolant subcooling
V	velocity of coolant
W	weight flow rate of coolant
δ	thickness, gap
Δ	difference
ρ	coolant density
ϕ	surface heat flux

Subscripts

$b\ell$	boundary layer
c	coolant
des	design
f	flow
h	heated
hc	hot channel
hst	hot streak
i	flow inlet
ib	incipient boiling
ℓ	locus

nom	nominal
o	flow outlet
ox	oxide
s	surface
x	cross sectional

Appendix D

NEUTRONICS PARAMETERS OF VARIOUS ALTERNATIVE OFFSET UNGRADED CORE DESIGNS AT BOC

Figure No.[a]	R. T. Primm ID No.[b]	Fueled volume (L)	Number of elements	Fueled length (mm)	^{235}U loading (kg)	Reactivity	Rendement (m^{-2})
B.7	2 (50)	41	2	310	22	1.252	3.287
B.10	3 (50)	41	3	208	22	1.248	2.924
B.11	4 (50)	50	3	254	22	1.273	2.757
B.12	5 (50)	60	3	304	22	1.281	2.598
B.8	6 (50)	50	2	379	22	1.273	3.082
B.8	6 (50)	50	2	379	19.5	1.262	3.139
B.9	7 (50)	60	2	455	22	1.292	2.887
	8	50	2	455	22	1.206	3.045
B.16	9 (50)	60	3	304	22	1.288	2.544
B.13	10 (50)	70	3	354	22	1.291	2.465
B.17	11 (50)	60	2	200	28	1.264	2.600
B.18	13 (50)	50	2	310	22	1.259	3.071
B.19	14 (50)	50	2	333	22	1.252	3.064
B.21	15 (50)	70	2	466	22	1.289	2.733
B.28	Baseline	67.4	2	449	22	1.285	2.770
B.33	Baseline[c]	67.4	2	449	22	1.317	2.826
B.33	Baseline[c]	67.4	2	449	17.5	1.295	2.927
	Milestone	66.5	2	467	16.3[d]	1.295[e]	3.034
	Milestone	66.5	2	467	14.5	1.283	3.088
	FPCD[f]	67.4	2	474	14.9	1.287[g]	3.058[h]
B.2	2 (130)	41	2	310	22	1.247	3.195
B.3	3 (118)[i]	41	3	208	22	1.239	2.755
B.5	5 (124)[j]	60	3	304	22	1.268	2.485
B.14	7 (130)	60	2	455	22	1.283	2.827
	14 (150)	50	2	333	22	1.241	1.283
B.6	12	50	2[k]	526	22	1.258	3.375
B.1	1 (150)	41	2[k]	431	22	1.254	3.423

[a]Appendix B.

[b]Number in parentheses is the plenum thickness (mm) between the fueled regions of the elements.

[c]Modified baseline design with CPBT thickness reduced to 12.5 mm and support post thickness reduced to 7 mm. The figure in Appendix B shows a fueled length of 453 mm, but the neutronics calculations assumed a length of 449 mm.

[d]Value at 14 d into the 350-MW(f) cycle = 1.084.

[e]Value at 14 d into the 350-MW(f) cycle = 3.130.

[f]Final preconceptual core design.

[g]Value at 14 d into the 350-MW(f) cycle = 1.062.

[h]Value at 14 d into the 350-MW(f) cycle = 3.177.

[i]Although designated 3 (118), the plenum thickness between fueled regions was probably 138 mm (in which case the plenum region between the ends of the aluminum fuel plates would be 118 mm).

[j]Although designated 5 (124), the plenum thickness between fueled regions was probably 144 mm (in which case the plenum region between the ends of the aluminum fuel plates would be 124 mm).

[k]In line.

Appendix E

CONFIRMATION OF RENDEMENT VS EFFECTIVE HEIGHT CORRELATION FOR THREE-ELEMENT CORES

The three-element core data in Table 4 of the main text were later amended and extended to cover a wider range of core volumes. The extended data set is shown in Table E.1 below.

These points are plotted, along with a least-squares fit straight line in Fig. E.1. The equation of the line (as determined by the TK SOLVER linear regression routine) is

$$\text{rendement} = 3.41 - 0.00064 \times \text{heated length per element} ,$$

and the correlation coefficient is 0.981. Over the range of interest, (heated lengths from about 300 to 500 mm) the values calculated from the equation differ by <0.25% from the values calculated from the formula, used by the PS-2 Committee, obtained from the three data points shown in Table 3 of the main text.

Table E.1. Effective core height and corrected rendement (adjusted to $K_{eff} = 1.25$) for three-element cores with 22-kg fuel loading

Fueled volume (L)	Plenum gap (mm)	Heated length (mm)	Effective height (mm)	K_{eff}	Rendement (m^{-2})	Corrected[a] rendement (m^{-2})	Figure No.[b]
41	50	208	774	1.248	2.924	2.91	B.10
41	138	208	1038	1.239	2.755	2.70	B.3
50	50	254	912	1.273	2.757	2.86	B.11
60	50	304	1062	1.281	2.598	2.73	B.12
60	144	304	1344	1.268	2.485	2.56	B.5
70	50	354	1212	1.291	2.465	2.63	B.13

[a] Corrected $K_{eff} = 1.25$.

[b] Appendix B.

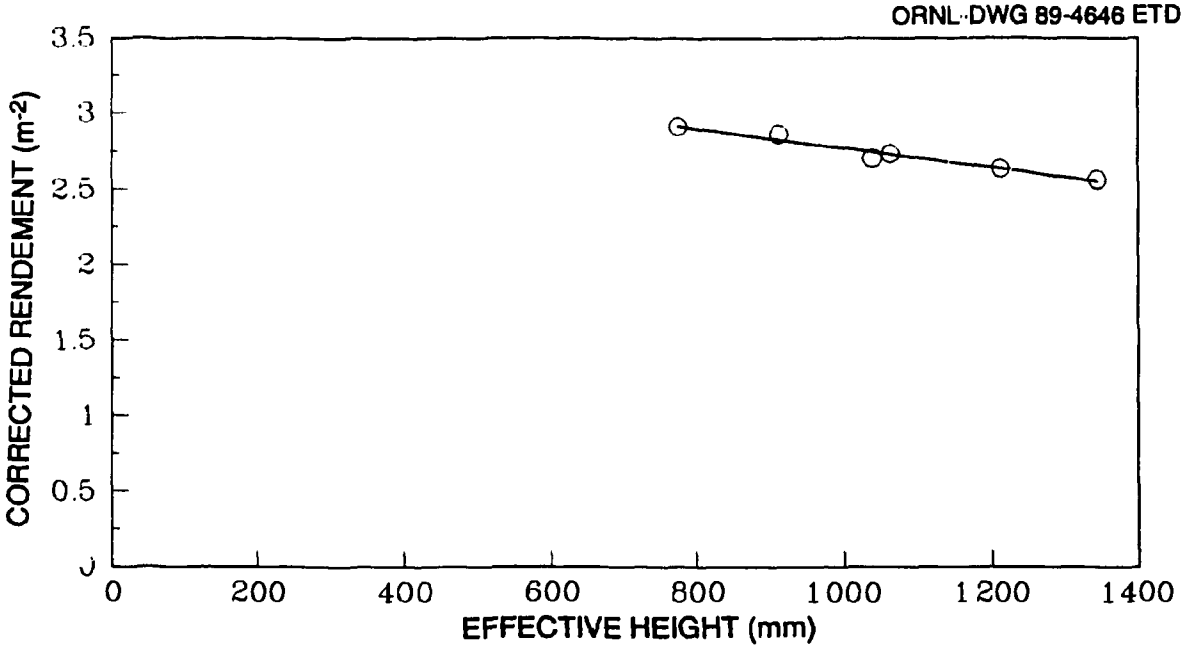

Fig. E.1. Corrected rendements vs effective height for three-element cores with 22-kg fuel cladding.

Appendix F

OXIDE FORMATION

It is known that under high heat flux conditions, a layer of low thermal conductivity boehmite (hydrated aluminum oxide) forms on the cladding of water-cooled, aluminum-fueled reactors. The phenomenon was studied during design of the HFIR, and a correlation between water interface temperature and oxide growth rate was derived by Greiss[1] on the basis of out-of-pile tests. The Greiss correlation did not include heat flux as a variable, except indirectly through its effect on surface temperature. Another correlation, from unpublished Savannah River Plant data, did include heat flux.[2] Recent analysis by INEL of experimental data from the ATR showed oxide thicknesses in the range of one-third to one-half that predicted by the Greiss correlation. Still more recently, results from out-of-pile experiments on the ANS corrosion loop at ORNL, under higher heat flux conditions than previously explored, showed oxide thicknesses of as little as one-third, or as much as three times the value predicted by the Griess correlation, depending upon water chemistry. The ANS tests and ATR data also indicated[3] that after some time the oxide layer spalls off, so that the temperature rise across the oxide, due to the heat flux, did not exceed ~140°C; however, after spallation voids or impurities in the aluminum substrate reduce the effective thermal conductivity of the clad and may unacceptably impair its integrity.

Clearly, there is much to be learned about the oxide growth phenomenon before its limiting effects on fuel plate heat flux can be defined accurately. However, enough is known to show that it may be a limiting issue.

Table F.1 shows clearly that oxide growth may be a limiting effect, especially if some of the high oxide growth rates observed so far in the ANS corrosion loop are indeed typical. The data were felt to be not yet conclusive, the full range of operating conditions having not yet been covered in the experimental tests.

Table F.1. Oxide effects

Core figure No.	Core volume (L)	Incipient boiling limit (MW)	Oxide thickness correlation used	EOC fuel centerline temperature limit (MW)	Time for oxide ΔT to reach 140°C (d)
7	41	276	Griess ÷ 3[a]	203	15
	41	276	½ × (Griess ÷ 3)[b]	229	20
	41	276	Modified Griess[c]	195	1
	41	276	½ × modified Griess	151	14
8	50	310	Griess ÷ 3	238	15
	50	310	Modified Griess	230	1
	50	310	½ × modified Griess	178	14
21	70	387	Griess ÷ 3	316	20
	70	387	½ × (Griess ÷ 3)	356	15
	70	387	Modified Griess	307	1
	70	387	½ × (modified Griess)	240	14
13	70	444	Griess ÷ 3	339	15
	70	444	Modified Griess	325	1

[a]The lowest growth rate observed in the ANS corrosion loop, under low pH conditions.

[b]The factor of ½ in this, and similar cases, accounts for the fact that the point of maximum power density (where the oxide growth rate is highest) moves during the cycle.

[c]A modified form of the Griess correlation, including heat flux as a variable, developed by W. R. Gambill to fit historical data and the ANS corrosion loop data.

However, the issue is a serious one, and so the PS-2 Committee discussed, and eventually listed, means by which the oxide growth effects might be mitigated. It was long known, for example, that the predicted oxide growth is extremely dependent on the water temperature in the hot spot region (e.g., in one case a 15% decrease in the temperature rise of the coolant water between inlet and hot spot reduced the calculated oxide thickness by a factor of 2 (Table F.2), thus providing several

Table F.2 Oxide growth rate for the PS-2 final preconceptual core/modified Griess

Power (MW)	Hot streak temperature (°C)	Hot spot temperature (°C)	Hot spot heat flux (MW/m^2)	Oxide failure thickness (mil)
250	102	188	11.38	0.48
300	112	213	13.66	1.04
350	122	240	15.94	2.0

possibilities for significantly reducing oxide growth. The following possible improvements to the oxide growth calculations and several possibilities for reducing oxide growth were discussed by the PS-2 Committee.

F.1 MORE COMPLETE (LESS CONSERVATIVE) CALCULATIONS OF OXIDE EFFECTS

- Correctly allow for the moving hot spot:
  - Because the hot spot moves, it is not possible for the power peak to coincide with the point of worst-case fuel loading except momentarily.
  - Movement of the control rods during the cycle will cause the hot spot to move.
  - Local fuel concentrations tend to burn out more rapidly than average fuel regions.
- Correctly allow for statistical combination of uncertainties in hot spot factors, etc.
- Correctly allow for the fact that the nuclear hot spot is usually close to the region where the fuel meat is thinnest, and therefore the thermal conductance across the fuel plate is highest.

F.2 DESIGN AND SPECIFICATION CHANGES

- Reduce inlet temperature (e.g., bigger, more expensive cooling towers and heat exchangers) or use river water as the heat sink.

- Improve QA on the plates and elements so that the worst-case deviations in coolant gap and local fuel concentrations are reduced and the hot spot factor is reduced.
- Increase the coolant velocity.

F.3 NEUTRONIC DESIGN CHANGES

- Take advantage of the larger cores to reduce the volumetric loading of the fuel and thereby increase fuel meat conductivity.
  - Also consider reducing fuel enrichment, which would permit more accurate fuel grading.
- Design the two elements differently so that, for example, the lower one (with the hot spot near the inlet) has a larger share of the power than the upper one (with the hot spot near the outlet).
- Optimize the fuel grading so that integrated oxide growth over the cycle is minimized.
  - We currently optimize for minimum peak/average nuclear power density ratio, which is not quite the same thing (e.g., we might grade the fuel so that the peak is close to the core inlets, not close to an outlet).

F.4 ENHANCEMENT R&D POSSIBILITIES

- Improve our knowledge of the expected oxide growth rate and behavior:
  - Most existing ANS loop measurements, at time of the PS-2 committee's work, have been made at higher average power densities and higher bulk water temperature than we expect in the new reference core.
- Increase the surface area in the core [e.g., decrease coolant gap and/or plate thickness (by ~0.1 mm or less)]:
  - Earlier ANS calculations showed that an 8 to 20% improvement in thermal margins might be achieved this way.
- All previous suggestions could be reconsidered and investigated such as different water chemistry, surface treatment, different cladding alloy, etc.

REFERENCES

1. J. C. Griess, H. C. Savage, and J. L. English, *Effect of Heat Flux on the Corrosion of Aluminum by Water. Part IV. Test Relative to the Advanced Test Reactor and Correlation with Previous Results*, ORNL-3541, Union Carbide Corp. Nuclear Div., Oak Ridge Natl. Lab., 1964.

2. R. S. Ordrejcin, *Evaluation of MARK-22 Cladding*, SRL memorandum DPST-83-324, 1983.

3. G. H. Hanson et al., *Report of the ANS Aluminum Cladding Corrosion Workshops*, ORNL/CONF-88-11203, Martin Marietta Energy Systems, Inc., Oak Ridge Natl. Lab.

ORNL/TM-11234

Internal Distribution

1. R. G. Alsmiller
2. Y. Y. Azmy
3. N. C. J. Chen
4. G. L. Copeland
5. F. C. Difilippo
6. W. R. Gambill
7. J. A. Getsi
8. M. A. Gildner
9. S. R. Greene
10. R. M. Harrington
11. D. T. Ingersoll
12. J. A. Johnson
13. M. Jordon
14. R. A. Lillie
15. R. Miller
16. B. H. Montgomery
17. F. R. Mynatt
18. L. C. Oakes
19. F. J. Peretz
20. R. T. Primm, III
21. C. C. Queen
22. J. S. Rayside
23. H. Reutler
24. A. E. Ruggles
25. T. L. Ryan
26. D. L. Selby
27. P. B. Thompson
28. H. E. Trammell
29-53. C. D. West
54. M. K. Wilkinson
55. G. T. Yahr
56. G. L. Yoder
57. ORNL Patent Section
58. Central Research Library
59. Document Reference Section
60-61. Labratory Records Department
62. Laboratory Records (RC)

External Distribution

63. P. Ageron, Institute Laue Langevin, 156X 38042, Grenoble Cedex, France
64. Takumi Asaoka, Deputy Director General, Tokai Research Establishment, Japan Atomic Energy Research Institute, Takaimure, Naka-gun, Ibaraki-ken, Tokyo 319-11, Japan
65. G. Bauer, KFA Julich, SNQ, P.O. Box 1913, D15170 Julich, West Germany
66. Dr. Klaus Böning, Fakultät Für Physik, Technische Universität München, D-8046 Garching, West Germany
67. H. A. Capote, Burns & Roe, 800 Kinderkamack Road, Oradell, NJ 07649
68. H. L. Dodds, Nuclear Engineering Department, University of Tennessee, Knoxville, TN 37996-2300.
69. Jack Dorning, Department of Nuclear Engineering and Engineering Physics, University of Virginia, Charlottesville, VA 22901
70. Dr. B. Chalmers Frazer, Materials Science Division, Office of Basic Energy Sciences, Office of Energy Research, U.S. Department of Energy, Germantown, ER-132, Washington, DC 20545
71. R. Fullwood, Building 130, Brookhaven National Laboratory, Upton, NY 11973
72. W. Glaser, Director, Institute Laue-Langevin, 156K, 38042 Grenobl Cedex, France

73. Dr. L. C. Ianniello, Deputy Associate Director, Office of Basic Energy Sciences, Office of Energy Research, U.S. Department of Energy, Germantown ER-11, Washington, DC 20545
74. Masashi Iizumi, Japan Atomic Energy Research Institute, 222, Uchisaiwai-cho, Chiyoda-ku, Tokyo, Japan
75. Professor K. Kanda, Research Reactor Institute, Kyoto University, Kumatori, Osaka 590-04, Japan
76. Nobuhiki Kunitomi, Osaka University, 1-1 Yamadaoka, Fuita-Shi, Osaka 565 Japan
77. J. A. Lake, Manager, Nuclear Engineering and Reactor Design, Idaho National Engineering Laboratory, P.O. Box 1625, Idaho Falls, ID 83415
78. Dale Lancaster, Georgia Institute of Technology, Atlanta, GA 30332
79. L. LeSage, Argonne National Laboratory, 9700 South Cass Avenue, Argonne, IL 60439
80. John Marks, Research and Test Reactor Fuel Elements, Babcock and Wilcox Co., P.O. Box 785, Lynchburg, VA 24505
81. John J. Rush, National Bureau of Standards, Washington, DC 20234
82. John M. Ryskamp, Idaho National Engineering Laboratory, P.O. Box 1625, Idaho Falls, ID 83415-3515
83. Professor T. Shibata, Kinki University, Kowakae, Hogashiosaka, Osaka 577, Japan
84. J. L. Snelgrove, Coordinator, Engineering Applications, RERTR Program, Argonne National Laboratory, 9700 South Cass Avenue, Argonne, IL 60439
85. Dr. D. K. Stevens, Associate Director, Office of Basic Energy Sciences, Office of Energy Research, Department of Energy, Germantown ER-10, Washington, DC 20545
86. Dr. Iran L. Thomas, Director, Materials Science Division, Office of Energy Research, U.S. Department of Energy, Germantown ER-13, Washington, DC 20545
87. R. P. Wadkins, Manager, Core Design and Analysis Unit, Idaho National Engineering Laboratory, EDG&G Idaho, P.O. Box 1625, Idaho Falls, ID 83415-3515
88. D. K. Wilfert, Energy Programs, U.S. Department of Energy, Oak Ridge Operations, P.O. Box 2001, Oak Ridge, TN 37831
89. R. J. Willard, U.S. Department of Energy, Oak Ridge Operations, P.O. Box 2001, Oak Ridge, TN 37831
90. Office of Assistant Manager for Energy Research and Development, Department of Energy, Oak Ridge Operations, P.O. Box 2001, Oak Ridge, TN 37831

91-100. Office of Scientific and Technical Information, P.O. Box 62, Oak Ridge, TN 37831